

SEDIMENTOLOGY OF BAYFILLS IN THE NESLEN
FORMATION, BOOK CLIFFS, USA, WITH SPECIAL FOCUS ON
THE IMPACT FROM EARLY COMPACTION ON THICKNESS-
AND LITHOFACIES DISTRIBUTION

Master in Geodynamics and Basin Studies

Julie Asdal Eriksen



Department of Earth Science

University of Bergen

June 2021

Abstract

The Neslen Formation of the Mesaverde Group (eastern Book Cliffs, Utah) accumulated along the western margins of the Western Interior Seaway. The formation is subdivided into Lower-, Middle-, and Upper Neslen Interval. The Lower Neslen Interval is composed of fluvial channel-fills and floodplain muds, overlain the marginal-marine interdistributary bay deposits of the Middle Neslen Interval, characterized by six vertically stacked bayfill units. Fluvial channel-fills and floodplain muds dominate the Upper Neslen Interval.

During burial of coastal plain deposits, sand-rich channel-fill deposits undergo less compaction than the surrounding floodplain muds, resulting in differential compaction. Early differential compaction is extensively documented in Holocene delta plain sediments, whereas fewer studies address early compaction in ancient delta plains and its effect on thickness and lithofacies characteristics of overlying deposits.

This MSc thesis investigates the vertical and lateral controls on thickness and lithofacies distribution of the three lowermost bayfill units within the Middle Neslen Interval, focusing on early differential compaction of the Lower Neslen Interval. Detailed documentation of lithofacies has been carried out by sedimentary logging and the larger-scale sedimentary architecture has been demonstrated through a number of correlation panels. Eleven lithofacies are identified in the lower delta plain deposits, and the interdistributary bay deposits are assigned to three facies associations; wave-dominated bayfill, bayhead delta, and sub-bay.

An interdistributary bayfill unit is a thin (1.7 - 6.3 m), upward-coarsening unit, a “parasequence”, bounded by allogenicly controlled flooding surfaces. As the tectonic subsidence is considered uniform in the study area, the stacking of bayfill units is driven by low-amplitude, high-frequency relative sea-level changes which had a profound effect in this low gradient and low relief environment. This study finds that the bayfill units become thinner and more sandstone-rich upwards in the succession, suggesting an overall decreasing rate of generation of accommodation space. Analyses of the sand- and shale-body geometries show that lateral variations in bayfill unit thickness and lithofacies distribution are vulnerable to early differential compaction of Lower Neslen Interval. The bayfill units exhibit a thinning above sandstone-rich channel-fill deposits concurrently with an increased abundance of sandstones relative to mudstones and increase in the amount of wave-generated structures. The effect decreases upwards in the bayfill successions and is usually absent after 7 - 8 meters of overburden. Lateral thickness variations are to some extent caused by autocompaction within the bayfill units and compaction of coals and organic-rich mudstones.

Adding knowledge of the effect of early differential compaction on bayfill unit thickness and lithofacies distribution will increase the understanding of reservoir architecture within lower delta plain reservoirs. A good understanding of reservoir architecture is crucial for improved quality of static and dynamic reservoir models. An improved understanding will also support drainage strategies and well planning.

Acknowledgements

This thesis is part of my MSc degree in Sedimentology at the Department of Earth Science at the University of Bergen. First and foremost, I would like to express my deepest gratitude to my supervisor, Professor William Helland-Hansen (University of Bergen), for his guidance, support, and motivation, and for always being available, despite the COVID-19 outbreak.

In addition, I would like to thank my co-supervisor, Jostein Kjærefjord (Equinor), for outlining the thesis and his invaluable assistance during the fieldwork and upcoming work with this project. I am grateful for the opportunity to conduct fieldwork in Utah and extend a great thanks to Equinor for funding the project.

A special thanks to my field partner, MSc candidate Tobias Hermansen, for excellent company and great discussions in the field. I would like to extend my sincere thanks to Sigrid and Torgeir for proofreading the thesis. Thank you to my fellow students for the great discussions, memories and the good atmosphere during my time at the University of Bergen. I am grateful for all the coffee breaks, field trips, and social gatherings during the fantastic years together at the Department of Earth Science.

Finally, I would like to thank my family and friends for being patient and supportive throughout these five years of study. Special thanks to Torgeir; your support, encouragement, and help have been essential to me.

Bergen, June 2021

Julie Asdal Eriksen

List of contents

1 INTRODUCTION	1
1.1 INTRODUCTION	1
1.2 PROJECT AIMS	1
1.3 STUDY AREA	2
2 GEOLOGICAL FRAMEWORK.....	4
2.1 STRUCTURAL SETTING.....	4
2.2 LATE CRETACEOUS STRATIGRAPHY	8
2.2.1 <i>Desert Member of the Blackhawk Formation</i>	10
2.2.2 <i>Castlegate Sandstone</i>	10
2.2.3 <i>Mancos Shale: Buck Tongue</i>	10
2.2.4 <i>Sego Sandstone</i>	11
2.2.5 <i>Neslen Formation</i>	11
2.2.6 <i>Farrer Formation</i>	15
2.2.7 <i>Tuscher Formation</i>	15
3 DATABASE AND METHODOLOGY.....	16
3.1 DATABASE	16
3.2 FIELDWORK AND METHODS	16
3.3 UNCERTAINTIES AND SOURCES OF ERROR.....	18
4 LITHOFACIES DESCRIPTION.....	20
4.1 LITHOFACIES 1A: CROSS-STRATIFIED SANDSTONE.....	22
4.2 LITHOFACIES 1B: SANDSTONE WITH WAVE-RIPPLE CROSS-LAMINATION AND SANDSTONE WITH HUMMOCKY CROSS-STRATIFICATION	24
4.2.1 <i>Sub-facies 1B1: Sandstone with hummocky cross-stratification</i>	24
4.2.2 <i>Sub-facies 1B2: Sandstone with wave-ripple cross-lamination</i>	26
4.3 LITHOFACIES 1C: BIOTURBATED SANDSTONE >DEGREE 2.....	28
4.4 LITHOFACIES 1D: CURRENT-RIPPLE CROSS-LAMINATED SANDSTONE.....	30
4.5 LITHOFACIES 2A: WAVE-RIPPLE CROSS-LAMINATED WAVY BEDDED HETEROLITH.....	31
4.6 LITHOFACIES 2A-C: CURRENT-RIPPLE CROSS-LAMINATED WAVY BEDDED HETEROLITH.....	34
4.7 LITHOFACIES 2B: CURRENT- OR WAVE-RIPPLED, WAVY- TO LENTICULAR BEDDED HETEROLITH	35
4.8 LITHOFACIES 3A: HORIZONTAL LAMINATED TO LENTICULAR BEDDED MUDSTONE	37
4.9 LITHOFACIES 3B: ROOTED AND ORGANIC-RICH MUDSTONE.....	38
4.10 COAL.....	40
5 FACIES ASSOCIATIONS	42
5.1 FACIES ASSOCIATION 1: FLUVIAL CHANNEL (FA1).....	43
5.2 FACIES ASSOCIATION 2: MARSH/LEVEE (FA2).....	45
5.3 FACIES ASSOCIATION 3: BAY DEPOSITS (FA3)	47
5.3.1 <i>Sub-facies association 3a: Wave-dominated bayfill (FA3a)</i>	48
5.3.2 <i>Sub-facies association 3b: Bayhead delta (FA3b)</i>	51
5.3.3 <i>Sub-facies association 3c: Sub-bay (FA3c)</i>	53
5.4 LOWER DELTA PLAIN DEPOSITS	54
5.5 CLASSIFICATION OF BAYFILL UNITS	57
5.5.1 <i>Definitions</i>	58
5.5.2 <i>Classification</i>	58
6 SAND- AND SHALE-BODY GEOMETRY	61

6.1 VERTICAL VARIATIONS IN GEOMETRY	61
6.1.1 <i>Distribution of facies associations</i>	61
6.1.2 <i>Bayfill unit thickness and percentage of mudstone</i>	61
6.1.3 <i>Description of bayfill units</i>	62
6.2 LATERAL VARIATIONS IN GEOMETRY	64
6.2.1 <i>Outer East Canyon</i>	64
6.2.2 <i>Exit Canyon</i>	69
6.2.3 <i>Keane Creek</i>	75
6.2.4 <i>East Canyon Window</i>	79
6.2.5 <i>Neslen Canyon</i>	84
7 ANALYSIS OF THE GEOMETRY	89
7.1 LATERAL VARIATIONS IN LITHOFACIES.....	90
7.1.1 <i>Wave- versus current-generated structures</i>	90
7.1.2 <i>Content of sandstone versus mudstone</i>	91
7.2 LATERAL THICKNESS VARIATIONS	92
7.3 OTHER FACTORS CONTROLLING LATERAL THICKNESS VARIATIONS.....	94
7.4 SUMMARY	95
8 CONTROLS OF THICKNESS WITHIN BAYFILL SUCCESSIONS.....	96
8.1 VERTICAL THICKNESS CONTROLS.....	96
8.1.1 <i>Autogenically versus allogenicly controlled flooding</i>	96
8.1.2 <i>Relative sea-level changes</i>	98
8.1.3 <i>Tectonic subsidence</i>	99
8.1.4 <i>Compaction-induced subsidence</i>	99
8.2 LATERAL THICKNESS CONTROLS.....	100
8.2.1 <i>Differential compaction</i>	100
9 CONCLUSIONS.....	103
LIST OF REFERENCES.....	104

APPENDIX I: Data from sedimentary logs

APPENDIX II: Sedimentary logs

APPENDIX III: Panoramic photos

1 Introduction

1.1 Introduction

The Campanian Neslen Formation crops out in the middle and eastern part of the Book Cliffs, Utah and Colorado. The formation represents a series of delta plain and interdistributary bay deposits prograding basinwards from the western margin of the Late Cretaceous, Western Interior Seaway. The formation is subdivided into three, with the Lower- and Upper Neslen Interval composed of fluvial deposits, whereas the Middle Neslen Interval is composed of marginal-marine interdistributary bay deposits.

As the Book Cliffs contain extensive, high-quality outcrops, the Neslen Formation represents an outcrop analog for numerous subsurface petroleum reservoirs. Previous studies have contributed to an improved understanding of facies architecture and a robust stratigraphic framework of the Neslen Formation (e.g., Kjærefjord, 1999; Willis, 2000; Hettinger & Kirschbaum, 2002; Kirschbaum & Hettinger, 2004; Shiers et al., 2014). Still, there are significant gaps in knowledge related to the development of bayfill successions, both surrounding the factors controlling the development of vertically stacked bayfill units and possible controls on lateral variations in thickness and lithofacies distribution of a bayfill unit. There is a lack of previous studies that focus on how the extent of early differential compaction in underlying strata affects the bayfill unit thickness and lithofacies distribution.

Sedimentary logging and establishing lithofacies and facies associations schemes add insights into these knowledge gaps. The relation between the underlying, fluvial deposits and the heterogeneities in the overlying interdistributary bay deposits is investigated by performing log correlations and analyzing the sand- and shale-body geometries. Differential compaction causes uneven space for sediments to fill due to variations in volume reduction, resulting in heterogeneities. Differential compaction has become a topic of interest in, e.g., hydrocarbon exploration and subsidence studies of Holocene delta plains. In order to improve the quality of static and dynamic reservoir models of lower delta plain deposits, early differential compaction within reservoirs should be further considered.

1.2 Project aims

This project aims to improve the understanding of the controls on lithofacies distribution and bayfill unit thickness in the three lowermost bayfill units in the Middle Neslen Interval, with special focus on early differential compaction in the Lower Neslen Interval. The aim is reached

by gaining insight into the spatial distribution of lithofacies within a laterally- and vertically defined interval. The following objectives have been carried out to reach the aim:

- Detailed sedimentary logging of the upper part of the Lower Neslen Interval and the three vertically stacked bayfill units of the Middle Neslen Interval at 19 different locations.
- Build detailed schemes of lithofacies and facies associations based on sedimentary logs.
- Perform correlation of sedimentary logs and study sand- and shale-body geometries.
- Investigate the controls of thickness and lithofacies distribution of the bayfill units vertically and laterally, focusing on differential compaction.

1.3 Study area

The study area is located along a ~6 km transect in the eastern part of Utah, USA, northeast in Grand County (Fig. 1.1). The area where the studied rocks are exposed is located approximately 65 km northwest of Grand Junction, Colorado, and covers ~10 km². The studied Neslen Formation is Campanian (Late Cretaceous) in age and crops out in Outer East Canyon, East Canyon Window, Neslen Canyon, Keane Creek, and Exit Canyon (Figs. 1.1 and 1.2). These canyons cut into the eastern part of the northwest - southeast trending Book Cliffs (Fig. 1.1), stretching approximately 250 km from the city of Helper, Utah, in the northwest to Grand Junction, Colorado, in the southeast.



Figure 1.1: The study area is located in the eastern part of Utah, USA. The studied outcrops are located in Outer East Canyon, East Canyon Window, Neslen Canyon, Keane Creek, and Exit Canyon. White, dashed line outline the Book Cliffs. Boxes A, B, C correlates to Figure 1.2A, B, C. Satellite images © Google Earth 2020.

The studied part of the Book Cliffs trends oblique to the east-west oriented depositional dip. Canyons cutting the cliff-face constitute excellent 3D exposures. The stratigraphic thickness of the Book Cliffs ranges from 300 m to 600 m, and the altitude in the study area is ~1600 ~1800

m. The study area comprises five main locations (Fig. 1.1), each with a varying number of logs (Table 1.1 and Fig. 1.2).

Table 1.1: The five main locations in the study area, showing the number of logs, the length of the transects, and the corresponding figures.

Location	Number of logs	Length of transect	Figure
Outer East Canyon	3	~100 m	1.2B
Exit Canyon	7	~300 m	1.2A
Keane Creek	3	~100 m	1.2C
East Canyon Window	4	~100 m	1.2C
Neslen Canyon	2	~200 m	1.2C

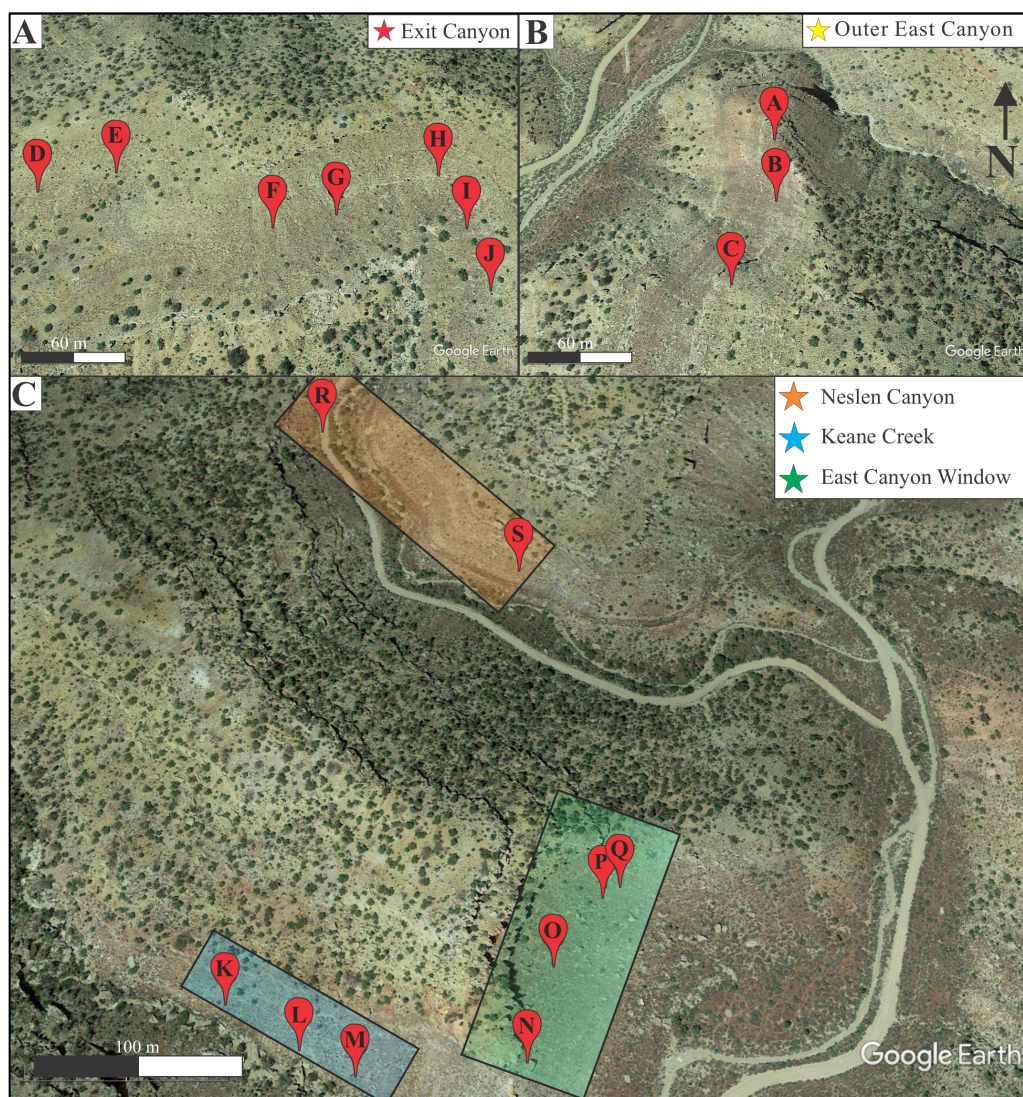


Figure 1.2: Close-up satellite images of the five main locations shown in Figure 1.1. A: Locations of the seven logs in Exit Canyon. B: Locations of the three logs in Outer East Canyon. C: Locations of the two logs in Neslen Canyon (orange), the three logs in Keane Creek (blue), and the four logs in East Canyon Window (green). Satellite images © Google Earth 2020.

2 Geological framework

2.1 Structural setting

The study area (Fig. 1.1) has undergone major tectonic phases, starting in the Carboniferous, when the North-American Plate detached from Pangea and started to drift towards the northwest (Kauffman & Caldwell, 1993). The western margin of the North-American Plate collided with the Pacific Farallon Plate, causing subduction of the Pacific Farallon Plate.

During Carboniferous, Triassic, and Jurassic, the sedimentation was dominated by fine-grained eolian deposits (e.g., Page Sandstone, Cedar Mesa Formation, Wingate Sandstone, Nugget Sandstone, Navajo Sandstone, and Slickrock Member) (Blakey et al., 1988). In the Late Jurassic, the Carboniferous to Jurassic stratigraphic succession is pushed up in a thrust belt, first as the Mesocordilleran High, and finally into the Sevier fold-and-thrust-belt. Generally, the Book Cliffs mostly exhibit grain-sizes no larger than fine- to medium-grained sandstone due to the overall fine-grained, eolian sedimentary rocks in the source area.

The Sevier fold-and-thrust-belt was in the period 140 Ma to 55 Ma characterized by thin-skinned deformation of the crust (Fig. 2.4) (Blakey & Ranney, 2018). Thin-skinned deformation and increased growth of the Sevier fold-and-thrust-belt led to the development of a foreland basin in the front (to the east) around 120 Ma, caused by isostatic adjustment adjacent to the thickened crust of the orogen (Kauffman & Caldwell, 1993; Blakey & Ranney, 2018). A foreland basin (Fig. 2.1) is characterized as a basin formed during compression. The asymmetric subsidence is of greatest magnitude close to the source area, resulting in thick proximal successions in the west, which is thinning eastward. This thesis' study area (Fig. 1.1) is located far out in the basin (~250 km from the source area). Hence, the subsidence in the study area is considered symmetrical. The foreland bulge was likely located just east of the study area during deposition of the Book Cliffs' stratigraphy (Fig. 2.1). Later, the foreland bulge (Douglas Creek Arch) defines the boundary between the upcoming Uinta and Piceance basins (Fig. 2.1 and 2.3B, C).

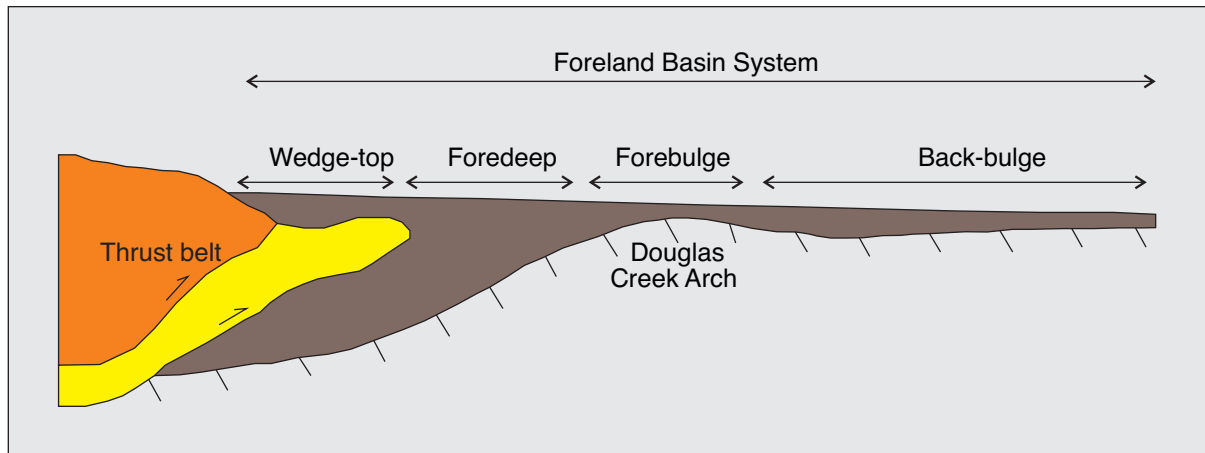


Figure 2.1: Illustration of a foreland basin system, with the Douglas Creek Arch as the forebulge in the study area. Modified from DeCelles & Giles (1996).

In the Aptian, the foreland basin was invaded and flooded by seawater from the north (Fig. 2.2). This was due to subsidence adjacent to the mountain system combined with high eustatic sea-level in the Late Cretaceous and led to the development of the Western Interior Seaway (Hintze, 1988; Kauffman & Caldwell, 1993). The Western Interior Seaway extended southwards from about 115 Ma and reached its maximum at 93 Ma (Turonian) (Hettinger & Kirschbaum, 2002; Blakey & Ranney, 2018). At that time, it extended from Alaska to the Gulf of Mexico (Fig. 2.2A) (Kauffman, 1984). Towards the end of the Late Cretaceous, the Western Interior Seaway gradually began to close from the south due to decreasing subsidence rates and high sedimentation rates (Blakey & Ranney, 2018). Parts of this foreland basin are exposed in the uplifted Colorado Plateau (Fig. 2.3A).

Sedimentation pattern in the Western Interior Seaway was affected by several factors such as subsidence, eustatic sea-level, climate, and thrusting in the source area. Thrusting and eustatic fluctuations resulted in variable sediment supply and fluctuating shoreline positions with periods of transgression and regression (Ryer et al., 1984; Johnson, 2003; Miall et al., 2008). Thrusting also caused volcanic activity. Several ash layers are observed within the Western Interior Seaway deposits (Blakey & Ranney, 2018), including two bentonite layers in the coal bed capping one of the studied bayfill units (Bayfill #2 unit, see Sub-chapter 2.2.5).

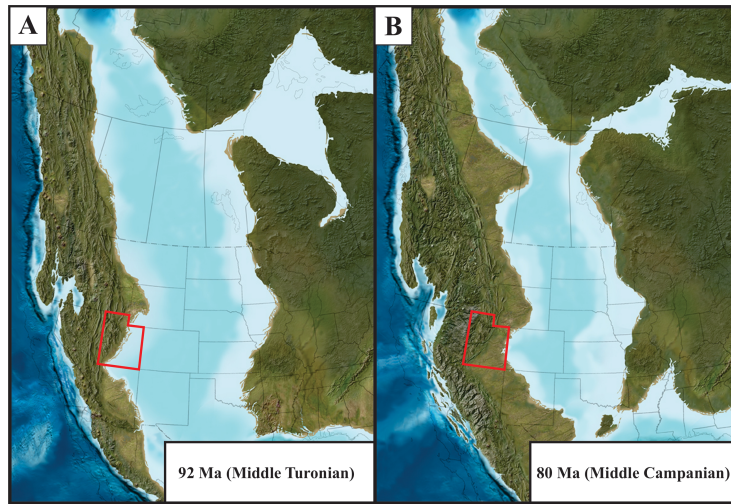


Figure 2.2: A: The Western Interior Seaway at its greatest extent in Middle Turonian (92 Ma). B: The Western Interior Seaway during deposition of the Mesaverde Group in Middle Campanian (80 Ma). Location of Utah in the red polygon. Maps from Blakey (2017).

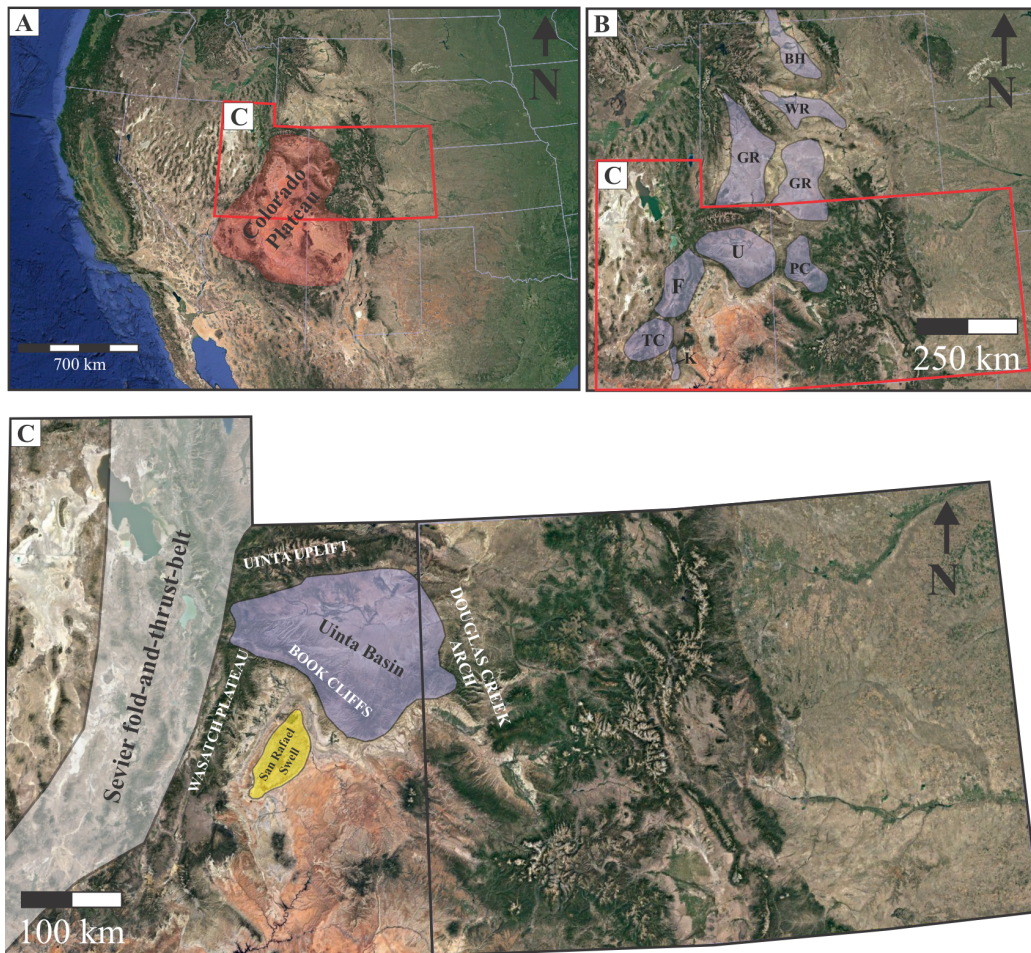


Figure 2.3: A: The Colorado Plateau. Location of Utah and Colorado in the red polygon. B: Distribution of Laramide depositional basins. BH: Bighorn, F: Flagstaff, GR: Greater Green River, K: Kaiparowitz, PC: Piceance Creek, TC: Table Cliffs, U: Uinta, WR: Wind River. Modified from Lawton (2008). C: The Uinta Basin shaded in purple, bounded by the Uinta Uplift in the north, the Douglas Creek Arch in the east, the San Rafael Swell in the south, and the Wasatch Plateau of the Sevier fold-and-thrust-belt in the west. Location of the Book Cliffs within the Uinta Basin is also shown. Satellite images © Google Earth 2020.

During the Latest Cretaceous and Cenozoic, the deformation style changed due to flattening of the subduction slab with increased compressional stresses (Fig. 2.4) (Keith, 1978; Erslev, 1993; Aschoff & Steel, 2011; Yonkee & Weil, 2015). Flattening of the subduction slab occurred as the Pacific Farallon Plate changed its westward direction to a south-eastward direction. Flat-slab subduction is a result of a thickened slab of oceanic volcanic plateau being subducted. This causes the subducting Farallon Plate to be more buoyant and the descent angle less steep (Fig. 2.4) (Blakey & Ranney, 2018). A less steep subduction angle moved the arc magmatism, and thus the axis of the Western Interior Seaway to the east. This led to cessation of deposition within the foreland basin. Whereas the earlier Sevier-style deformation was dominated by thin-skinned deformation and the development of a foreland basin, the flat-slab subduction and compressional stresses led to a transition into Laramide-style thick-skinned deformation and the development of uplifts and intermontane basins (Keith, 1978; Erslev, 1993; Roberts & Kirschbaum, 1995). This transformation caused the contiguous foreland basin to be locally partitioned by basement-involved structures from the Laramide uplifts (Fig. 2.4) (Aschoff & Steel, 2011).

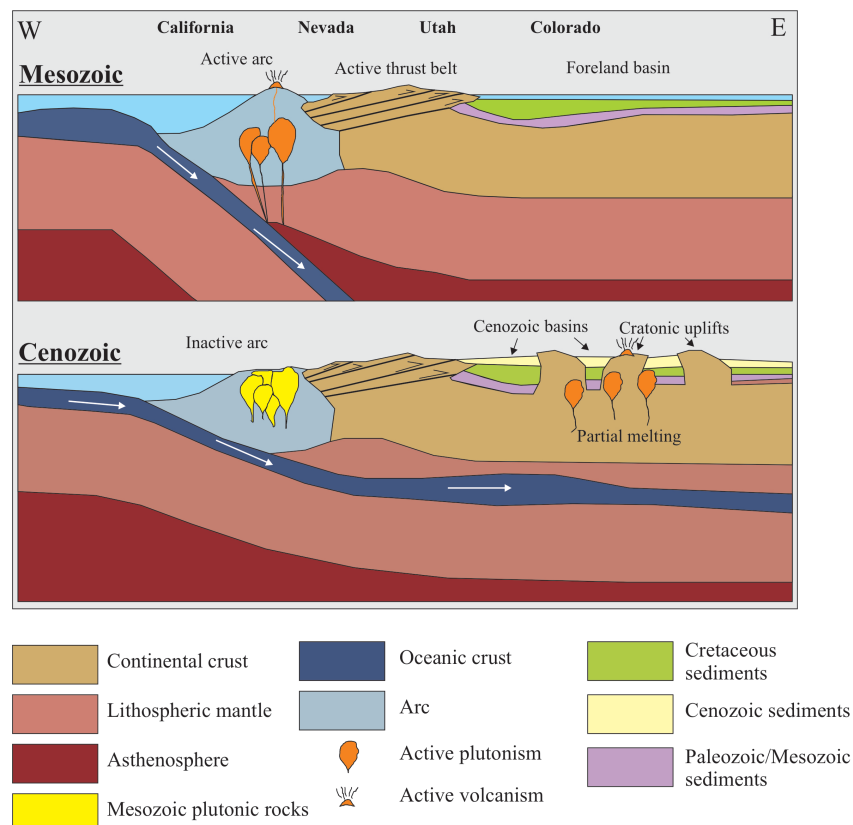


Figure 2.4: Cross-section from California to Colorado, showing two different subduction types in the study area. In the Mesozoic, the Sevier-style deformation dominated, with normal subduction with a steep angle, creating a foreland basin. In the Cenozoic, flat-slab subduction occurred, creating uplifts that partitioned the foreland basin. Modified from Frisch et al. (2011).

Several minor, rapidly subsiding depositional basins developed between individual Laramide uplifts, where subsidence rates exceeded sedimentation rates (Fig. 2.3B) (e.g., Ryder et al., 1976; Hintze, 1988; Krystinik & DeJarnett, 1995; Van Wagoner, 1995; Howell & Flint, 2003; Aschoff, 2010). The Laramide orogeny led to the uplift of today's Colorado Plateau and the Rocky Mountains. Uinta Basin is one of the minor, Laramide ponded basins of this period and is today located in the eastern part of Utah (Krystinik & DeJarnett, 1995; Van Wagoner, 1995). The Uinta Basin is bounded by the Sevier fold-and-thrust-belt in the west, the Uinta Mountains in the north, the San Rafael Swell in the south, and the Douglas Creek Arch in the east (Fig. 2.3C) (Sonntag et al., 2014). About 3 km of siliciclastic and carbonate deposits accumulated in the Uinta depocenter from Late Cretaceous to Eocene time (Ryder et al., 1976). The sediments that accumulated in the ponded basins during the Laramide uplifts originated from the eastern side of the western highlands and consisted of a mixture of continental and shallow marine sediments. Coarse-grained sediments accumulated adjacent to the highlands, whereas finer-grained sediments accumulated in the basin's central parts. The Uinta Basin was inundated by a transgression during Eocene time, creating Lake Uinta and accumulation of lacustrine sediments (Johnson, 1985).

2.2 Late Cretaceous stratigraphy

Sediments eroded from the Sevier fold-and-thrust-belt were transported and deposited into the foreland basin during Campanian time. Several clastic wedges were formed and the Mesaverde Group comprises one wedge (Fig. 2.5) (Willis, 2000). Depositional dip was primarily towards the east, and the margin was characterized as a ramp margin lacking shelf break (Howell & Flint, 2003). Lateral variations in lithology and thickness in east-west- and north-south direction are observed within the Mesaverde Group in the Uinta Basin (Van Wagoner, 1995; Willis & Gabel, 2001; Aschoff, 2010). According to Hettinger & Kirschbaum (2002) and Aschoff (2010), several depositional environments are observed within the Mesaverde Group. During deposition of the Mesaverde Group, transgressions and regressions caused oscillation between the marine Mancos Shale tongues and the Mesaverde Group sandstones and shales.

The clastic deposits of the Cretaceous foreland basin were described early by several authors (e.g., Spieker, 1946; Young, 1955; Fisher et al., 1960). The Late Cretaceous stratigraphy in the study area is subdivided into Desert Member of Blackhawk Formation, Castlegate Sandstone, Buck Tongue of the Mancos Shale, Sego Sandstone, Neslen Formation, Farrer Formation, and

Tuscher Formation (Fisher et al., 1960) (Fig. 2.5), all part of the extensively studied Campanian Mesaverde Group in eastern Utah, USA (Shiers et al., 2014).

The Late Cretaceous Mesaverde Group comprises shallow-marine, coastal-plain, and alluvial-plain deposits (Harper, 2011). Mesaverde Group originates from a clastic system prograding into the foreland basin from the Western Interior Seaway's western margin. Neslen Formation, the main focus of this thesis, is deposited as a part of a clastic eastward-thinning wedge that prograded eastwards from the Sevier fold-and-thrust-belt into the Western Interior Seaway.

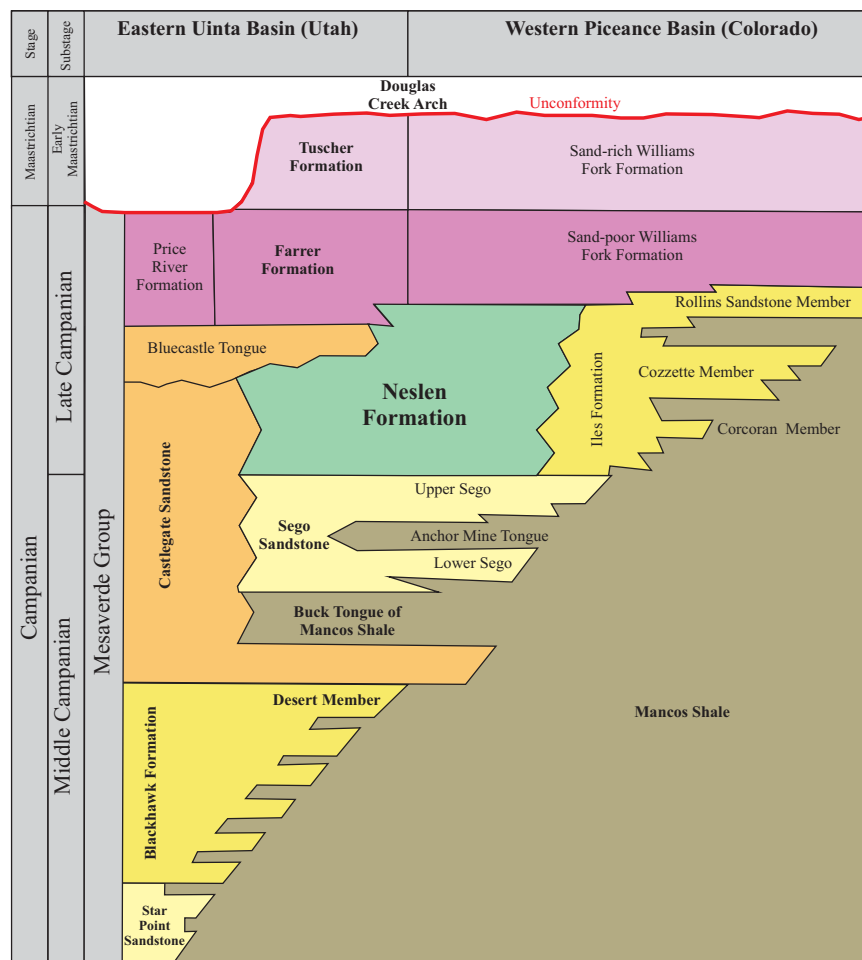


Figure 2.5: Generalized stratigraphic chart of the Campanian Mesaverde Group and overlying strata from Eastern Uinta Basin (Utah) to Western Piceance Basin (Colorado), Book Cliffs, USA. Douglas Creek Arch defines the boundary between Uinta Basin and Piceance Basin. Modified after Fenn (2012).

Large fluvial megafans and clastic systems fed the western shorelines with sediments derived from the Sevier fold-and-thrust-belt (Roberts & Kirschbaum, 1995). The sedimentation within the basin varied from thick, coarse-grained, marginal- to shallow-marine sandstone-sequences in the west to fine-grained, marine deposits with calcareous and silty shales and carbonates farther east (Kauffman, 1984; Hintze, 1988). The shoreline position fluctuated due to variations in sediment supply and accommodation, caused by factors such as eustasy, subsidence,

hinterland tectonics, and climate (Aschoff et al., 2018). Well-known sandstone units (e.g., Mesaverde Group) interbedded with shale bodies (e.g., Mancos Shale) were deposited during this stage (Blakey & Ranney, 2018). A description of the sandstones and formations of the Mesaverde Group within the study area follows (in ascending order, from oldest to youngest).

2.2.1 Desert Member of the Blackhawk Formation

Only the uppermost member of the Blackhawk Formation, the Desert Member, is developed in the study area (Fig. 2.5). The Desert Member is one out of six sandstone-dominated members separated by the Mancos Shale, unconformably overlain by the Castlegate Sandstone (Fisher et al., 1960; Hettinger & Kirschbaum, 2002). It contains fine- to medium-grained sandstones, mudrocks, shales, and coals interpreted as coastal plain and shoreface deposits (Hettinger & Kirschbaum, 2002). Van Wagoner (1995) interprets valley-fill deposits where the base of the Desert Member represents an unconformity (Desert Sequence Boundary).

2.2.2 Castlegate Sandstone

The Castlegate Sandstone is composed of laterally extensive sandstone sheets that unconformably overlie the Blackhawk Formation (Lawton, 1986) (Fig. 2.5). To the west of the study area, the formation comprises a continuous, thick sandstone. Within the study area, only the lowermost part of the Castlegate Sandstone is present, as the middle/upper part passes into several formations (in order from oldest to youngest); Buck Tongue of the Mancos Shale, Sego Sandstone, and Neslen Formation (Franczyk et al., 1990). The middle/upper Castlegate Sandstone deposits are interpreted as fluvial and estuarine deposits (Lawton, 1986; Van Wagoner, 1995). Van Wagoner (1995) suggested an eastward transition from the Castlegate Sandstone into shoreface strata. Hence, in the study area, the Castlegate Sandstone consists of upward-coarsening shoreface deposits (Fig. 2.6).



Figure 2.6: Photo showing the stratigraphy in the entrance to the study area, where Castlegate Sandstone (red), Buck Tongue of the Mancos Shale (green), Sego Sandstone (yellow), Anchor Mine Tongue of the Mancos Shale (green), and Neslen Formation (orange) is shown. Photo: Jostein Kjærefjord.

2.2.3 Mancos Shale: Buck Tongue

The Buck Tongue of the Mancos Shale is located on top of the Lower Castlegate Sandstone and below the Sego Sandstone in the study area (Figs. 2.5 and 2.6). This open-marine shale

pinches out into the Castlegate Sandstone landwards (westwards) and the main body of the Mancos Shale basinwards (eastwards) (Fig. 2.5). Its base is erosional, interpreted as a transgressive wave ravinement surface (Van Wagoner et al., 1990). Its upper contact to the Segoe Sandstone is mostly conformable (Fisher et al., 1960), but locally unconformable (Van Wagoner et al., 1990; Willis, 2000; Willis & Gabel, 2001).

2.2.4 Segoe Sandstone

The Segoe Sandstone was first described by Fisher (1936) in Segoe Canyon, Utah, as a ~55 m thick unit with sandstones and mudstones. The Segoe Sandstone is divided into two parts in the study area; Lower Segoe and Upper Segoe, separated by the westward-thinning open marine shales of the Anchor Mine Tongue of the Mancos Shale (Figs. 2.5 and 2.6). Segoe Sandstone is stratigraphically located on top of the Buck Tongue of Mancos Shale and overlain by the Neslen Formation (Figs. 2.5 and 2.6). In Colorado, east of the study area, the Segoe Sandstone is overlain by the Corcoran Member of the Iles Formation. Farther to the east, it passes into the open marine Mancos Shale. West of the study area, the Segoe Sandstone passes into the Castlegate Sandstone. The Segoe Sandstone comprises deposits of lower shoreface and nearshore marine- (Young, 1955), estuarine- (Van Wagoner, 1992), and tide-dominated delta deposits (Willis & Gabel, 2001).

2.2.5 Neslen Formation

The Neslen Formation was first described as a ~98 m thick coal-bearing unit with shales, siltstones, and sandstones in Neslen Canyon, Utah, by Fisher (1936). The thickness of the Neslen Formation varies from 40 m most landwards (westwards) to 120 m at the Utah - Colorado border (Shiers et al., 2014), with an average thickness of ~110 m (Kjærefjord, 1999). Neslen Formation is located between the underlying Segoe Sandstone and the overlying Farrer Formation (Figs. 2.5 and 2.6). Van Wagoner (1992) suggests that the lower limit of the Neslen Formation is placed at the Neslen Sequence Boundary (SB) (Fig. 2.7). Neslen Formation is interpreted as low gradient coastal plain-, lower alluvial plain- (Franczyk et al., 1990; Shiers et al., 2014), estuarine- and interdistributary bay deposits (Kjærefjord et al., 2021, Accepted). Neslen Formation passes into the fluvial-dominated Upper Castlegate Sandstone landwards (westwards) and into the shallow-marine Cozzette- and Corcoran Members of Iles Formation basinwards (eastwards) (Fig. 2.5) (Kirschbaum & Hettinger, 2004). In general, the Corcoran Member is identified by deposits of fluvial-, tidal-, and shoreface environments. The Cozzette Member is characterized by tidal-, estuarine-, and shoreface environments (Kirschbaum &

Hettinger, 2004). The Cozzette- and Corcoran Members acted as barrier islands during deposition of the Middle Neslen Interval, where the tidal- and shoreface deposits interpreted by Kirschbaum & Hettinger (2004) are related to the barrier islands. The estuarine deposits are associated with the five sequence boundaries (Neslen SB, Corcoran SB, Buck SB, Cozzette SB, and Bluecastle SB) interpreted in the Neslen Formation (Fig. 2.7).

Earlier studies subdivide the Neslen Formation into three distinct intervals; Palisade Coal Zone, Ballard Coal Zone, and Chesterfield Coal Zone (Fig. 2.7) based on thinner coal beds between sand-bodies (Fisher, 1936; Kirschbaum & Hettinger, 2004; Shiers et al., 2014). In this thesis, a threefold subdivision of Neslen Formation based on differences in facies associations related to stratigraphic architecture rather than lithological variations is used: Lower Neslen Interval, Middle Neslen Interval, and Upper Neslen Interval (Fig. 2.7). Lower Neslen Interval and the lowermost part of the Middle Neslen Interval passes into the Corcoran Member eastwards. In contrast, the upper part of the Middle Neslen Interval and Upper Neslen Interval passes into Cozzette Member eastwards. This thesis uses this threefold subdivision (Fig. 2.7), and a more detailed explanation of the intervals follows.

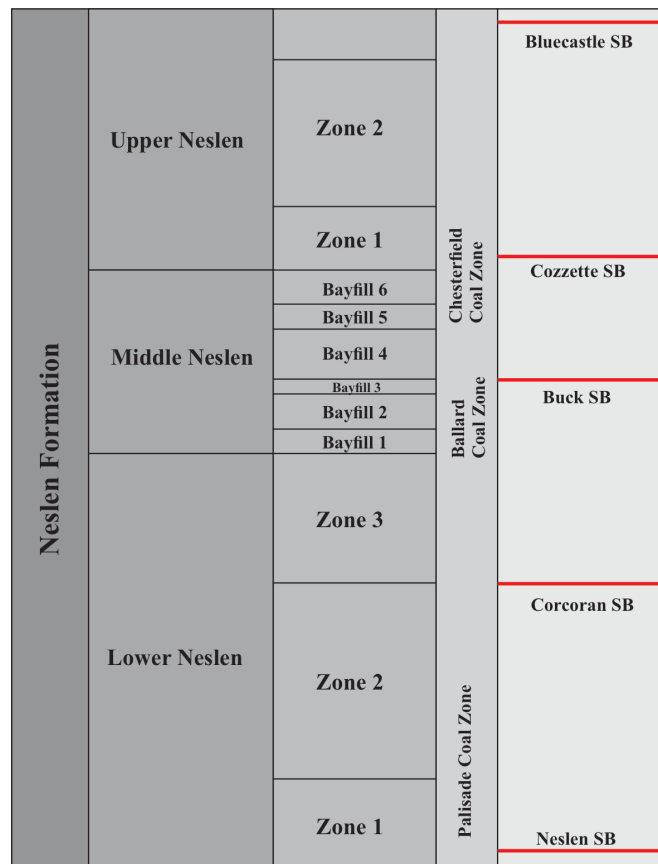


Figure 2.7: Stratigraphy of the Neslen Formation, with the subdivision into Lower-, Middle-, and Upper Neslen Interval by Kjærefjord et al. (2021, Accepted). Red lines represent the sequence boundaries interpreted by Kirschbaum & Hettinger (2004). Figure modified from Kjærefjord et al. (2021, Accepted).

Lower Neslen Interval

The Lower Neslen Interval (Fig. 2.7) is composed of coastal plain deposits, comprising fluvial channels, floodplain fines, crevasses, and coals (Kjærefjord et al., 2021, Accepted). The interval is subdivided into three zones (Zone 1 - 3) based on fluvial channel style. Zones 1 and 3 have a higher sand content than Zone 2, probably due to less generation of accommodation and following channel amalgamation (Kjærefjord et al., 2018).

Zone 1 is characterized by a high proportion of multistorey fluvial channel bodies with low tidal influence (Kjærefjord et al., 2018). The high proportion of fluvial channel facies association suggests a relatively low rate of generation of accommodation during deposition (Kjærefjord et al., 2018). The Neslen SB is a major erosional surface, mapped across several locations (e.g., Van Wagoner, 1992; Kirschbaum & Hettinger, 2004). The position of the Neslen SB varies, but Kjærefjord et al. (2018) place it within Zone 1 (Fig. 2.7). The surface cuts through different strata but is typically characterized by floodplain fines or tidally influenced deposits that overlie either shoreface, offshore transition, or offshore deposits (Kirschbaum & Hettinger, 2004). In the study area (Fig. 1.1), Kjærefjord et al. (2018) describe fluvial channel-fill followed by tidally influenced deposits and floodplain fines above the erosional cut. The erosional cut is interpreted to have formed during falling relative sea-level, and the following fluvial channel-fill is interpreted as deposited during a lowstand systems tract. The overlying tidally influenced deposits are associated with a marine flooding during a transgressive systems tract, resulting in an estuarine depositional setting (Kirschbaum & Hettinger, 2004; Kjærefjord et al., 2018).

Progradational coastal plain units overlie the Zone 1 deposits. Zone 2 mainly comprises floodplain deposits with thick coal beds and some bayfill deposits (Kjærefjord et al., 2018). Channel-fill deposits are rarely observed. The lower sand content in Zone 2 is consistent with a higher rate of generation of accommodation. These deposits are associated with the highstand systems tract (Kirschbaum & Hettinger, 2004). Zone 2 has an upper boundary that may be related to the Corcoran SB (Fig. 2.7) (Kjærefjord et al., 2021, Accepted).

Zone 3 is characterized by meandering, amalgamated fluvial channel-fill deposits, and marginal-marine, estuarine deposits, with the Corcoran SB as its lower boundary (Fig. 2.7) and a flooding surface as its upper boundary (Kjærefjord et al., 2018). An incision is observed in the lower part, associated with the Corcoran SB and a falling relative sea-level. The incised valley is filled with fluvial deposits capped by heterolithic bedding caused by tidal influence,

interpreted as deposits of lowstand- and transgressive systems tracts (Kirschbaum & Hettinger, 2004). The flooding surface marks the upper boundary of the Lower Neslen Interval.

Middle Neslen Interval

The Middle Neslen Interval (Fig. 2.7), located on top of the flooding surface, is interpreted as a part of the highstand or transgressive systems tract (Kirschbaum & Hettinger, 2004; Kjærefjord et al., 2018). In the study area, this interval comprises six vertically stacked bayfill units (Bayfill #1 - #6 units, from the base upwards) (Fig. 2.7), separated by short-lived allogenic flooding surfaces (Kjærefjord et al., 2018). The sedimentary succession is dominated by tabular, upward-coarsening marginal-marine interdistributary bays deposits, representing a landward shift in facies from the Lower Neslen Interval. Fining upwards distributary channel-fill deposits are found along the bay margins (Kjærefjord et al., 2018). East of the study area, wave-dominated shoreface deposits are observed, located at the seaward side of barrier islands or as linear coastlines (Kirschbaum & Hettinger, 2004).

The incisive Buck SB of Kirschbaum & Hettinger (2004) is positioned on top of Bayfill #3 unit (Fig. 2.7) and affects underlying units to varying degrees, depending on location. The erosional cut creates an incision into underlying bayfill deposits, and the incised valley is filled with estuarine tidal channel, -bar, and -flat deposits. These deposits are overlain bayfill deposits, suggesting an overall rise in relative sea-level (Kjærefjord et al., 2021, Accepted).

Upper Neslen Interval

The Upper Neslen Interval (Fig. 2.7) comprises coastal plain deposits. Zone 1 is characterized by multistorey, amalgamated channels from a period of low accommodation (Kjærefjord et al., 2021, Accepted). These channels are associated with the Cozzette SB (Kirschbaum & Hettinger, 2004), a non-incisive sequence boundary. The channel-fill consists of point bars, possibly modulated by tidal processes (Kjærefjord et al., 2021, Accepted).

Zone 2 consists of coaly floodplain fines with dispersed channel-fill deposits related to a period of higher rate of generation of accommodation. According to Kjærefjord et al. (2021, Accepted), varying thickness of Zone 2 suggests variability in sand- and coal content, as well as a changing degree of erosion by the overlying Bluecastle SB (Kirschbaum & Hettinger, 2004).

2.2.6 Farrer Formation

The Farrer Formation was described by Fisher (1936) for its exposure in Coal Canyon, Utah. In the study area, the Farrer Formation overlies the Neslen Formation and is overlain by the Tuscher Formation (Fig. 2.5). Farther west, it overlies the Bluecastle Tongue of the Castlegate Sandstone. It passes into the Price River Formation landwards (westwards) and to the sand-poor Williams Fork Formation basinwards (eastwards) (Fig. 2.5) (Kirschbaum & Hettinger, 2004; Shiers et al., 2014). The deposits comprise massive sandstones and shales with locally, thin coal lenses. Sandstones exhibit cross-stratification (Fisher, 1936), and fluvial channels and floodplains of meandering fluvial systems are suggested as depositional environments (Lawton, 1986).

2.2.7 Tuscher Formation

The Tuscher Formation was named by Fisher (1936) and overlies the Farrer Formation in the study area (Fisher et al., 1960; Lawton, 1986) (Fig. 2.5). Compared to the underlying Farrer Formation, it is composed of thicker and lighter-colored sandstones separated by thin shale beds (Hettinger & Kirschbaum, 2002). The formation passes into the Williams Fork Formation basinwards (eastwards) (Fig. 2.5). Lawton (1986) interpreted the Tuscher Formation to have been deposited within a fluvial system of meandering and braided rivers.

3 Database and methodology

3.1 Database

This study is based on the following data:

- Sedimentological descriptions of the Neslen Formation at 19 locations (Appendix III).
- Outcrop photos shot by the author.
- Published papers.

The sedimentary logging was carried out in Utah in August - September 2019. 19 locations were visited along the Book Cliffs in eastern Utah (Fig. 1.2). Logging took place in five canyons, with <100 m distance between the logs within the areas (Fig. 1.2). The thickness of the logged sections varies from 8 m to 29 m, depending on the outcrop's availability and how much of the Lower Neslen Interval is accessible and included. In some areas, the Bayfill #1 unit is missing or covered, resulting in shorter logs. The total thickness of the logged sections is 319 m, where 195 m are logged at a 1:20 scale and 124 m at a 1:200 scale.




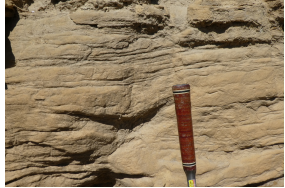

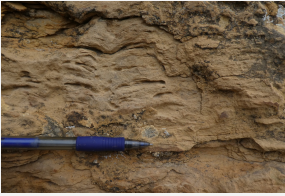

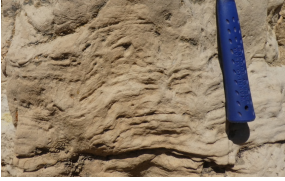
3.2 Fieldwork and methods

The following equipment was used during the fieldwork:

- Logging paper (millimeter paper) was used for precise logging and to obtain a clear and tidy log with necessary information.
- A hand lens, together with a grain-size card, was used to define the grain-size.
- A geological hammer was used to break rock samples for the examination of grain-size and sedimentary structures.
- A mattock/shovel was used for digging and removing debris material in front of the outcrops.
- Coordinates for the locations were obtained by using a GPS.

The sedimentary logging involved descriptions of lithology, grain-size distribution, bed thickness, bed contacts, degree of bioturbation, and sedimentary structures. The Bayfill units #1 - #3 in the Middle Neslen Interval were logged at 1:20 scale to obtain all small-scale variations. Underlying strata in Lower Neslen Interval were logged at 1:200 scale due to less vertical variability. Lithology was subdivided into five categories: mudstone, sandy mudstone, muddy sandstone, sandstone, and coal. The degree of bioturbation ranges from 0 - 3, and the definition of bioturbation degrees is shown in Table 3.1.

Table 3.1: Definition of the bioturbation degrees used in the sedimentary descriptions.

Bioturbation degree	Symbol in logs	Description	Photo
0 - none		Bioturbation absent	
1 - low		Sparse bioturbation with few discrete traces	
2 - moderate		Moderate bioturbation, primary structures are visible but disturbed	
3 - high		Complete bioturbation, primary structures almost completely disturbed	

Based on the mentioned definitions, eleven lithofacies were established (described in Chapter 4). Lithofacies, combined with the larger-scale architecture of the outcrops, were the basis for defining the facies associations (described in Chapter 5).

After returning from fieldwork, all logs were redrawn and digitized at the University of Bergen, using CoreIDRAW (vector graphics editor). Lithofacies thicknesses were retrieved from CoreIDRAW by using a measuring tool after customizing the page size to the scale. All the lithofacies thicknesses were transferred into an Excel spreadsheet for further calculations.

To get panoramic images of the outcrops (Appendix III), several photos with much overlap were taken in the field. The photos are merged in Adobe Photoshop for further use in correlation panels in Chapter 6. Workflow in Figure 3.1 illustrates how merging of photos is performed.

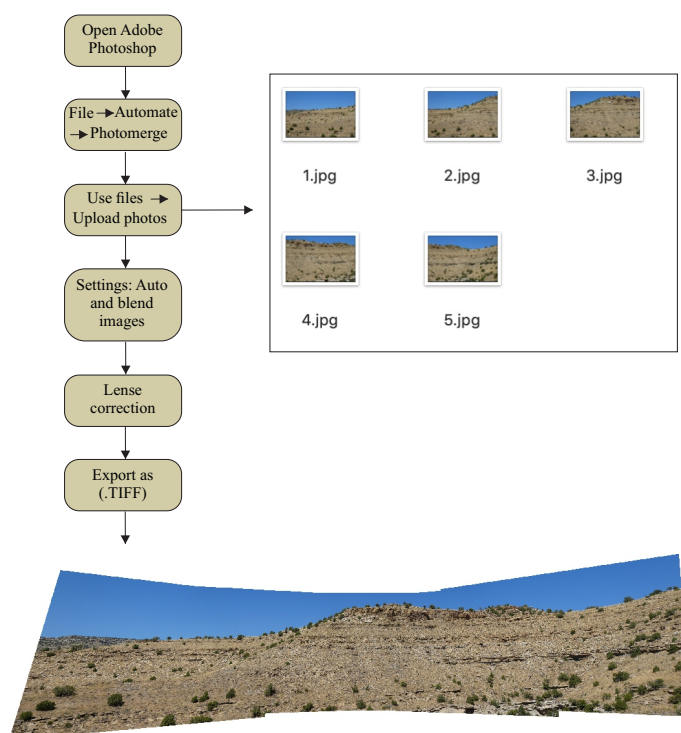


Figure 3.1: Workflow used when merging the photos in Adobe Photoshop to obtain images of the outcrops as a whole.

3.3 Uncertainties and sources of error

Addressing the sedimentary logs and following correlations, it is important to consider the sources of error. Uncertainties related to logging, interpreting, digitizing, and correlation must be taken into consideration.

First of all, there are uncertainties related to logging. In some intervals, it can be challenging to determine which sedimentary structure is present. Covered areas also are sources of errors both regarding measuring of sloped areas, descriptions and interpretations of lithofacies and facies associations, and lateral correlations over several covered meters. Availability and steepness of slopes made it challenging to log perfectly vertical sections. Thus, smaller lateral shifts occur upwards in the logs. A consequential source of error could be found in the facies associations interpretation, as it is based on the lithofacies' thicknesses.

The merging of outcrop photos in Adobe Photoshop may have led to small errors in the outputs. The photos can, to some extent, be slightly angled or elevated in relation to each other, which may cause smaller distortions. However, as these merged photos cover up to several hundred meters, the distortions pose little uncertainty, which is most likely insignificant in this study.

It is also worth mentioning the uncertainty related to the lateral correlation of logged sections. Every meter between the logs could not be walked out in every area due to availability. This means that there are uncertainties in linking logged sections and the correlation of lithofacies along the outcrops. Photos and the dipping direction of possible inclined layers are used to obtain information in these areas.

4 Lithofacies description

Eleven different lithofacies and sub-facies are identified within the lower delta plain deposits in the study area (Fig. 1.1). The following chapter presents a description and interpretation of the lithofacies. The Lithofacies 1 includes those with sandstone lithology, Lithofacies 2 has a heterolithic lithology, while mudstone lithology comprises Lithofacies 3. Lithofacies 1 is further subdivided into 1A, 1B, 1C, and 1D, the Lithofacies 2 into 2A, 2A-C, and 2B, and the Lithofacies 3 is subdivided into 3A and 3B. Table 4.1 presents the lithofacies and their main characteristics, and a more detailed description and interpretation follows.

Table 4.1: Overview of lithofacies identified in the study area.

Lithology	Lithofacies	Sub-facies	Grain-size	Thickness	Bioturbation (0 - 1 - 2 - 3)	Photos	Log
Sandstone	1A Cross-stratified sandstone		Very fine upper - medium lower sandstone	20 cm - 840 cm	0	Figure 4.2	Figure 4.1
	1B Sandstone with wave-ripple cross-lamination or hummocky cross-stratification	1B#1 Sandstone with hummocky cross-stratification	Very fine lower - fine lower sandstone	4 cm - 160 cm	0 - 2	Figure 4.3	Figure 4.4
		1B#2 Sandstone with wave-ripple cross-lamination	Very fine lower - fine lower sandstone	2 - 50 cm	0 - 3	Figure 4.6	Figure 4.5
	1C Bioturbated sandstone >degree 2		Very fine lower - fine lower sandstone	22 cm - 90 cm	3	Figure 4.7	Figure 4.8
	1D Current-ripple cross-laminated sandstone		Very fine lower - fine lower sandstone	2 cm - 420 cm	0 - 2	Figure 4.9	Figure 4.10
Heterolith	2A Wave-ripple cross-laminated wavy bedded heterolith		Mudstone and very fine lower - very fine upper sandstone	2 cm - 112 cm	0 - 2	Figure 4.11	Figure 4.12
	2A-C Current-ripple cross-laminated wavy bedded heterolith		Mudstone and very fine lower - very fine upper sandstone	2 cm - 378 cm	0 - 2	Figure 4.13	Figure 4.1
	2B Current- or wave-rippled, wavy-to lenticular bedded heterolith		Mudstone and very fine lower - very fine upper sandstone	2 cm - 460 cm	0 - 2	Figure 4.15	Figure 4.14
Mudstone	3A Horizontal laminated to lenticular bedded mudstone		Mudstone	2 cm - 496 cm	0 - 1	Figure 4.17	Figure 4.16
	3B Rooted and organic-rich mudstone		Mudstone	4 cm - 218 cm	0 - 1	Figure 4.19	Figure 4.18
Coal	Coal			14 cm - 90 cm	0	Figure 4.20	Figure 4.18

4.1 Lithofacies 1A: Cross-stratified sandstone

Description

Lithofacies 1A consists of non-graded, very fine-grained to medium-grained sandstone with planar and tangential cross-stratification (Fig. 4.2). Cross-stratified sandstone is present in Lower Neslen Interval. The thickness of Lithofacies 1A ranges from 20 cm to 840 cm, and based on 15 observations (n=15), the mean thickness is ~120 cm. Within Lithofacies 1A, the sets of cross-stratification are 10 - 40 cm thick, and the number of sets extends from one to several tens. Typical for Lithofacies 1A is an erosive base (Fig. 4.2C), marking a transition into underlying layers. The significance of the erosive bases varies from no relief to tens of centimeters of relief. Generally, bioturbation is absent (degree 0). Lithofacies 1A often occur with current-ripple cross-lamination (Lithofacies 1D) on top, or commonly in alternation with heterolithic wave- or current-ripple cross-lamination (Lithofacies 2A and 2A-C) (Figs. 4.1 and 4.2A, B). Mud drapes occur along the foreset surfaces and at the base of the sets (Fig. 4.2A, B).

Interpretation

Planar cross-stratification indicates migration of 2D dunes (Ashley, 1990) and represents tractional deposition. Dunes can occur in various environments, and the association of lithofacies is needed for further interpretation (Bhattacharya & Walker, 1991). Planar cross-stratification reflects deposition in the lower flow regime of a unidirectional current. Erosive bases suggest deposition from tractive, turbulent currents. The presence of mud drapes associated along foreset surfaces or as bottomsets reflects a flow with fluctuating energy. Mud drapes are deposited in slack-water periods with current speeds close to zero, possibly caused by tidal reversals. Wave-ripple cross-lamination is indicative of oscillatory currents. Heterolithic wave-ripple cross-lamination and mud drapes along the foreset surfaces may be evidences of proximity to a marine environment influenced by tides.

Log H, Exit Canyon

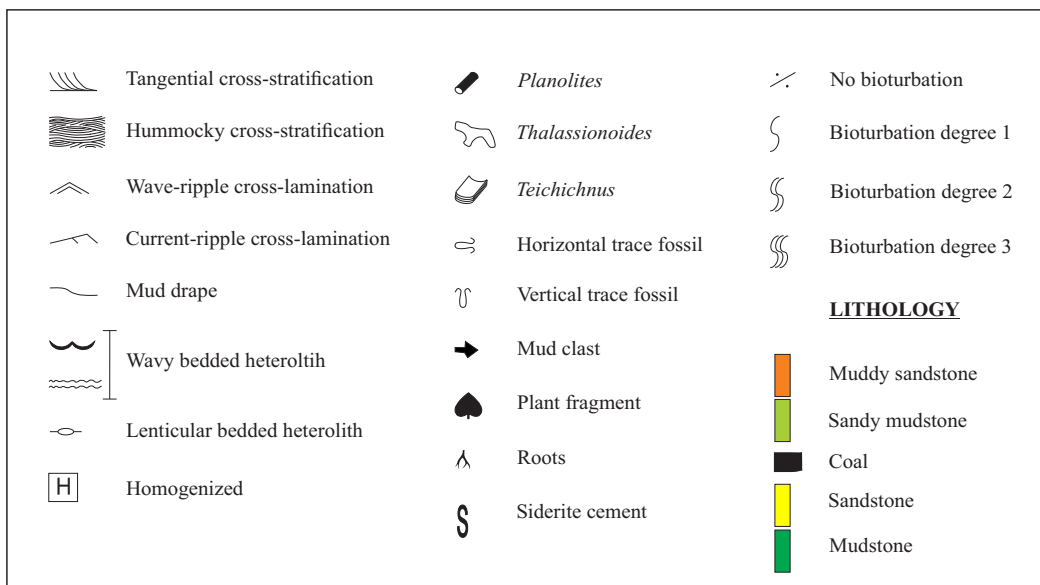
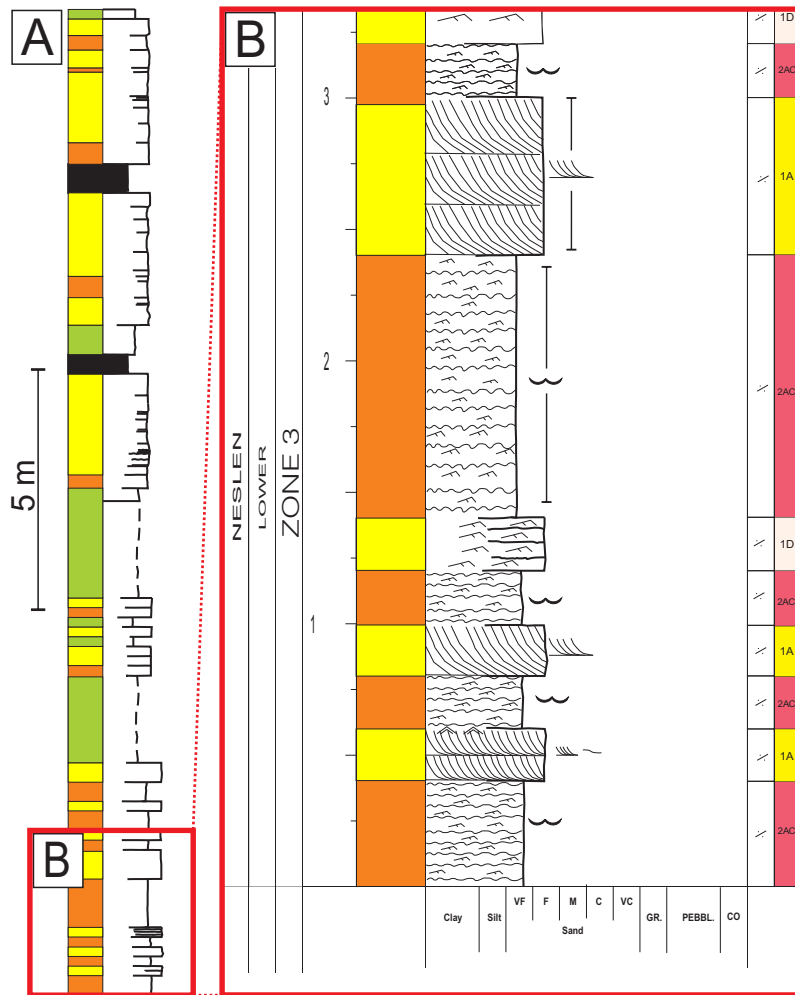


Figure 4.1: A: Sedimentary log from Exit Canyon, log H (Fig. 1.2). B: Excerpt from the lowermost 3 m showing Lithofacies 1A in alternation with current-ripple cross-laminated wavy bedded heterolith (Lithofacies 2A-C) and current-ripple cross-laminated sandstone (Lithofacies 1D). The legend is valid for all the lithofacies and facies association descriptions.

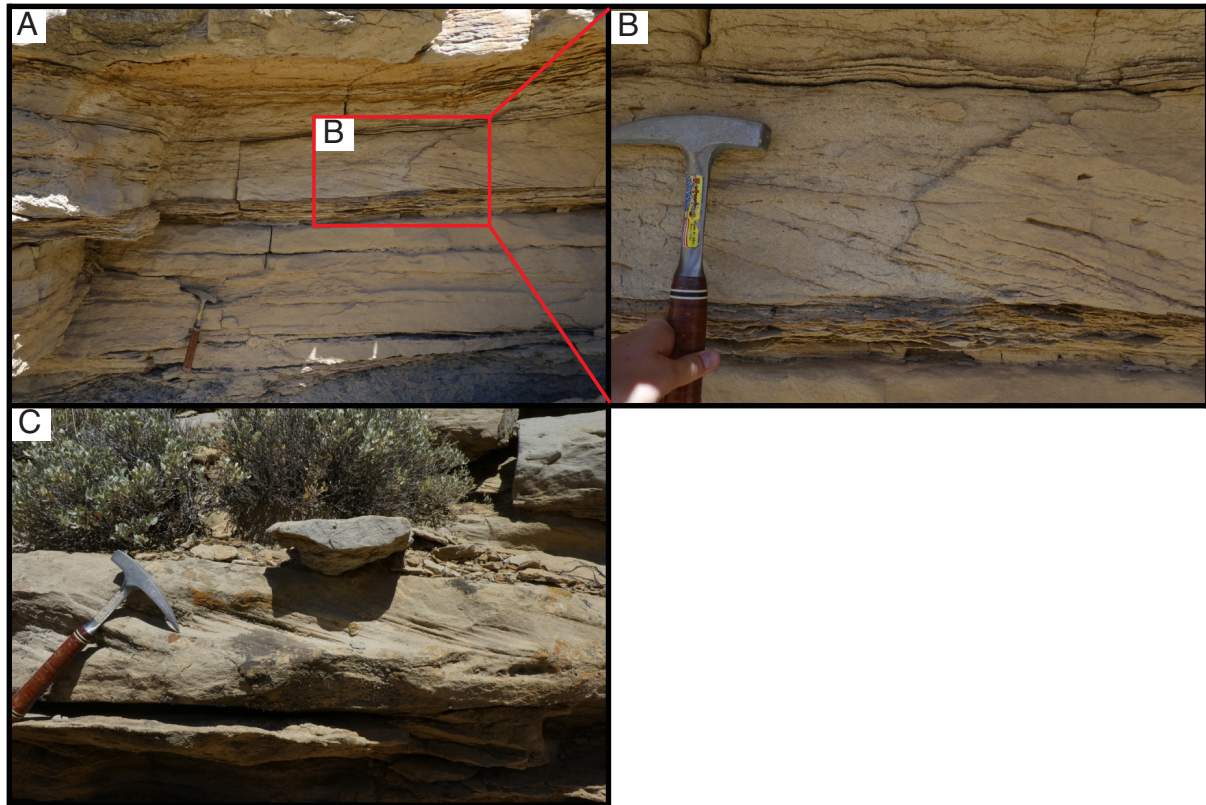


Figure 4.2: Photos of Lithofacies 1A. A: Alternating cross-stratified sandstone and heteroliths in Lower Neslen Interval, Exit Canyon, log H (Fig. 1.2). B: Close-up photo showing current-ripple cross-laminated wavy bedded heterolith (Lithofacies 2A-C) in the lowermost part followed by tangential cross-stratified sandstone with mud drapes (Lithofacies 1A). The uppermost part shows a 1 cm layer of wave-ripple cross-laminated wavy bedded heterolith (Lithofacies 2A) capped by current-ripple cross-laminated wavy bedded heterolith (Lithofacies 2A-C). C: Sandstone with tangential cross-stratification (Lithofacies 1A) with an erosive base in Lower Neslen Interval, Exit Canyon, log H (Fig. 1.2).

4.2 Lithofacies 1B: Sandstone with wave-ripple cross-lamination and sandstone with hummocky cross-stratification

Lithofacies 1B is composed of Sub-facies 1B1 and 1B2, including sandstone with wave-ripple cross-lamination and sandstone with hummocky cross-stratification. Volumetrically, Lithofacies 1B is an essential lithofacies in the study area.

4.2.1 Sub-facies 1B1: Sandstone with hummocky cross-stratification

Description

Hummocky cross-stratified (HCS) and swaley cross-stratified (SCS) sandstone, primarily small-scale, make up the Sub-facies 1B1 (Fig. 4.3). Internal stratification shows both a convex-up (hummocks) trend and a concave-up (swales) trend, with slightly inclined strata. Sub-facies 1B1 is present in the Middle Neslen Interval. The degree of bioturbation extends from none to moderate (degree 0 - 2) (Fig. 4.3), and the grain-size ranges from very fine-grained to fine-grained sandstone. *Skolithos* is the most common trace fossil. In Exit Canyon (Fig. 1.2), *Bergaueria* resting trace is observed within a few intervals. The thickness of Sub-facies 1B1

ranges from 4 cm to 160 cm, with a mean thickness of 25 cm (n=130). Within Sub-facies 1B1, the thickness of the cross-stratified sets rarely exceeds 30 cm. Hummocks wavelengths are up to 3 m, but small-scale hummocks with a wavelength of 30 - 100 cm dominate. In some intervals, Sub-facies 1B1 contains mud clasts and plant fragments. Mudstone- and heterolithic lithofacies are commonly interbedded with Sub-facies 1B1. Wave-ripple cross-laminated sandstone (Sub-facies 1B2) and current-ripple cross-laminated sandstone (Lithofacies 1D) are also present together with Sub-facies 1B1 (Fig. 4.4). In the case of alternation between Sub-facies 1B1 and 1B2, the HCS sandstone often has a wave-reworked top.

Interpretation

The deposition of HCS and SCS sandstone results from a combined flow, including an intense and complex wave activity (Collinson et al., 2006). HCS sandstone deposition indicates a strong oscillatory component and a weaker unidirectional component (Southward et al., 1990; Dumas et al., 2005; Dumas & Arnott, 2006), a condition which is typical at the seabed during storms. The deposition also depends on sufficient sediment aggradation rates to preserve the bedforms. SCS sandstone deposition indicates a more energetic unidirectional component and increased orbital velocity than HCS sandstone, creating an erosive basal surface. Sandstone with HCS and SCS is deposited below fair-weather wave-base and above storm-weather wave-base (Collinson et al., 2006). The reason for variability in hummock's wavelength is not widely appreciated, but it is suggested to be related to the wave orbital diameter, affected by the water depth (Yang et al., 2006). Shorter hummock wavelengths indicate shallower water in a more landward position. None to a moderate degree of bioturbation suggests deposition in an environment with significant energy. Presence of *Bergaueria* may indicate deposition in shallow water (Crimes & Anderson, 1985; Benyoucef et al., 2017) or wave-dominated prograding deltas (Bhatt & Patel, 2017). Mudstone- and heterolithic lithofacies suggest calmer periods with less energy. Sub-facies 1B1 interbedded with wave-ripple cross-lamination (Sub-facies 1B2) reflects fluctuations between a combined flow and an oscillatory flow. The alternation between Sub-facies 1B1 and current-ripple cross-laminated sandstone (Lithofacies 1D) indicates a change from a combined flow (1B1) to a unidirectional flow (1D). In cases where the HCS sandstone has a wave-reworked top, the oscillatory flow is dominant.

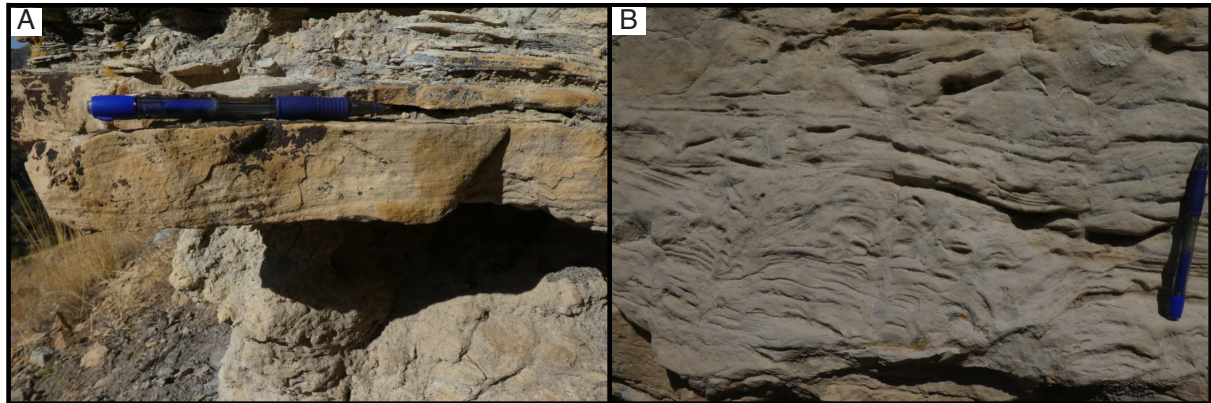


Figure 4.3: Photos of Lithofacies 1B1. A: Sandstone with HCS with a short wavelength in Middle Neslen Interval, Exit Canyon, log G (Fig. 1.2). B: Bioturbated sandstone with HCS in Middle Neslen Interval, Neslen Canyon, log S (Fig. 1.2).

Log G, Exit Canyon

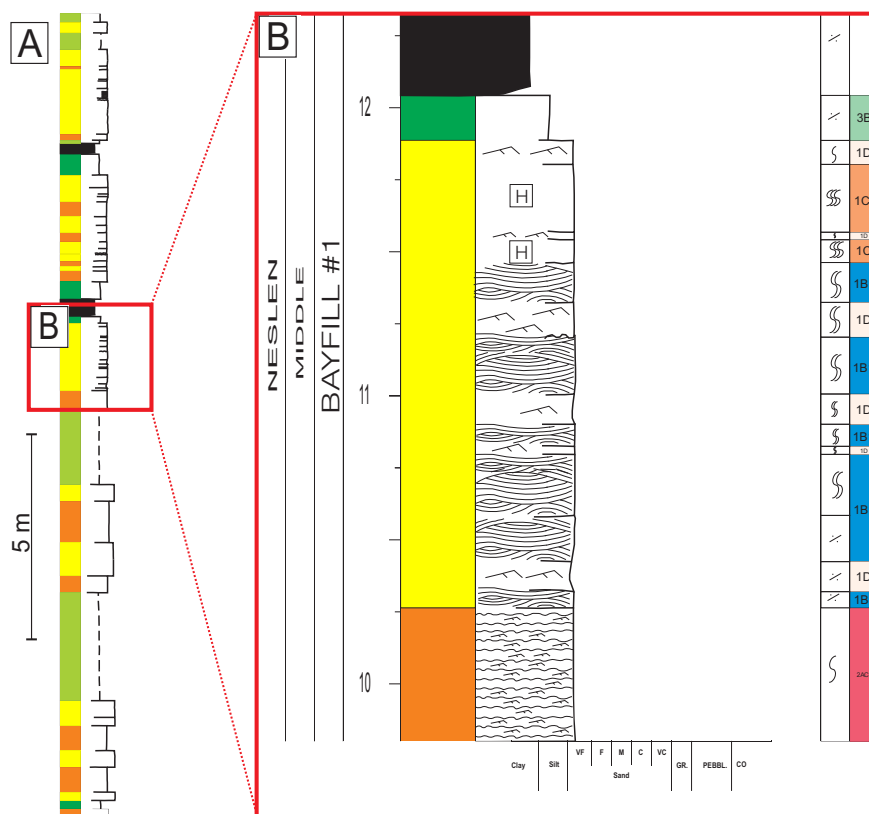


Figure 4.4: A: Sedimentary log from Exit Canyon, log G (Fig. 1.2). B: Excerpt from Bayfill #1 unit showing Sub-facies 1B1 in alternation with current-ripple cross-laminated sandstone (Lithofacies 1D). The degree of bioturbation increases upwards, and Sub-facies 1B1 is capped by bioturbated sandstone >degree 2.

4.2.2 Sub-facies 1B2: Sandstone with wave-ripple cross-lamination

Description

Sub-facies 1B2 consists of wave-ripple cross-laminated sandstone and is present in the Middle Neslen Interval. The thickness of Sub-facies 1B2 ranges from 2 - 50 cm, and the mean thickness is ~11 cm (n=64). Individual ripples have a height of 1 - 5 cm and are often observed in sets of

two or more ripples stacked vertically. The grain-size ranges from very fine-grained to fine-grained sandstone, and the degree of bioturbation varies from none to high (degree 0 - 3). A wave reworked cross-set top appears in several intervals. Mud clasts are present within Sub-facies 1B2 at some localities (Fig. 4.6A). Sub-facies 1B2 is commonly interbedded with Sub-facies 1B1 (Figs. 4.5 and 4.6B) and occasionally with current-ripple cross-laminated sandstone (Lithofacies 1D).

Interpretation

In general, ripples form by water movement over a sand substratum. Four main factors control the size, spacing, and symmetry of wave-ripples: maximum wave-orbital velocity at the bed, asymmetry of orbital velocities, mean grain-size, and wave period (Collinson et al., 2006). Internal lamination indicates whether the current's strength has been equally strong in both directions. A current with a forward motion stronger than backward motion often results in internal lamination showing through-cross-lamination. Therefore, some wave-ripples are result of a combined flow.

Log A, Outer East Canyon

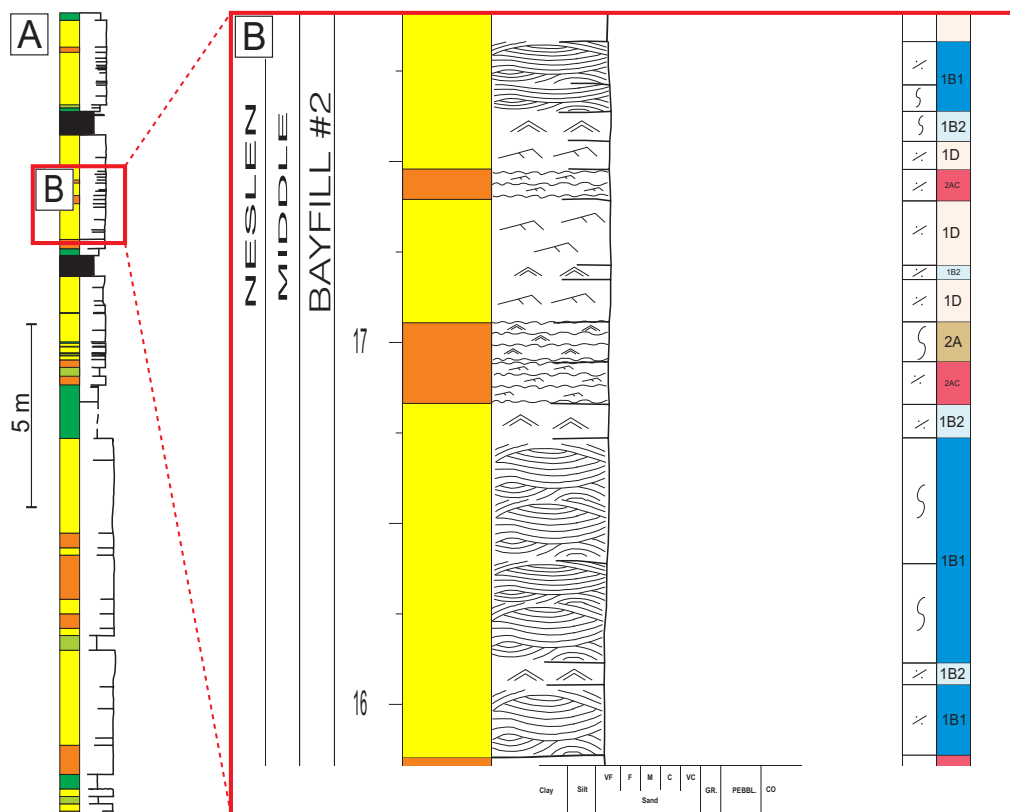


Figure 4.5: A: Sedimentary log from Outer East Canyon, log A (Fig. 1.2). B: Excerpt from Bayfill #2 unit showing Sub-facies 1B2 in alternation with hummocky cross-stratified sandstone (Sub-facies 1B1) and current-ripple cross-lamination (Lithofacies 1D).

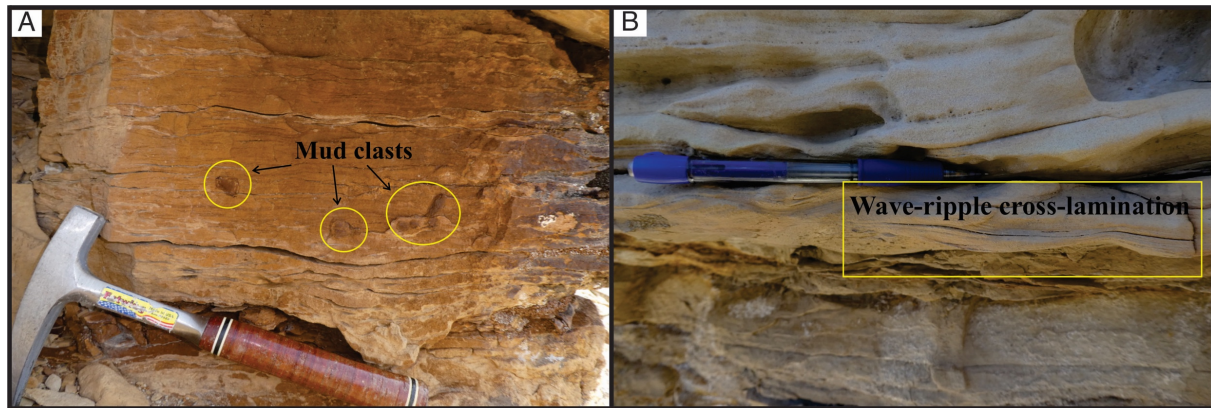


Figure 4.6: Photos of Lithofacies 1B2. A: Sandstone with wave-ripple cross-lamination and mud clasts in Middle Neslen Interval, Exit Canyon, log E (Fig. 1.2). B: Sandstone with wave-ripple cross-lamination in the middle part of the photo followed by HCS sandstone (Sub-facies 1B1) in the upper part. Middle Neslen Interval, Exit Canyon, log F (Fig. 1.2).

4.3 Lithofacies 1C: Bioturbated sandstone >degree 2

Description

Lithofacies 1C consists of very fine-grained to fine-grained sandstone with a high degree of bioturbation (degree 3) (Fig. 4.7). In most cases, Lithofacies 1C is completely bioturbated, and primary sedimentary structures are mostly destroyed. Organic matter is common in Lithofacies 1C. Within some intervals, hummocky cross-stratification show tendencies of strong bioturbation. Lithofacies 1C is represented with lithofacies thicknesses of 22 - 90 cm, with a mean thickness of 36 cm (n=15). The heavily bioturbated sandstone is present in Neslen Canyon, Outer East Canyon, and Exit Canyon (Figs. 1.1 and 1.2), commonly in the upper parts of the bayfill units. Above and below Lithofacies 1C, both heterolithic lithology and sandstones are common. Lithofacies 1C is under- or overlain by coals in some localities. Both deposits generated by marine and non-marine processes border Lithofacies 1C. Trace fossils are dominated by *Planolites* and *Thalassinoides* (Figs. 4.7 and 4.8). *Planolites* is a horizontal, tunnel-shaped trace fossil, and *Thalassinoides* has an irregular network of tunnels mainly observed on or underneath bedding planes.

Interpretation

Sedimentary structures, together with trace fossils, can provide important information. Trace fossils record in situ life and behavior, unlike many body fossils. They represent events during or shortly after deposition of the sediments (Collinson et al., 2006). The high amount of bioturbation and organic matter within Lithofacies 1C suggests deposition in an environment with relatively low energy and a low sedimentation rate (Kjærefjord, 1999). *Planolites* reflects sandy-silty lagoon/shelf-sea conditions below fair-weather wave-base. The horizontal traces indicate low energy. *Thalassinoides* is characteristic of marine origin and indicates deposition

in marine-to-brackish water (Tonkin, 2012). Storm waves are likely to affect the deposits due to the presence of hummocky cross-stratification.

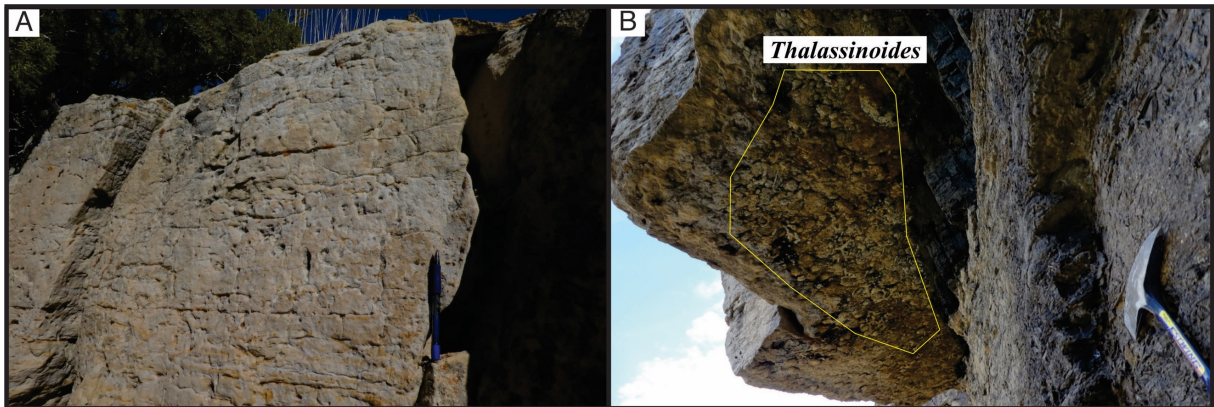


Figure 4.7: Photos of Lithofacies 1C. A: Strongly bioturbated sandstone with roots in Middle Neslen Interval, Exit Canyon, log J (Fig. 1.2). B: Sandstone with *Thalassinoides* at the base in Middle Neslen Interval, Neslen Canyon, log S (Fig. 1.2).

Log S, Neslen Canyon

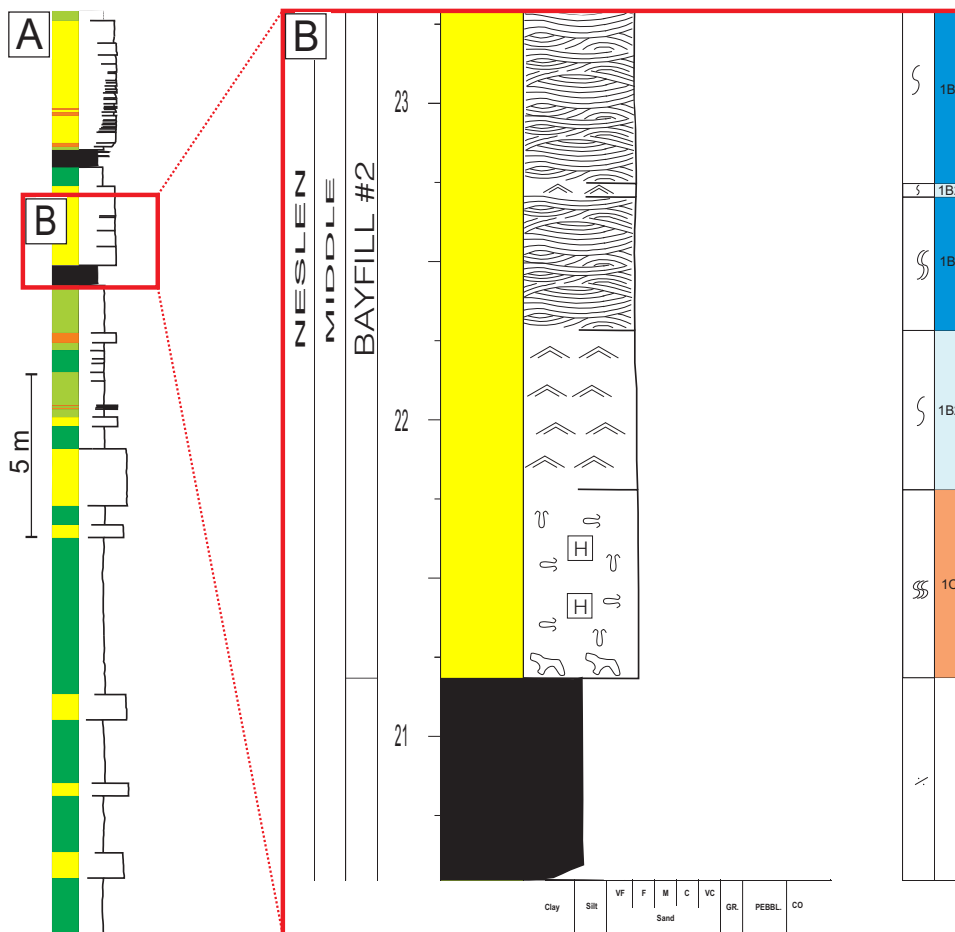


Figure 4.8: A: Sedimentary log from Neslen Canyon, log S (Fig. 1.2). B: Excerpt from Bayfill #1 and #2 units. Lithofacies 1C has *Thalassinoides* at the base, and there are traces of burrows in the interval. Lithofacies 1C is mostly homogenized by bioturbation.

4.4 Lithofacies 1D: Current-ripple cross-laminated sandstone

Description

Lithofacies 1D consists of current-ripple cross-laminated sandstone and is present in Lower Neslen Interval and Middle Neslen Interval at most locations. An erosive base is observed in some logs (Fig. 4.9A). By volume and quantity, Lithofacies 1D is most common in the study area, with an average thickness of 35 cm (n=269). The thickness ranges from 2 cm to 420 cm. Lithofacies 1D is represented by very fine-grained to fine-grained sandstone. Individual sets of ripples have a thickness of <1 - 4 cm. Plant fragments and mud clasts are present (Fig. 4.10), and wave reworking of the top is common. The degree of bioturbation is generally low, rarely exceeding moderate (degree 1 - 2). The visibility of the internal lamination varies, but the crest is commonly preserved. Internal lamination shows inclined laminae dipping in one direction. Lithofacies 1D is typically interbedded with Lithofacies 1B and more mudstone-rich deposits.

Interpretation

Internal cross-lamination results from ripple migration and the crest's asymmetry indicates a unidirectional flow (Collinson et al., 2006). The low degree of bioturbation reflects an energetic environment, and plant fragments suggest deposition in an environment relatively close to the coast. According to Collinson et al. (2006), current-ripples are formed both in shallow water and deep water through ocean-bottom currents. Seen in combination with observations such as plant fragments and alternation with Lithofacies 1B, Lithofacies 1D is suggested to be deposited in relatively shallow water with proximity to the coast, by a unidirectional flow.

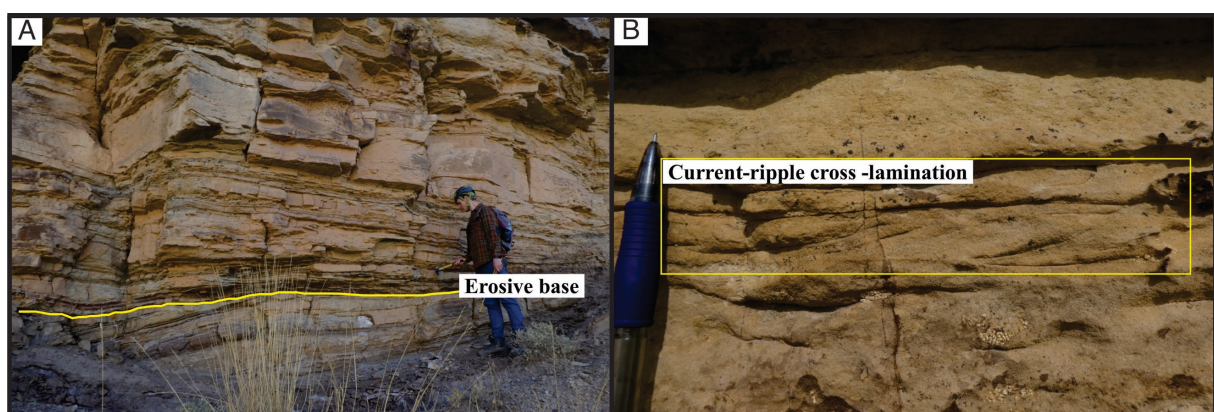


Figure 4.9: Photos of Lithofacies 1D. A: Outcrop showing an erosive base of Lithofacies 1D in Lower Neslen Interval, Outer East Canyon, log A (Fig. 1.2). B: Sandstone with current-ripple cross-lamination in Bayfill #3 unit, Middle Neslen Interval, Exit Canyon, log E (Fig. 1.2).

Log K, Keane Creek

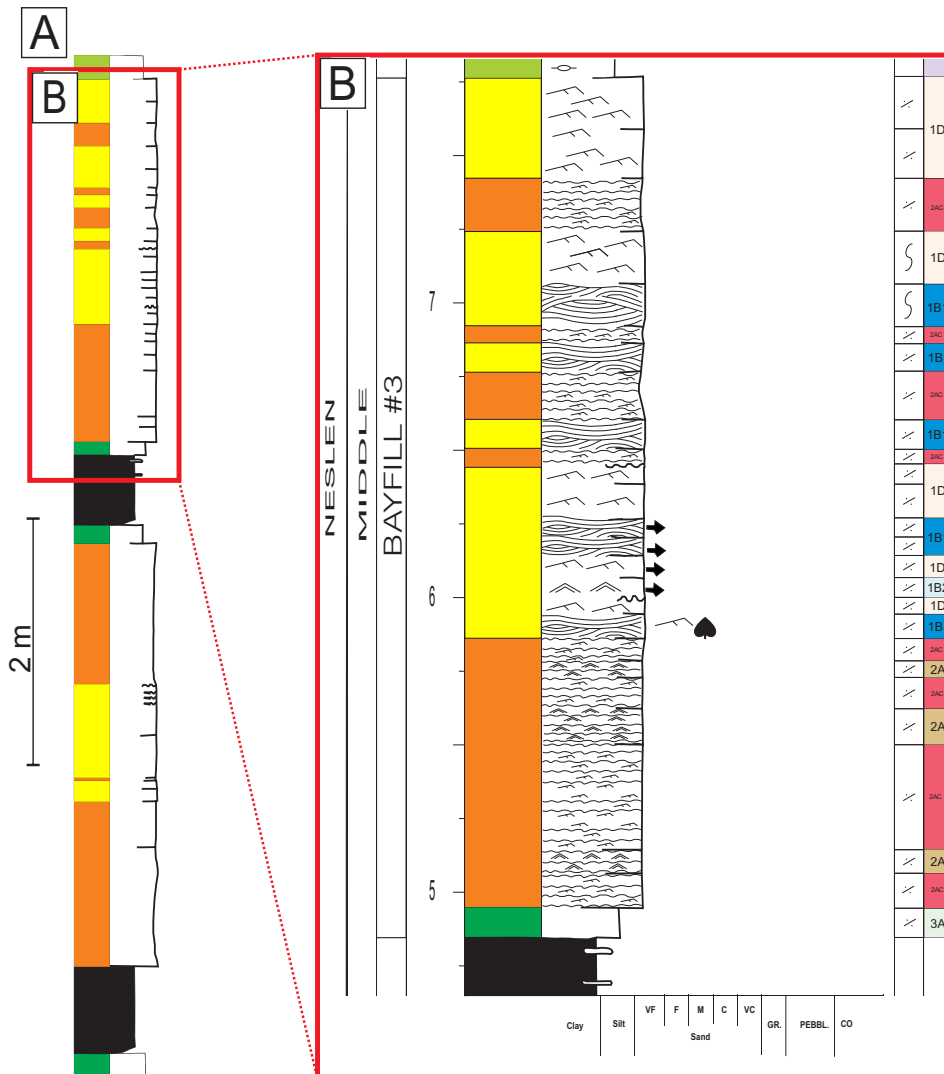


Figure 4.10: A: Sedimentary log from Keane Creek, log K (Fig. 1.2). B: Excerpt from Bayfill #3 unit. Lithofacies 1D is present with mud clasts and in alternation with sandstone and heterolithic lithofacies.

4.5 Lithofacies 2A: Wave-ripple cross-laminated wavy bedded heterolith

Description

Lithofacies 2A is observed in the Middle Neslen Interval within all the studied bayfill units. Lithofacies 2A exhibits interbedding of mixed sandstone and mudstone lithologies. The heterolithic lithology is characterized by wavy bedding due to continuous layers of both sand and mud (Fig. 4.11). The sandstone component consists of very fine-grained sandstone that exhibits wave-ripple cross-lamination. Occasionally, the sandstone component is observed with small-scale hummocky cross-lamination (Fig. 4.11B) or single current-ripple cross-lamination sets. The rippled sandstone component constitutes a larger proportion than the mudstone layers. Lithofacies 2A has an average thickness of 18 cm (n=34) and is represented by lithofacies

thicknesses of 2 - 112 cm. Wood fragments, roots, and millimeter-scale sand-filled syneresis cracks are present within Lithofacies 2A. Degree of bioturbation ranges from none to moderate (degree 0 - 2). Dominant trace fossils are *Planolites* and *Thalassinoides*. *Thalassinoides* is typically visible on the bedding planes (Fig. 4.12). This lithofacies occurs in association with lenticular bedded heteroliths (Lithofacies 2B) and the sandstone Lithofacies 1B and 1D.

Interpretation

Heterolithic bedding indicates fluctuating energy during deposition, where the sandstone represents periods of higher energy. Intervals with mudstone reflect deposition of suspended load between energetic events. Wave-ripple cross-lamination suggests deposition from an oscillatory current, and the preservation of wave-ripple cross-lamination indicates deposition above storm-weather wave-base. Anyway, the existence of wave-ripple cross-lamination suggests deposition below fair-weather wave-base (Bhattacharya & Walker, 1991). Small-scale hummocky cross-lamination reflects periods of increased energy from a combined flow. Syneresis cracks may be an indicator of brackish water with salinity changes (Burst, 1965). Brackish water is a result of periodic freshwater influx due to seasonal variations in river runoff and storm periods (Kjærefjord, 1999). The formation of syneresis cracks is due to loss of pore water from the sediments caused by reorganization of clay particles with high porosity. Reorganization occurs through spontaneous de-flocculation due to salinity-induced differences in the pore water (Pratt, 1998; Collinson et al., 2006). Plummer & Gostin (1981) also suggest that syneresis cracks, combined with a low degree of bioturbation, imply rapid deposition. The alternation between Lithofacies 2A and the lenticular bedded heteroliths (Lithofacies 2B) reflects a change in energy due to a significantly higher mudstone content in Lithofacies 2B. Sandstone Lithofacies 1B and 1D indicate higher energy than the heterolithic Lithofacies 2A, suggesting variations in water depth. The roots, syneresis cracks, the low degree of bioturbation, but with some marine trace fossils, suggest deposition in a marginal-marine, brackish water environment.

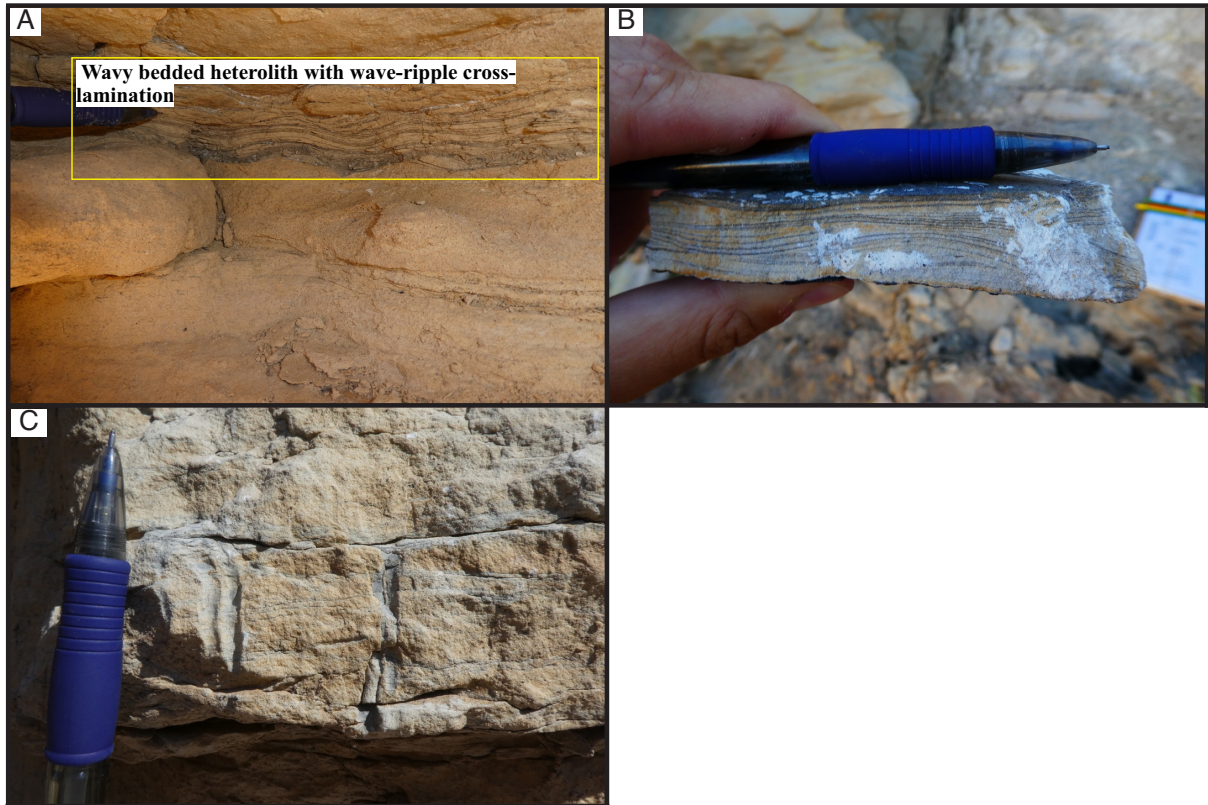


Figure 4.11: Photos of Lithofacies 2A. A: Wavy bedded heterolith with wave-ripple cross-lamination in Bayfill #3 unit, Middle Neslen Interval, Neslen Canyon, log S (Fig. 1.2). B: Wavy bedded heterolith with small-scale hummocky cross-lamination in Bayfill #1 unit, Middle Neslen Interval, Outer East Canyon, log C (Fig. 1.2). C: Wavy bedded heterolith with wave-ripple cross-lamination and bioturbation in Bayfill #2 unit, Middle Neslen Interval, Keane Creek, log M (Fig. 1.2).

Log M, Keane Creek

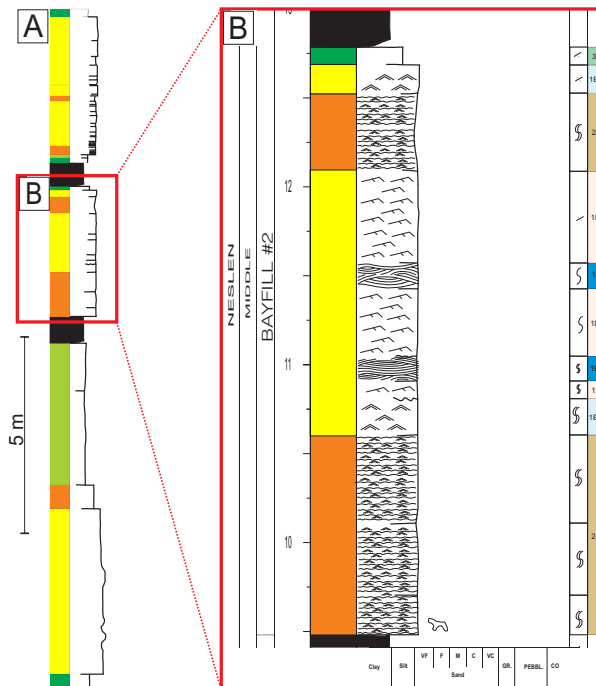


Figure 4.12: A: Sedimentary log from Keane Creek, log M (Fig. 1.2). B: Excerpt from Bayfill #2 unit showing Lithofacies 2A in the log. Lithofacies 2A is present with deposits from other marine processes and deposits from unidirectional currents (Lithofacies 1D). *Thalassinoides* is present at the base of the Lithofacies 2A.

4.6 Lithofacies 2A-C: Current-ripple cross-laminated wavy bedded heterolith

Description

Lithofacies 2A-C is present in the Lower- and Middle Neslen Interval. Lithofacies 2A-C consists of mudstones encasing rippled sandstones. Heterolithic Lithofacies 2A-C exhibits wavy bedding with current-ripple cross-lamination (Fig. 4.13). The mudstone content is lower than the sandstone content. Rippled sand layers have a grain-size of very fine-grained sandstone. The layers are 2 - 378 cm thick, with a mean thickness of 37 cm (n=120). Due to the mudstone component, Lithofacies 2A-C typically form slopes in the landscape. Plant fragments are common, and the degree of bioturbation is generally none to moderate (degree 0 - 2). A few areas have a higher degree of bioturbation where the trace fossil *Thalassinoides* is present on the bedding planes. Lithofacies 2A-C is often interbedded with sandstone Lithofacies 1A and 1D (Fig. 4.1).

Interpretation

The heterolithic bedding reflects fluctuating energy during deposition, where the sandstone component is linked to periods of more energy, and the mudstone component is related to periods of low energy and deposition from suspended load. Current-ripple cross-lamination indicates deposition from a unidirectional current. A high net/gross sand ratio represents dominance of deposition during high-energy periods, possibly augmented by erosion of finer-grained material. Alternation between Lithofacies 2A-C and 1A/1D reflects fluctuations in stream capacity and velocity. The presence of plant fragments suggests deposition in a marine setting close to the shore. The low degree of bioturbation suggests deposition in a stressed environment, either due to an anoxic water column or water salinity fluctuations.

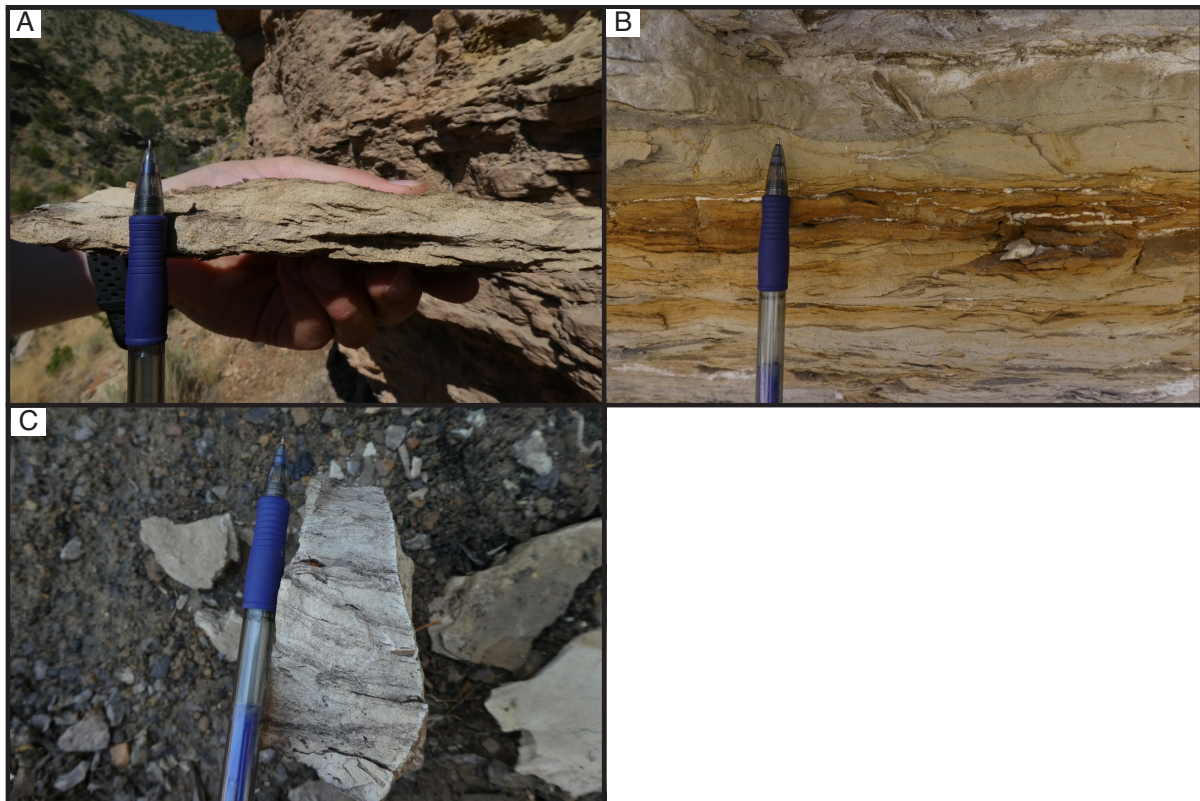


Figure 4.13: Photos of Lithofacies 2A-C, showing a relatively high net/gross sand ratio. A: Wavy bedded heterolith with current-ripple cross-lamination and plant fragments in Bayfill #3 unit, Middle Neslen Interval, Keane Creek, log L (Fig. 1.2). B: Wavy bedded heterolith with current-ripple cross-lamination in Bayfill #3 unit, Middle Neslen Interval, Neslen Canyon, log R (Fig. 1.2). C: Sample with wavy bedded heterolith with current-ripple cross-lamination in Bayfill #2 unit, Middle Neslen Interval, Neslen Canyon, log R (Fig. 1.2).

4.7 Lithofacies 2B: Current- or wave-rippled, wavy- to lenticular bedded heterolith

Description

Lithofacies 2B is present in Lower- and Middle Neslen Interval. The minimum Lithofacies 2B thickness is 2 cm, and the maximum thickness is 460 cm. The mean thickness is 71 cm (n=53). The heterolith exhibits wavy- to lenticular bedding, containing either wave- or current-ripple cross-lamination (Fig. 4.15). Sandstone and mudstone layer thickness varies from a few millimeters to 3 - 4 cm. The sand component consists of very fine-grained sandstone and is present as incoherent, light-colored lenses between the mudstone. Lithofacies 2B has a low net/gross sand ratio, where the mudstone component constitutes >70%. The degree of bioturbation in Lithofacies 2B ranges from absent to moderate (degree 0 - 2). Dominant trace fossils are *Planolites* and *Teichichnus*. In the Lower Neslen Interval, Lithofacies 2B is often observed interbedded with Lithofacies 1D (Fig. 4.14). In the Middle Neslen Interval, the lithofacies is alternated with heterolithic lithofacies (2A and 2A-C) (Fig. 4.15B). Lithofacies 2B often forms slopes in the landscape.

Interpretation

The alternation between mudstone and sandstone lithologies within Lithofacies 2B indicates fluctuating energy during deposition. Sandstone lenses represent periods of higher energy. The dominant mudstone component indicates deposition from suspension fallout, suggesting a low-energy setting periodically interrupted by processes bringing sand into the environment. Physical sedimentary structures as wave-ripples and current-ripples indicate that the current can be unidirectional or oscillatory. The low degree of bioturbation and the presence of *Planolites* and *Teichichnus* indicates deposition in a proximal setting, probably in a brackish-water environment.

Log C, Outer East Canyon 3

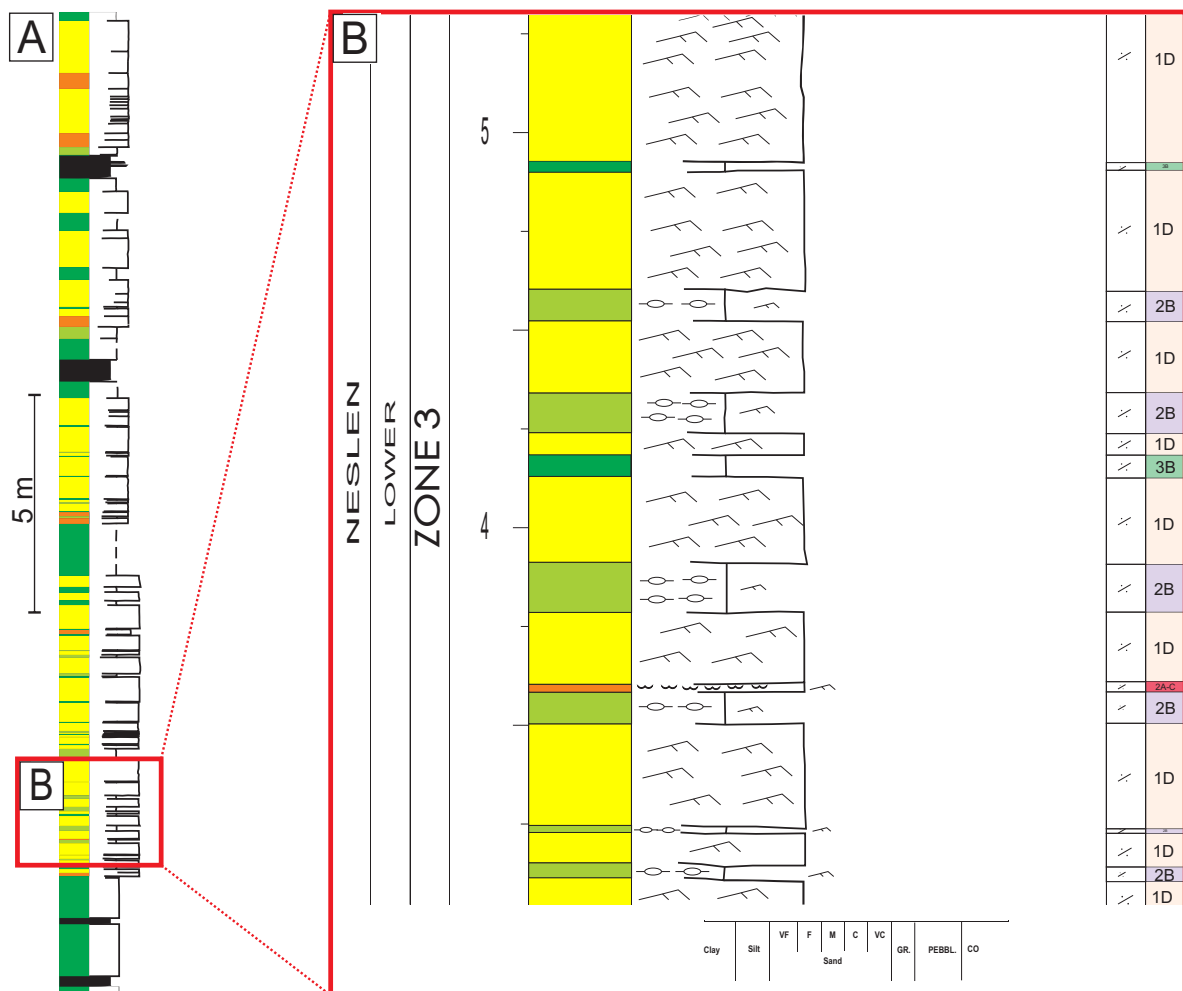


Figure 4.14: A: Sedimentary log from Outer East Canyon, log C (Fig. 1.2). B: Excerpt from Lower Neslen Interval showing Lithofacies 2B in the log. Lithofacies 2B is here present in alternation with sandstone with current-ripple cross-lamination (Lithofacies 1D).

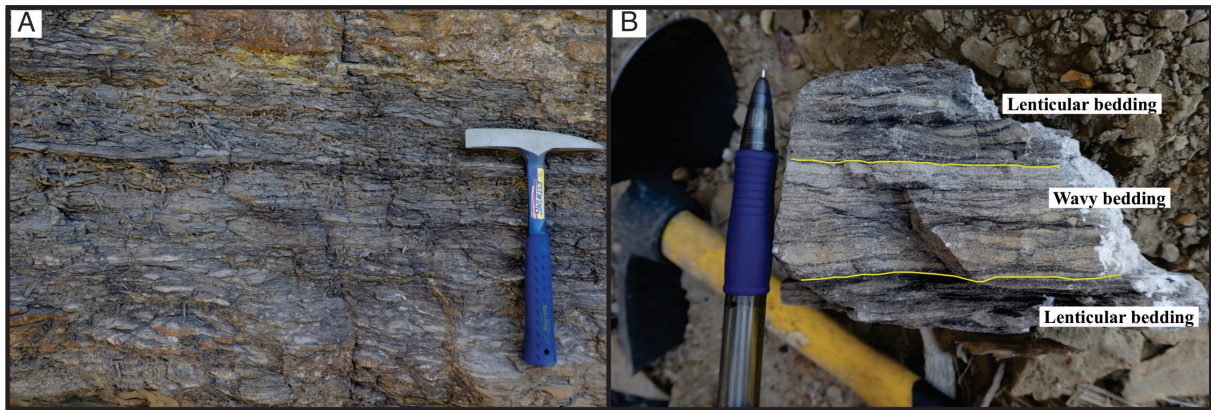


Figure 4.15: Photos of Lithofacies 2B. Both photos are showing a relatively low net/gross sand ratio. A: Lenticular bedded heterolith with current-ripple cross-lamination and plant fragments in Bayfill #1 unit, Middle Neslen Interval, Neslen Canyon, log S (Fig. 1.2). B: Sample with wavy- (middle part) and lenticular (lowermost and uppermost part) bedded heterolith in Bayfill #3 unit, Middle Neslen Interval, Outer East Canyon, log C (Fig. 1.2).

4.8 Lithofacies 3A: Horizontal laminated to lenticular bedded mudstone

Description

Lithofacies 3A is commonly structureless but occasionally composed of horizontal laminated to slightly lenticular bedded mudstone (Fig. 4.17). Silt- and sandstones are present as streaks of a lighter color, and the mudstone is dark grey. Lithofacies 3A is observed in the Middle Neslen Interval in most of the logs. Within the bayfill units, Lithofacies 3A is typically observed at the base, with a gradual transition into wavy- or lenticular bedded heteroliths. In some logs, it is observed in alternation with Lithofacies 1B and heterolithic lithofacies. The average thickness of Lithofacies 3A is 56 cm (n=37), ranging from 2 cm to 460 cm. The degree of bioturbation is absent to low (degree 0 - 1). Observations show siderite cemented beds and nodules within and above Lithofacies 3A (Figs. 4.16 and 4.17A). Due to the high mudstone content, Lithofacies 3A often forms slopes in the landscape (Fig. 4.17B).

Interpretation

Due to the amount of mudstone, the deposition of Lithofacies 3A has probably taken place in a low-energy environment. The gradual transition into, or alternation with, heterolithic bedding or sandstone, indicates a marginal-marine depositional environment. Lithofacies 3A is interpreted as deposited below storm-weather wave-base. Thin sandstone or siltstone streaks are interpreted as deposited from suspension fallout after periods of higher energy (Raaf et al., 1977), such as storms. Subsequently, the storm deposits may be wave-reworked. Siderite nodules and cementation can be found both in marine and terrestrial settings. According to Mozley & Wersin (1992), $\delta^{13}C$ values of siderite can indicate whether the depositional environment is continental or marine. However, such analyses are not carried out in this study.

Log S, Neslen Canyon 1

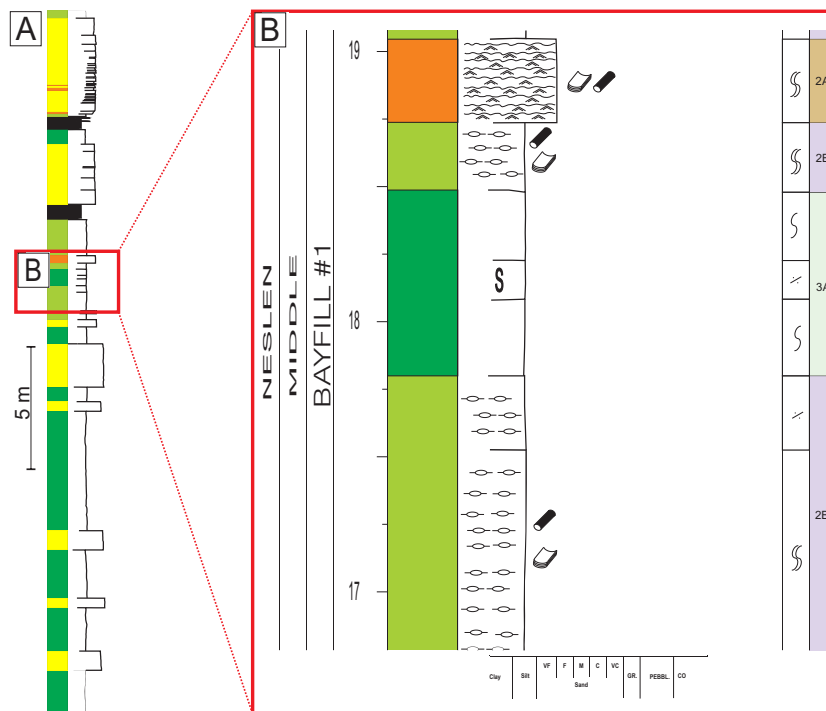


Figure 4.16: A: Sedimentary log from Neslen Canyon, log S (Fig. 1.2). B: Excerpt from Bayfill #1 unit showing Lithofacies 3A in the log. Lithofacies 3A is without any distinct structures, and there is about 20 cm of siderite cementation within the lithofacies. Lithofacies 3A is interbedded with heterolithic deposits of marine and non-marine processes.

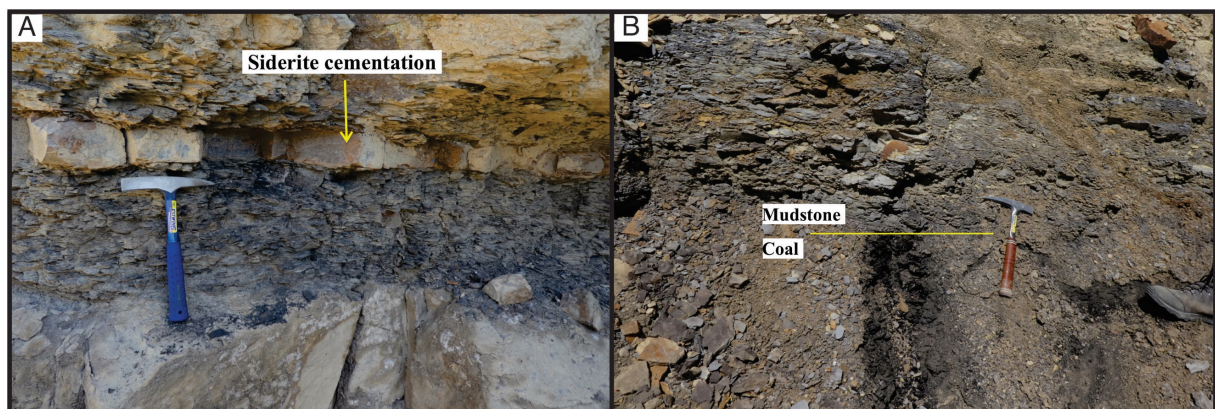


Figure 4.17: Photos of Lithofacies 3A. A: Lithofacies 3A with siderite cementation in Bayfill #1 unit, Middle Neslen Interval, Neslen Canyon, log S (Fig. 1.2). B: Lithofacies 3A above a coal bed in Bayfill #2 unit, Middle Neslen Interval, Exit Canyon, log F (Fig. 1.2).

4.9 Lithofacies 3B: Rooted and organic-rich mudstone

Description

Lithofacies 3B is composed of rooted and organic-rich, dark grey mudstone, observed in the Lower- and Middle Neslen Interval. The thickness varies from 2 cm to 496 cm, and the mean thickness is 64 cm (n=74). Bioturbation is absent (degree 0). Coal interbeds up to 6 - 7 cm are observed (Fig. 4.19A), but Lithofacies 3B in the Middle Neslen Interval is overlain thicker coal

beds (Fig. 4.18). Lithofacies 3B forms slopes and is often poorly exposed in outcrops. In the Lower Neslen Interval, Lithofacies 3B is observed interbedded with Lithofacies 1A and 1D.

Interpretation

Abundant coals and roots within Lithofacies 3B indicate subaerial exposure during deposition (Kjærefjord, 1999; Kirschbaum & Hettinger, 2004). Coal deposition depends on the accumulation of organic-rich material and limited input of clastic sediments (McCabe, 1985). According to Kirschbaum & Hettinger (2004), organic-rich mudstone with coal represents deposition in wetlands. The alternation between Lithofacies 3B and sandstone Lithofacies 1A and 1D suggests crevasse splay interbeds, and alternation on a smaller scale may represent levee deposition (Elliott, 1974).

Log S, Neslen Canyon

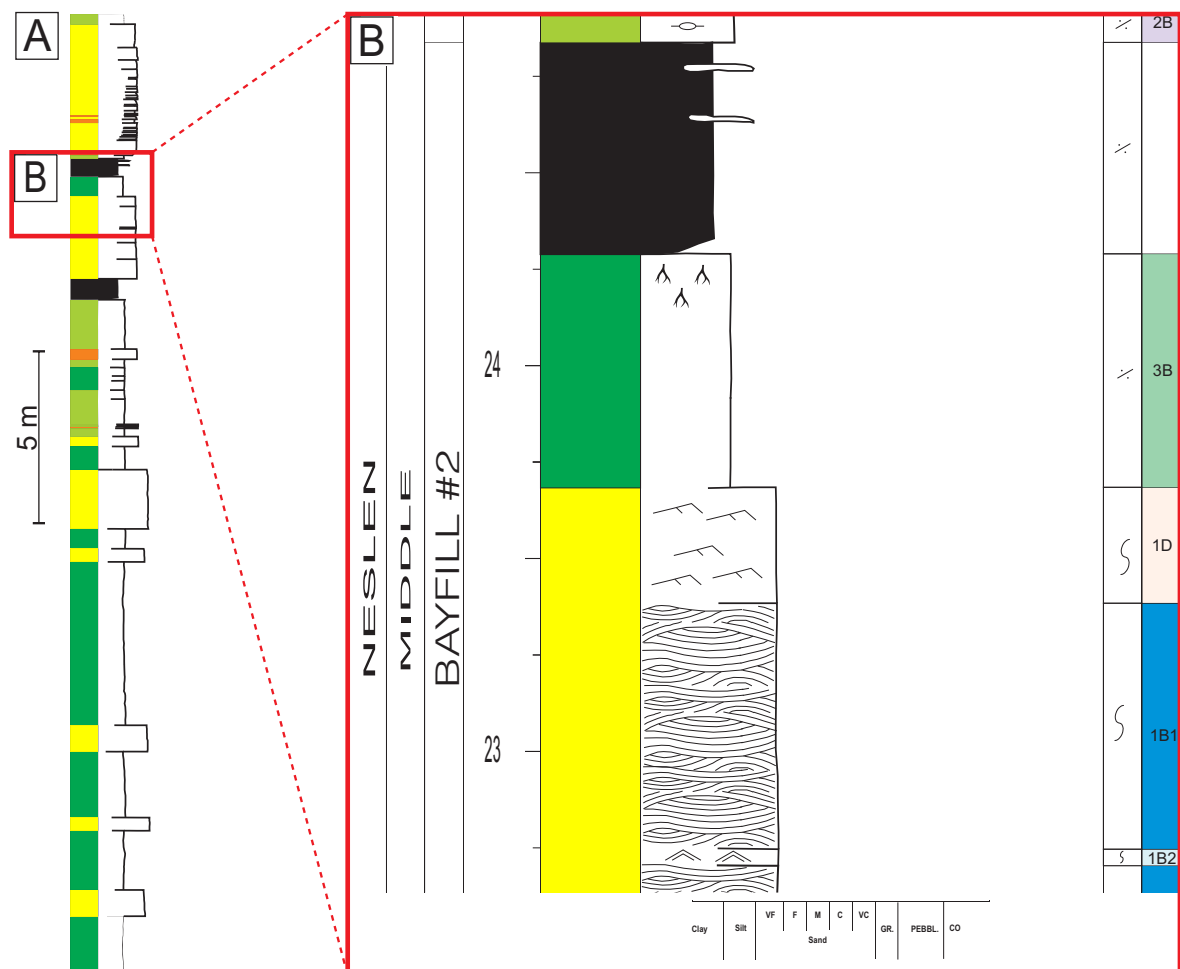


Figure 4.18: A: Sedimentary log from Neslen Canyon, log S (Fig. 1.2). B: Excerpt from Bayfill #2 unit showing Lithofacies 3B in the log, with a coal bed on top. Lithofacies 3B have roots in the upper part. The coal bed is ~50 cm, containing two bentonite layers.

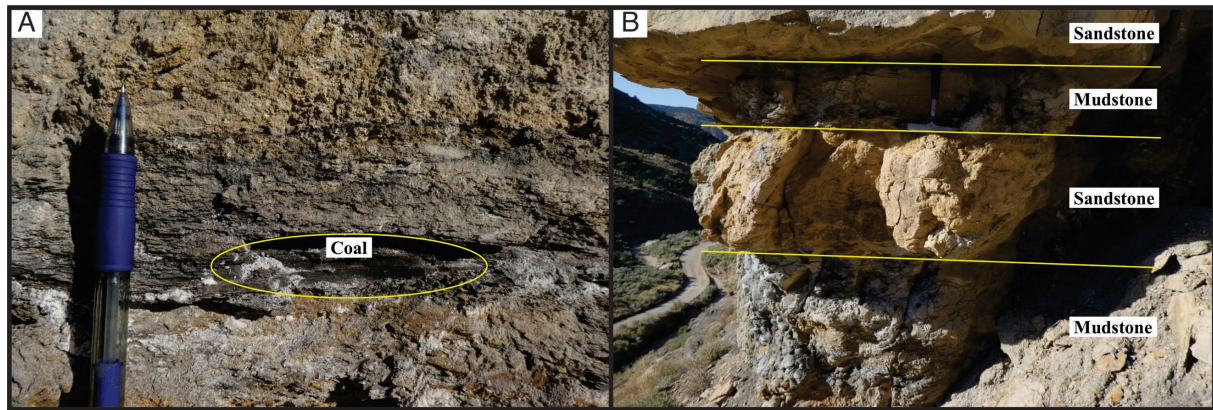


Figure 4.19: Photos of Lithofacies 3B. A: Organic rich mudstone with a coal layer in Lower Neslen Interval, Exit Canyon, log G (Fig. 1.2). B: Alternating mudstone and sandstone with current-ripple cross-lamination in Lower Neslen Interval, East Canyon Window, log N (Fig. 1.2).

4.10 Coal

Description

At least two coal beds are present at every location, defining the tops of Bayfill units #1 and #2 (Fig. 4.20). The coal beds separating the bayfill units have a uniform thickness in most of the logs. Out of 40 coal bed measurements, the thickness ranges from 14 cm to 90 cm. The mean thickness is 52 cm. The coal bed in Bayfill #2 unit comprises one or two thin, grey-brown lamina of volcanic ash; bentonites (Figs. 4.18 and 4.20C). Observed bentonites have a thickness up to 3 - 4 cm. The sediments exhibit a white color extending a few meters down in units below coal beds, especially in the Bayfill #2 unit.. Rootlets are commonly observed as extending downwards from the coal bed (Fig. 4.18).

Interpretation

Laterally extensive coal beds suggest subaerial exposure. Coal reflects limited clastic sedimentation and is developed during sustained accumulation of organic material within a protected and reducing environment (McCabe, 1985). The whitish color below the coal is formed by organic acid, and the affected areas are called leached zones. The acids have caused diagenetic mineral leaching to the underlying zones, forming so-called “whitecaps” (Taylor et al., 2000; Taylor & Machent, 2010). Roots beneath the lithofacies suggest in-situ accumulation of peat. Peat can accumulate from organic matter below stagnant water in a reducing environment (McCabe, 1985).

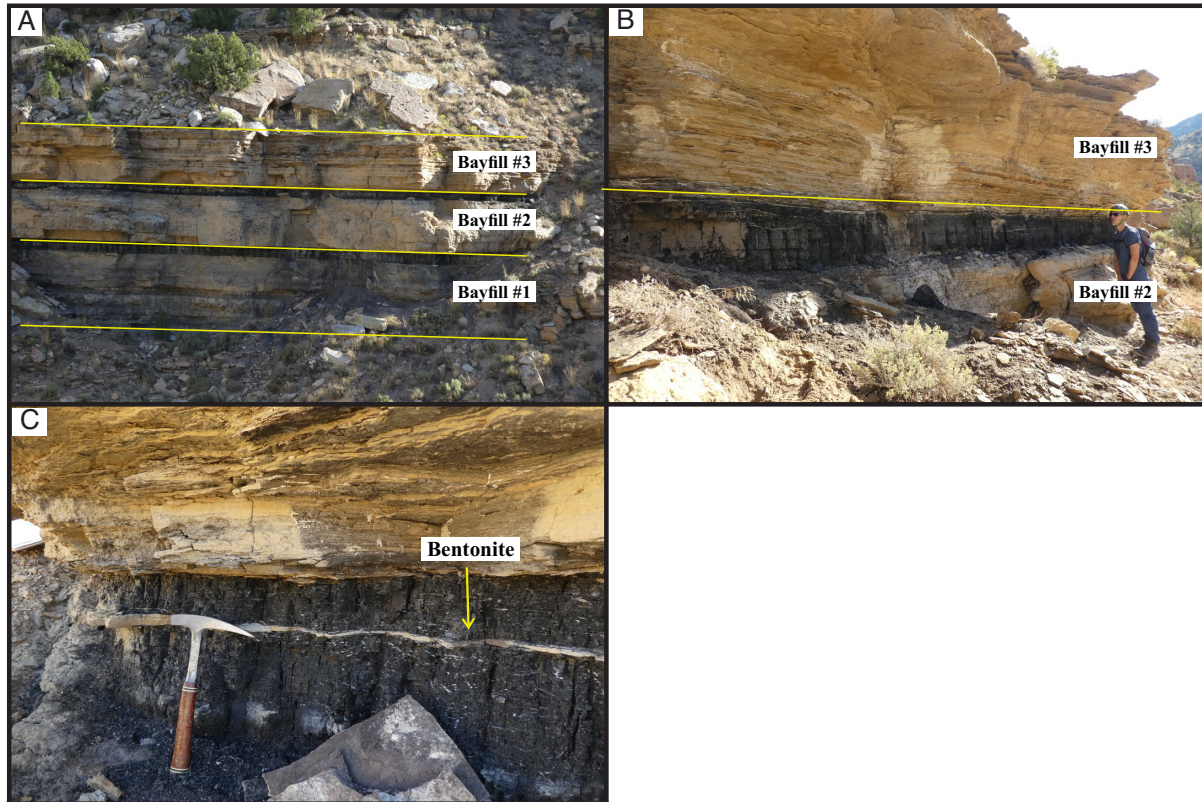


Figure 4.20: Photos of coal. A: Overview of Bayfill units #1 - #3 (Neslen Formation) separated by coal beds in Neslen Canyon. Log S (Fig. 1.2) in Neslen Canyon is made by walking along the slope to the right. B: Coal bed with bentonites between sandstones, in Bayfill #2 unit, Middle Neslen Interval, Keane Creek, log K (Fig. 1.2). C: Coal bed with bentonite in Bayfill #2 unit, Middle Neslen Interval, Outer East Canyon, log B (Fig. 1.2).

5 Facies associations

The lithofacies (Table 4.1) themselves (Chapter 4) are not distinctive of any particular depositional environment. The sedimentary logs show that stacking of lithofacies is rarely random but most often occurs in preferred patterns. Based on combinations of the lithofacies, a number of facies associations are established. The following Sub-chapters 5.1, 5.2, and 5.3 describe and interpret the different facies associations. Sub-chapter 5.4 explains the spatial distribution of the facies associations within the lower delta plain environment, and Sub-chapter 5.5 addresses a classification of bay deposits.

Three distinct facies associations are recognized within the study area (Table 5.1), all of them representing sub-environments related to a lower delta plain setting. A subdivision into three different bay deposits is suggested based on the mud versus sand content and the relative importance of current- versus wave-generated structures.

Table 5.1: Overview of facies associations of the lower delta plain deposits in the study area.

Facies association	Interpretation	Sub-facies association	Typical lithofacies	Mud content	Relative importance of current- versus wave-generated structures
FA1	Fluvial channel		1A, 1B, 1D, 2A, 2A-C, 3B		
FA2	Marsh/levee		3B, 1D, 1A		
FA3	Bay deposits	FA3a Wave-dominated bayfill	1B, 1C, 1D, 2A, 2B, 3A	<60%	>50% wave-generated
		FA3b Bayhead delta	(1B), 1D, 2A, 2B, 3A	<60%	>50% current-generated
		FA3c Sub-bay	2A, 2B, 3A	>60%	

Figure 5.1 shows the spatial organization of facies associations within a lower delta plain setting:

- The fluvial channel facies association is present where a fluvial channel approaches the marine realm. The channel system is then typically bifurcating.
- The deposits of the marsh and levee facies association are interpreted to have been deposited adjacent to the channels.
- The deposits of the wave-dominated bayfill facies association are interpreted to have been deposited in the middle and outer parts of a bay in areas less sheltered from wave-energy.

- The deposits of the bayhead delta facies association are interpreted to have been deposited at the mouth of channels that extend into central parts of a bay and indicate deposition closer to the fluvial channel.
- The deposits of the sub-bay facies association are interpreted to have been deposited in a more sheltered area, often behind barrier islands, causing a low-energy environment only occasionally interrupted by storm waves.

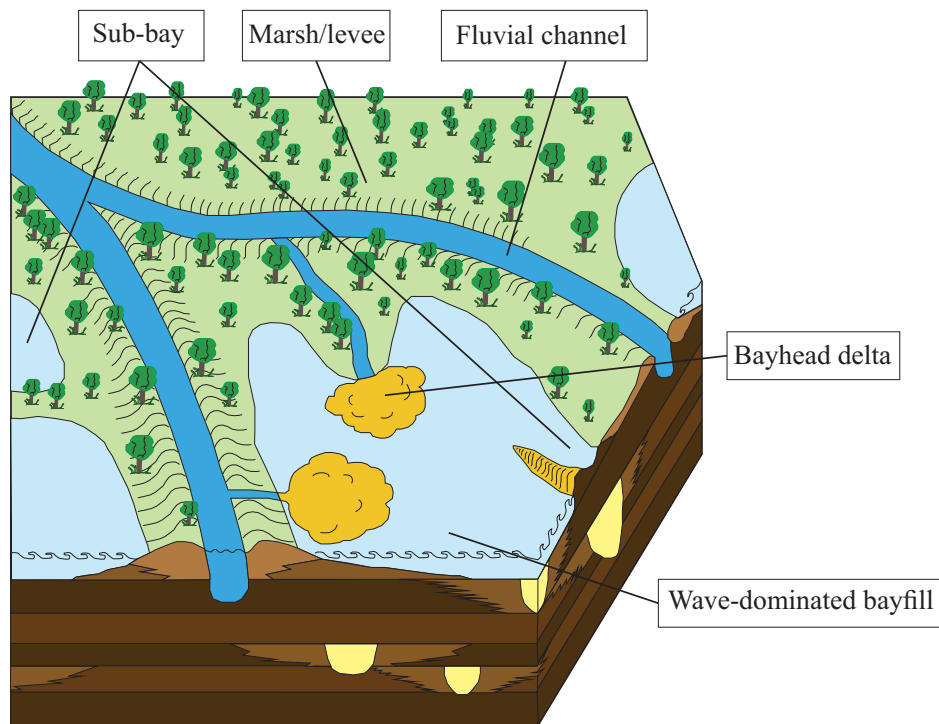


Figure 5.1: Spatial distribution of lower delta plain facies associations: Fluvial channel, marsh/levee, sub-bay, bayhead delta, and wave-dominated bayfill. Modified from Kjærefjord (1999).

5.1 Facies association 1: Fluvial channel (FA1)

Description

Facies association 1 (FA1) ranges in thickness from 5 - 13 m and comprises continuous sandstone packages of varying thickness, up to 8.4 m. The sandstone packages contain primary sedimentary structures such as cross-stratification and cross-lamination (Lithofacies 1A, 1D) and are often interbedded with thinner heteroliths containing wave-ripple- or current-ripple cross-lamination (Lithofacies 2A and 2A-C) and mudstones (Lithofacies 3B) (Figs. 5.2 and 5.3). Cross-stratified beds and current-ripple cross-laminated beds may exhibit wave-reworked tops. Above is wave-ripple cross-lamination. The sandstone packages in the lower part of FA1 typically display cross-stratification (Lithofacies 1A), trending towards cross-lamination (Lithofacies 1D) in the upper part. Bioturbation is absent in the cross-stratified sandstone. Rippled heteroliths and sandstones have a higher degree of bioturbation, containing traces of *Planolites* and *Thalassinoides*. Mud drapes are

occasionally observed along the cross-stratified sandstone's foreset surfaces, and an erosive base is common for the cross-stratified sandstone packages.

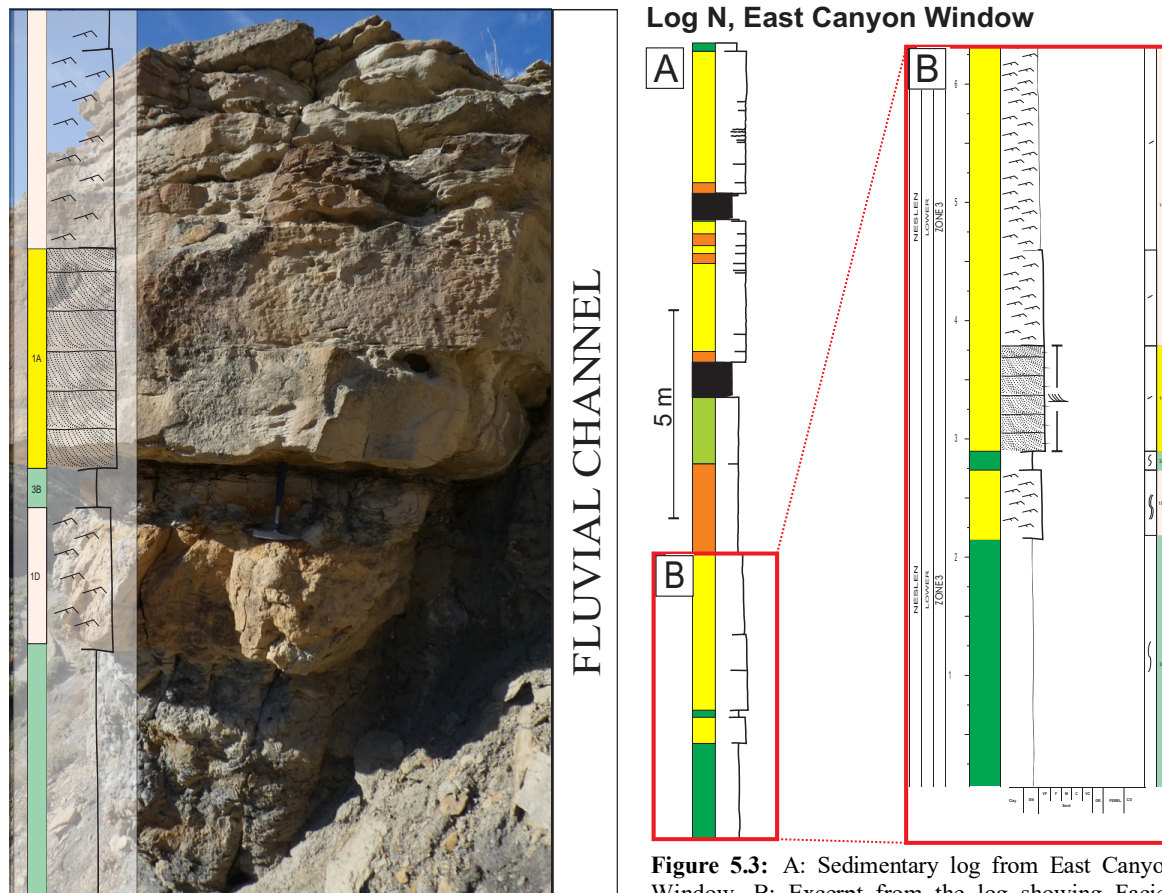


Figure 5.2: Photo of Facies association 1 (fluvial channel). The succession shows alternation between sandstone (FA1) and mudstone (FA2). A part of the sedimentary log (Fig. 5.3) is included. From Lower Neslen Interval, East Canyon Window, log N (Fig. 1.2).

Figure 5.3: A: Sedimentary log from East Canyon Window. B: Excerpt from the log showing Facies association 1 (fluvial channel) in the Lower Neslen Interval. The succession shows alternation between sandstone (FA1) and mudstone (FA2). This part correlates to the photo in Figure 5.2. From Lower Neslen Interval, East Canyon Window, log N (Fig.

Interpretation

The presence of cross-stratification suggests deposition from tractive, unidirectional currents, as cross-stratification reflects migration of 2D- or 3D-dunes (Ashley, 1990; Li & Bhattacharya, 2014). Mud drapes along foreset surfaces indicate fluctuating energy during deposition, which may be caused by tidal influence (Li & Bhattacharya, 2014). This implies that the facies association is found near the marine realm, but it can still be at a great distance as tidal modulation can occur up to a few hundred kilometers up in the fluvial channels (Dalrymple & Choi, 2007). Trace fossils and wave-ripple cross-lamination may be indicators of an environment that is, at least, partly marine, as *Planolites* and *Thalassinoides* reflects a brackish environment. The transition from asymmetrical- to symmetrical ripples indicates a decrease in unidirectional energy, causing a wave-reworked top of the cross-stratified and current-rippled

sandstones. Heteroliths capping the cross-stratification also indicate a waning flow (Li & Bhattacharya, 2014).

The brackish to marine indicators suggest deposition in the distal end of a fluvial channel on the marine-influenced lower delta plain. Deposition could be within a fluvial channel (Kjærefjord, 1999; Payenberg et al., 2003), possibly associated with a bay environment (Li & Bhattacharya, 2014). Varying thickness of the sandstone beds (2 cm - 8.4 m) indicates different parts of the environment. Thicker beds are interpreted as deposits of main fluvial channels (Dreyer, 1990), while thinner, more laterally extensive beds are interpreted to result from permanent crevasse channels (Elliott, 1974).

5.2 Facies association 2: Marsh/levee (FA2)

Description

Facies association 2 (FA2) is typically 40 cm to 5 m thick, composed of rooted and organic-rich mudstone (Lithofacies 3B) interbedded with 14 - 78 cm thick coal beds (Figs. 5.4 and 5.5), 4 - 52 cm of current-ripple cross-laminated sandstone beds and 40 - 80 cm thick cross-laminated sandstone beds (Lithofacies 1D, 1A). Alternation between Lithofacies 3B and Lithofacies 1D/1A is observed on centimeter to decimeter scale and decimeter to meter scale. FA2 is also observed without intervening sandstones. The coal beds are 52 cm thick on average, often including thin grey laminae of volcanic ash (bentonites).

Usually, the packages are relatively thin compared to the bay deposits of Facies association 3. In the Middle Neslen Interval (Fig. 2.7), FA2 is commonly stratigraphically positioned between bay deposits (Facies association 3), separating the bayfill units from each other. In these positions, the coal beds are often present above the mudstone beds (Lithofacies 3B). Mudstones with coal interbeds are also observed in the Lower Neslen Interval (Fig. 2.7), but usually, this interval consists of mudstones (Lithofacies 3B) interbedded with sandstones with unidirectional primary sedimentary structures (Lithofacies 1A/1D). Some of the sandstone packages exhibit erosive bases.

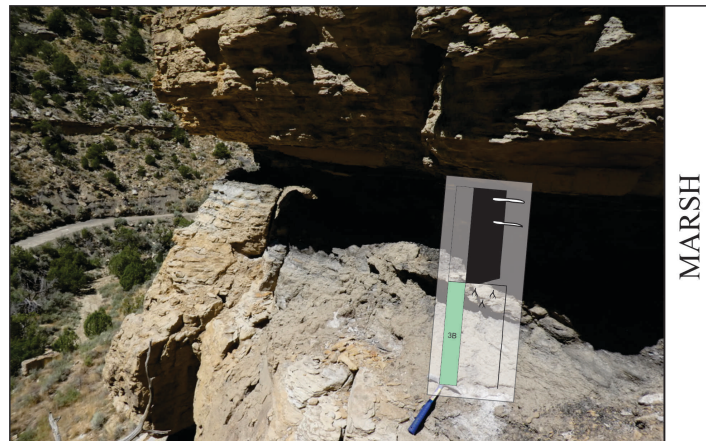


Figure 5.4: Photo of Facies association 1 (marsh). The succession shows organic-rich mudstone capped by a 55 cm coal layer with bentonites. A part of the sedimentary log (Fig. 5.5) is included in the photo where the relevant facies association is interpreted. From the upper part of Bayfill #2 unit, Middle Neslen Interval, Neslen Canyon, log S (Fig. 1.2).

Log S, Neslen Canyon

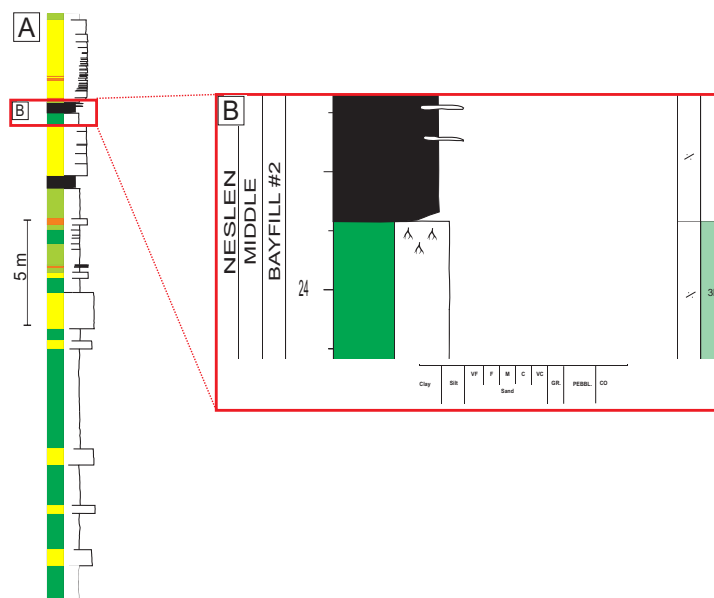


Figure 5.5: A: Sedimentary log from Neslen Canyon, log S (Fig. 1.2). B: Excerpt from the log showing Facies association 2 (marsh), in the upper part of Bayfill #2 unit, Middle Neslen Interval. The succession shows organic-rich mudstone capped by a 55 cm coal layer with bentonites. This part correlates to the photo in Figure 5.4.

Interpretation

The presence of rooted- and organic-rich mudstone indicates paleosols (Mack et al., 1993), which, together with coal beds, indicate subaerial exposure. Sandstone beds interbedded with mudstone and structures pointing to unidirectional currents are interpreted as crevasse splays (Kjærefjord, 1999). Crevasse splays result from floodwater transferred from the channels to the marsh and interdistributary bays by small crevasse channels (Allen, 1965; Coleman, 1969; Arndorfer, 1973). A crevasse channel is formed by sediment-laden water that cuts through the levee crest during flooding in a fluvial channel. According to Elliott (1974), Kjærefjord (1999)

and Kjærefjord et al. (2021, Accepted), the rapid, small-scale alternation between rooted, organic-rich mudstones (Lithofacies 3B) and sandstones with unidirectional primary structures may also be indicative for levee deposition. Interaction of crevasse splay interbeds, levee deposition, coal beds, and the rooted, organic-rich mudstones is indicative of a vegetated marsh (Kjærefjord, 1999).

5.3 Facies association 3: Bay deposits (FA3)

Typical for lower delta plain deposits are areally extensive bayfills originating in interdistributary bays separating distributary channels (Coleman & Prior, 1982). Bayfills often form several vertical stacked units separated by marsh deposits (Bhattacharya, 2010). Interdistributary bays are defined as part of the area between distributary channels, together with tidal channels, crevasse splays and -channels, levees, marshes, and swamps (Coleman & Gagliano, 1964; Coleman & Prior, 1982). Bays are often 1 - 5 m deep, rarely exceeding 7 - 8 m depth, with brackish or marine water (Elliott, 1974; Coleman & Prior, 1982; Kjærefjord, 1999). Sediments deposited sub-aquatically within a bay make up a bayfill succession (Kjærefjord, 1999). The three following sub-facies associations are deposited as part of a bayfill succession and occur in close association with each other. Coleman & Prior (1982) explain the development of stacked bayfill units as part of a sedimentary cycle, where early compaction and subsidence causes inundation by marine water after the infilling of an interdistributary bay. Figure 5.6 shows the distribution of unit thicknesses and facies associations in the Bayfill units #1, #2, and #3, further described in the respective facies associations.

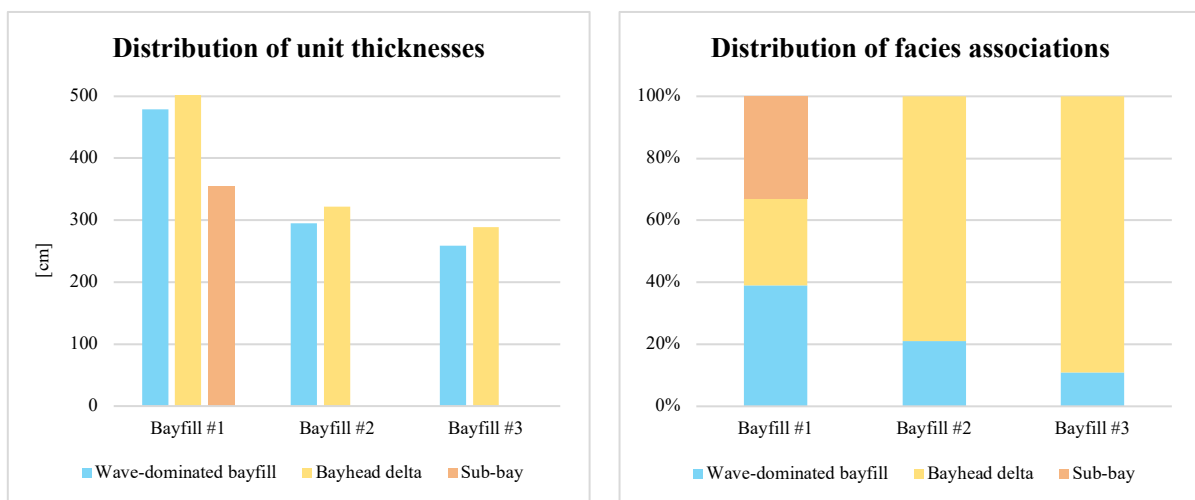


Figure 5.6: Left: Distribution of the thicknesses of the facies association 3 (wave-dominated bayfill, bayhead delta, and sub-bay) in the Bayfill units #1, #2, and #3. Right: Distribution of facies association 3 (wave-dominated bayfill, bayhead delta, and sub-bay) within the Bayfill units #1, #2, and #3.

5.3.1 Sub-facies association 3a: Wave-dominated bayfill (FA3a)

Description

In the study area, the wave-dominated bayfill sub-facies association (FA3a) makes up 25% of all the studied bayfill units (n=56). Amongst Bayfill #1 units (n=18), ~39% is FA3a, ~21% amongst Bayfill #2 units (n=19) is FA3a, and ~11% of Bayfill #3 units (n=19) is FA3a (Fig. 5.6). Average thicknesses of FA3a Bayfill units #1, #2, and #3 are ~479 cm (n=7), ~299 cm (n=4), and ~259 (n=2) cm (Fig. 5.6), respectively, from the studied logs. The thickness of FA3a ranges from 1.8 m to 4.8 m. Sub-facies association 3a displays an upward-coarsening trend from mudstones at the base to heteroliths and further into sandstones (Figs. 5.7 and 5.8). The top may be rooted and capped by marsh deposits (FA2). Note that not all studied bayfill units display this gradual transition, but most of them have a mudstone-dominated base composed of Lithofacies 3A, with a thickness ranging from 4 - 146 cm. Above the mudstone-dominated interval, several locations demonstrate an alternation between sandstone and mudstone/heterolithic beds, with thicknesses from 78 - 320 cm. The heteroliths show wavy- to lenticular bedding and are dominated by wave-ripple cross-lamination (Lithofacies 2A and 2B). Heteroliths typically have none to moderate bioturbation degree, containing trace fossils of *Planolites*, *Thalassinoides*, and *Teichichnus*. Syneresis cracks are observed in some of the heterolithic intervals lacking bioturbation.

Primary sedimentary structures in the 64 - 250 cm thick sandstone intervals are wave-ripple cross-lamination (Sub-facies 1B2) and small-scale hummocky cross-stratification (Sub-facies 1B1). These sandstone intervals have a bioturbation degree ranging from none to high. Some intervals display sandstones where primary sedimentary structures are destroyed by pervasive burrowing (Lithofacies 1C). The trace fossil assemblage in sandstones is dominated by *Skolithos*, *Thalassinoides*, *Bergaueria*, and *Planolites*. The sandstones also exhibit current-ripple cross-lamination (Lithofacies 1D), in some places with a wave-reworked top and in alternation with Lithofacies 1B and 2A.



Figure 5.7: Photo of Facies association 3a (wave-dominated bayfill). The wave-dominated bayfill unit shows an upward-coarsening trend and primary sedimentary structures dominated by wave-generated processes. A part of the sedimentary log f (Fig. 5.8) is included in the photo where the relevant facies association is interpreted. The red lines mark the top and bottom of the bayfill unit. From Bayfill #1 unit, Middle Neslen Interval, in Outer East Canyon, log C (Fig. 1.2).

Log C, Outer East Canyon

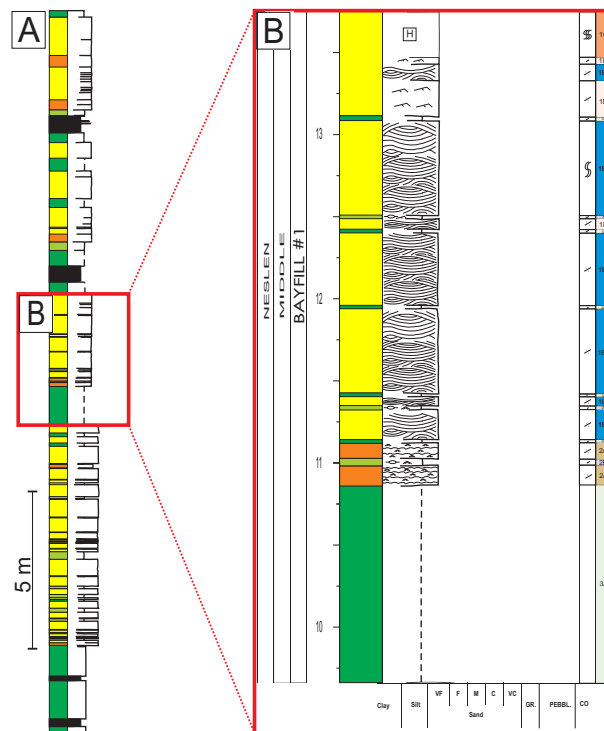


Figure 5.8: A: Sedimentary log from Outer East Canyon, log C (Fig. 1.2). B: Excerpt from the log showing Facies association 3 (wave-dominated bayfill), in Bayfill #1 unit, Middle Neslen Interval. The succession shows an upward-coarsening trend and primary sedimentary structures dominated by wave-generated processes. This part correlates to the photo in Figure 5.7.

Interpretation

Lithofacies 3A is interpreted as deposited in a low-energy marginal-marine environment mostly below local storm-weather wave-base, occasionally influenced by storm-generated waves. The upwards change into Lithofacies 2B and 2A with syneresis cracks represents a decreasing water depth, reflected in increasing energy level, more influence from waves, and input from saline water from storms. Completely bioturbated sandstones (Lithofacies 1C) are interpreted as deposited below fair-weather wave-base within a relatively low-energy environment compared to Lithofacies 1B. The wave-reworked sandstones (Lithofacies 1B) are interpreted as shallow-marine deposits in an area with more wave-energy than the underlying units. Instances of alternation with Lithofacies 1D suggest deposition from sheet floods, generated by distributary channels spilling sediment-laden water into the interdistributary bay (Coleman & Gagliano, 1964; Elliott, 1974, 1986).

The overall upward-coarsening trend from mudstones through heteroliths and further into sandstones reflects upward-shallowing and progradation of a bay shoreline. Relatively thin upward-coarsening packages indicate shallow water. Hence, open sea progradation is eliminated. The proximity of the sandstone source is interpreted to increase upwards in the successions. A prograding shoreline moves the depositional surface upwards from a deeper environment depositing mudstones and heteroliths below local storm-weather wave-base, to a more energetic environment above fair-weather wave-base, depositing sandstones. Areas above fair-weather wave-base are too high-energetic to preserve mudstones. Brackish-water trace fossils indicate a marginal-marine setting (Coleman & Prior, 1982), more likely in a protected environment than in an open marine environment (MacEachern et al., 2005; MacEachern et al., 2010). Primary sedimentary structures point at waves as a central depositional agent. The dominance of wave-generated structures, the upward-coarsening trend, and association with marsh deposits vertically and other bay facies associations laterally in FA3a suggest gradual infilling of wave-dominated interdistributary bays, therefore, interpreted as a wave-dominated bayfill.

The wave-dominated bayfill is most common in the middle and outer parts of bays (Fig. 5.1) (Kjærefjord, 1999). Occasionally, the lithofacies association is present in the inner parts of the bays.

5.3.2 Sub-facies association 3b: Bayhead delta (FA3b)

Description

Out of the 56 studied bayfill units, bayhead delta (FA3b) constitutes 64% and make up ~28% of Bayfill #1 units (n=18), ~79% of Bayfill #2 units (n=19), and ~89% of Bayfill #3 units (n=19) (Fig. 5.6). The thickness of FA3b ranges from 1.7 m to 6.3 m in the studied logs, with average thicknesses of ~507 cm in Bayfill #1 unit (n=5), ~322 cm in Bayfill #2 unit (n=15), and ~293 cm in Bayfill #3 unit (n=17) (Fig. 5.6). Sub-facies association 3b comprises an upward-coarsening unit grading from mudstone (2 - 140 cm) through heteroliths (10 - 500 cm) and passing into sandstone (14 - 330 cm) (Figs. 5.9 and 5.10). The top is usually rooted and capped by marsh deposits (FA2). Mudstones and heteroliths in the lower part are similar to the ones in Sub-facies association 3a. Some of the FA3b intervals have heteroliths in the lower part where pure mudstone is absent. A typical succession has mudstone (Lithofacies 3A) or lenticular bedded heteroliths (Lithofacies 2B) at the base, grading into wavy bedded heteroliths (Lithofacies 2A/2A-C), followed by sandstones. Wavy bedded heteroliths display both wave- and current-ripple cross-lamination, but the latter is dominant. The mudstone/heterolithic component has none to moderate degree of bioturbation, with trace fossils dominated by *Thalassinoides* and *Planolites*. The sandstones typically show current-ripple cross-lamination (Lithofacies 1D) with absence of trace fossils, occasionally interbedded with deposits generated by wave-processes, with trace fossil assemblage dominated by *Bergaueria* and *Skolithos*.

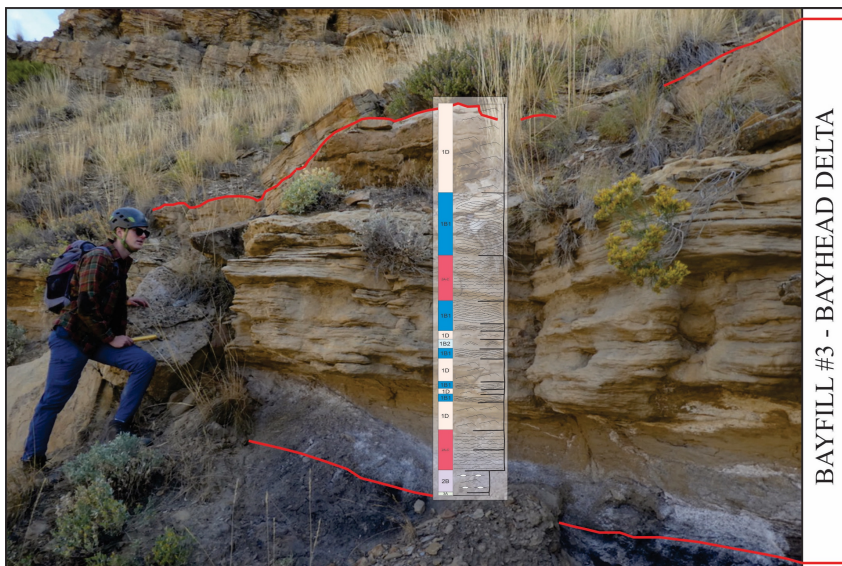


Figure 5.9: Photo of Facies association 3b (bayhead delta). The succession shows an upward-coarsening trend and primary sedimentary structures dominated by current-generated processes. A part of the sedimentary log (Fig. 5.10) is included in the photo where the relevant facies association is interpreted. The red lines mark the top and bottom of the bayfill unit. From Bayfill #3 unit, Middle Neslen Interval, in Outer East Canyon, log C (Fig. 1.2).

Log C, Outer East Canyon

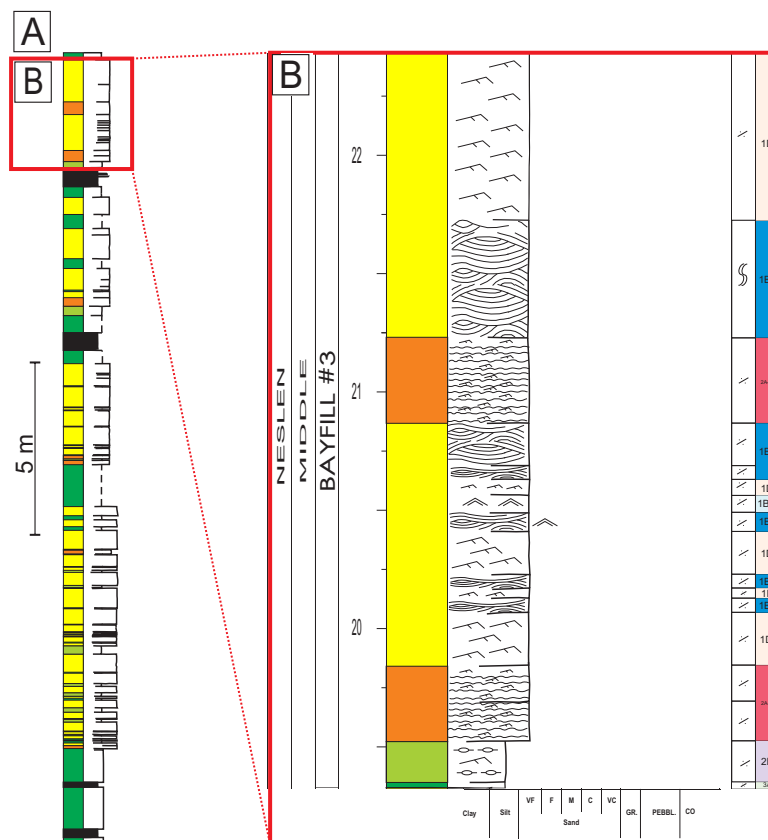


Figure 5.10: A: Sedimentary log from Outer East Canyon, log C (Fig. 1.2). B: Excerpt from the log showing Facies association 3b (bayhead delta) in Bayfill #3 unit, Middle Neslen Interval. The succession shows an upward-coarsening trend and primary sedimentary structures dominated by current-generated processes. This part correlates to the photo in Figure 5.9.

Interpretation

Primary sedimentary structures suggest deposition predominantly under conditions of unidirectional currents in an environment with active sediment transport. Deposition at a bayhead delta will normally be a consequence of small, permanent crevasse channels that extend into central parts of an interdistributary bay, resulting in an upward-coarsening bayfill unit (Kjærefjord, 1999). Hence, the overall upward-coarsening trend indicates increased proximity to the source further up in the successions. Wave-influenced heteroliths (Lithofacies 2A and 2B) are interpreted to have been deposited in front of the current-ripple cross-laminated sandstone at the distal part of the bayhead delta. Bayhead deltas form in the transition from confined- to unconfined river mouths, where changes in flow conditions occur (Wright, 1977). The channel's current velocity decreases when reaching a standing body of water, causing coarser-grained sediments to deposit rapidly. During progradation of a delta, the channels erode into the delta (Kjærefjord, 1999). Wave-influenced heteroliths with bioturbation suggest a buoyancy-dominated river mouth. Such river mouths appear where the river extends into the

bay as a freshwater plume, making a wedge of salt- or brackish water below the freshwater (Coleman & Wright, 1975; Elliott, 1986).

In a lower delta plain setting, bayhead deltas are most common in inner, more local parts of a bay and less common in the middle and outer parts of a bay (Fig. 5.1) (Kjærefjord, 1999).

5.3.3 Sub-facies association 3c: Sub-bay (FA3c)

Description

The sub-bay sub-facies association (FA3c) has an average thickness of ~354 cm (n=6) (Fig. 5.6) in the studied locations, ranging from 2.9 - 5.4 m. FA3c is only present in Bayfill #1 unit and makes up ~33% of the studied Bayfill #1 units (n=18) (Fig. 5.6) and 11% of all the studied bayfill units (n=56). Sub-facies association 3c is composed of lithologies of mudstone, muddy heteroliths, and sandy heteroliths (Figs. 5.11 and 5.12). In general, FA3c is more fine-grained than the above-mentioned sub-facies associations and consists of a higher proportion of mud. Short intervals with sandstone occur. FA3c typically consists of wavy- or lenticular bedded heteroliths with either wave- or current-ripple cross-lamination (Lithofacies 2A, 2A-C, and 2B) and mudstones (Lithofacies 3A). The degree of bioturbation ranges from none to high. The intervals of high bioturbation are typically sandstone-dominated (Lithofacies 1C). *Planolites* and *Teichichnus* predominate the trace fossil assemblage. The sub-facies association 3c is often observed with intervals of siderite cementation or siderite nodules within the mudstones. Syneresis cracks are abundant in some of the mudstone-dominated heterolithic beds. FA3c is capped by marsh deposits with ~50 cm thick coal beds.



Figure 5.11: Photo of Facies association 3c (sub-bay). The sub-bay succession shows a slightly upward-coarsening trend but is generally dominated by mudstones and heteroliths. A part of the lithofacies log (Fig. 5.12) is included in the photo where the relevant facies association is interpreted. The red lines mark the top and bottom of the bayfill unit. From Bayfill #1 unit, Middle Neslen Interval, in Keane Creek, log M (Fig. 1.2).

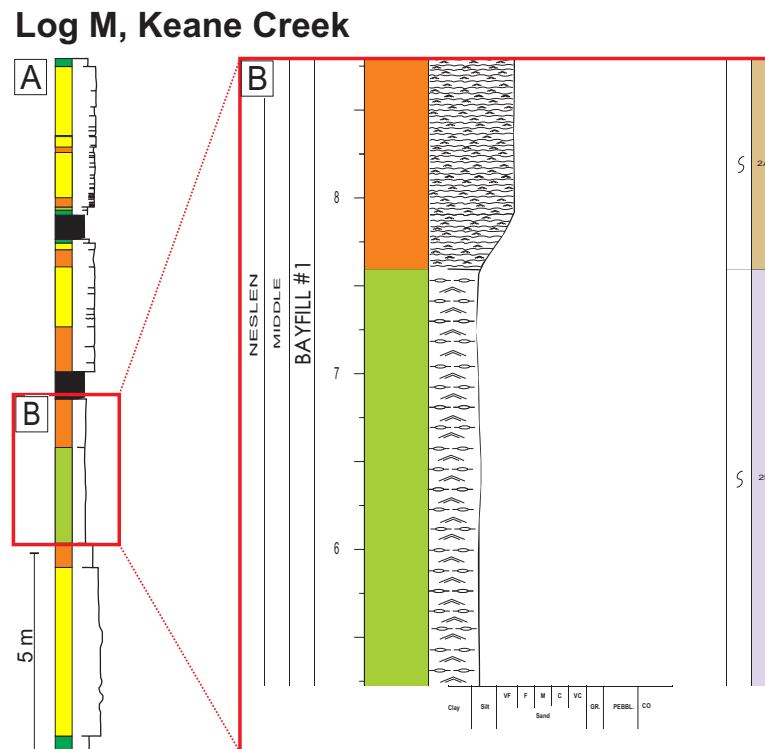


Figure 5.12: A: Sedimentary log from Keane Creek, log M (Fig. 1.2). B: Excerpt from the log showing Facies association 3c (sub-bay) in Bayfill #1 unit, Middle Neslen Interval. The sub-bay succession shows a slightly upward-coarsening trend but is generally dominated by mudstones and heteroliths. This part correlates to the photo in Figure 5.11.

Interpretation

Trace fossil assemblage and syneresis cracks reflect brackish-water with salinity fluctuations and low energy in a proximal setting. Intervals dominated by grain-sizes in the sand-fraction indicate periods of storm waves transporting the sand into a calm, low energetic environment. FA3c is suggested as deposited along the margins of a bay sheltered from wave energy (Fig. 5.1) (Kjærefjord et al., 2021, Accepted), typical behind wave-generated spits or bayhead deltas (Kjærefjord, 1999). According to studies by Kjærefjord (1999), sub-bay deposits have an areal extension of less than 1 km, grading rapidly into marsh, bayhead deltas, or wave-dominated deltas over distances of 200 – 300 m (Kjærefjord et al., 2021, Accepted).

5.4 Lower delta plain deposits

Facies association 3 consists of three types of sub-facies associations, all deposited within a bayfill succession, as part of the lower delta plain deposits. Their spatial organization within the lower delta plain is indicated in Figure 5.1. The bayhead delta is located in connection to the channel mouths, as they are deposited during progradation of smaller deltas within interdistributary bays. The wave-dominated bayfill is located most seaward at a location open to a wide lagoon where a significant wave fetch can build up substantial waves to rework the

sediments deposited. The sub-bay is sheltered from wave energy by spits or bayhead deltas building out into the bay.

Several observations are indicative of bay deposits, such as the relatively thin (1.7 - 6.3 m) deposits caused by limited accommodation space. Brackish trace fossils also indicate the infilling of an interdistributary bay. The range of bayfill unit thicknesses suggests variations in available accommodation space. Syneresis cracks also support the interpretations as bays, as bays typically have brackish water and salinity fluctuations. Salinity fluctuations may be seasonal (changes in freshwater discharge) or due to allogenic controls (crevasses splaying into the bay or the formation of new bayhead deltas).

The upward-coarsening trend of the bayfill units represents an upward-shallowing package with increasing energy over time, suggesting a progradational system. The capping of bayfill units by subaerial deposits indicates complete infilling of the available accommodation space (Kjærefjord et al., 2021, Accepted). Vertical stacking of bayfill units (Fig. 5.13) reflects repetitive periods of progradation, separated by flooding surfaces. A flooding surface causes reestablishment of an interdistributary bay and is interpreted to be positioned between the marsh/levee deposits (FA2) below and the bayfill units (FA3) above.

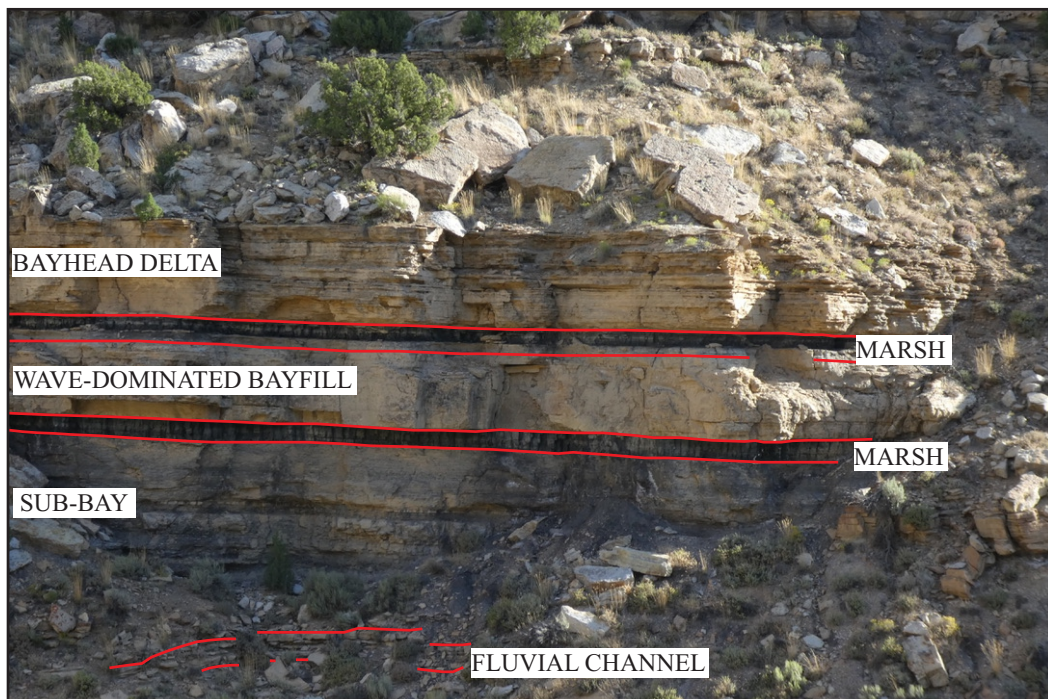


Figure 5.13: Photo showing the vertical stacking of bayfill units, separated by marsh facies association. A fluvial channel is present underneath the bayfill units. From Neslen Canyon, log S (Fig. 1.2).

The infilling of an interdistributary bay is dominated by incursions from distributaries, with crevasse deposits that build out in bays between or adjacent to distributary channels and extend seaward (Coleman & Prior, 1982). Sedimentary infilling of an interdistributary bay is described in a four-phase model by Elliott (1974) (Fig. 5.14). The model considers a distributary channel that recently avulsed into an interdistributary bay.

In the first phase (Fig. 5.14A), the levees of the distributary channel are absent or less developed. Consequently, relatively low-energy overbank sheet floods are likely to occur during flood events. During this stage, the sedimentation is dominated by mud deposition in central (deeper) parts of the interdistributary bay. These mud deposits coincide with the mudstones observed in the lower part of the studied bayfill units. At this stage, the bay is less affected by river processes but dominated by wave processes. Typically, the wave-dominated bayfill facies association is common during this stage. Repetitive flood events result in vertical accretion of levees at the bay margin. The distributary channel is more defined and mature in the second phase (Fig. 5.14B). The water level in the channel can reach higher elevations than in the bay. During a flood, the levees break, forming a crevasse splay. Typical for the crevasse splay is sand deposition with a downstream transition into heterolithic deposits (Smith et al., 1989). The third phase (Fig. 5.14C) initiates when the gradient between the channel and the bay is removed after filling the areas adjacent to levee breaks. Crevasse channels migrate across the initial splay lobe, causing deposition of minor mouth bars at the crevasse channel mouths. The bayhead delta facies association is typically related to this stage, as they represent deposition during the transition from confined- to unconfined river mouths. As the system builds out into the interdistributary bay, the sediments are gradually getting coarser. Some parts of the interdistributary bay become sheltered behind the bayhead delta building out, creating an area typical for the sub-bay facies association. In the last phase (Fig. 5.14D), the levees get higher, and the crevasse channels become permanent. During the next flood, an avulsion of the distributary river is likely. The process repeats itself as the system is now back to its initial position.

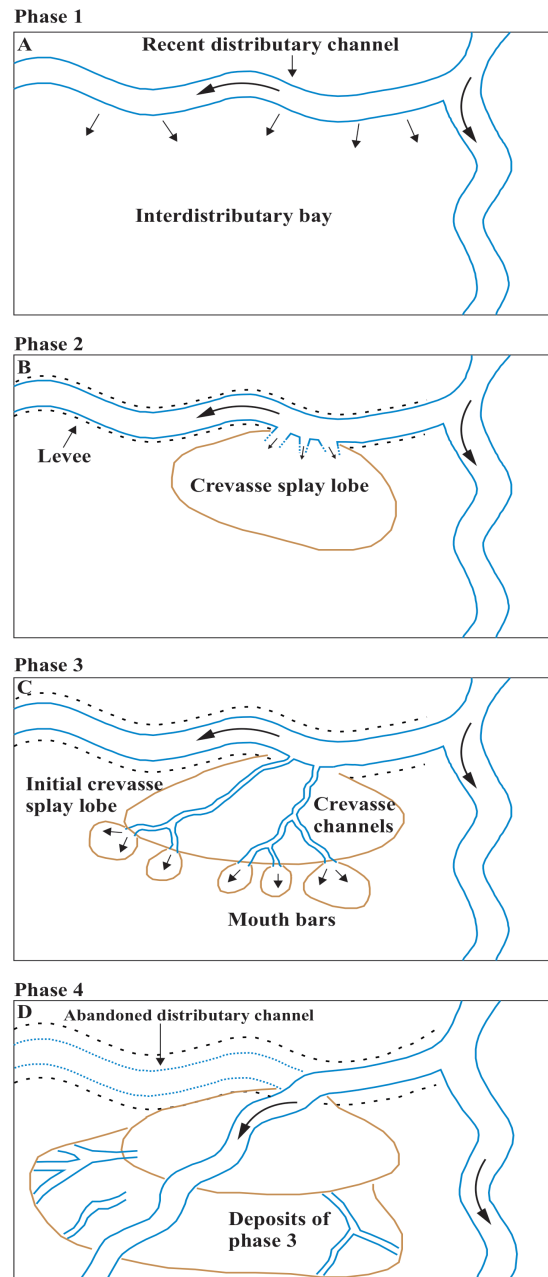


Figure 5.14: A four-step model showing the infilling of an interdistributary bay, with a channel that recently avulsed into the bay. A: Poorly developed levees causing overbank sheet floods to deposit mud in the central parts of the interdistributary bay. B: The distributary channel is more defined due to levees. Parts of levees break during a flood, making a sand-rich crevasse splay lobe. C: When the area adjacent to the river fills in, the gradient between the channel and the bay becomes low. Crevasse channels migrate across the initial splay lobe in «B». D: Levees build up and crevasse channels get permanent. The distributary river may avulse during the next flood event. The figure is modified from Elliott (1974).

5.5 Classification of bayfill units

The described facies associations are interpreted to be deposited within the interdistributary bay area. This sub-chapter contains definitions of the concepts *interdistributary bayfill* and *interdistributary bayfill unit*, followed by an explanation of the classification of the bayfill units.

5.5.1 Definitions

An *interdistributary bayfill* is described as facies associations deposited within an interdistributary bay, formed on a delta plain between distributary channels. This area is situated in a low gradient area open to the sea, often sheltered behind a barrier island (Kjærefjord et al., 2018). Barrier islands protect against wave-energy, causing too low energy in the bay to redistribute the sediments into a linear shoreline. The environment is characterized by the interaction of both wave- and river processes, where river processes build out bayhead deltas and wave processes redistribute the sediments. Factors such as vegetation may affect the degree of reworking and redistribution (Kjærefjord et al., 2018).

An *interdistributary bayfill unit* is defined as a parasequence bounded by allogenic flooding surfaces at its base and top, normally due to changes in sediment supply and/or relative sea-level (Kjærefjord et al., 2021, Accepted). Internal shifting of deltaic lobes may also occur, resulting in autogenic surfaces that can be observed within the bayfill units. The studied sections comprise three vertical stacked interdistributary bayfill units, Bayfill units #1, #2, and #3, from the base upwards. Layers of coal are present between the bayfill units. Coal beds indicate complete infilling of available accommodation space (Kjærefjord et al., 2021, Accepted). The bayfill units display vertical and lateral variability in the environmental setting, expressed by variations in thickness and lithofacies. In general, the thickness and size of a bayfill unit vary with the depth of the bay (Kjærefjord et al., 2018).

5.5.2 Classification

The different facies associations found in the interdistributary bay deposits within the study area are divided into three classes. The classification of bayfill units into sub-bay, bayhead delta, or wave-dominated bayfill used by Kjærefjord et al. (2018) has been approached in this thesis.

As shown in Table 5.2, the lithofacies have different approximate percentages of mudstone. The lithofacies are divided into two main groups, based on the main agent generating the structures: unidirectional currents or oscillatory currents. The structures mainly generated by unidirectional currents are hereafter referred to as current-generated structures, and the ones mainly generated by oscillatory currents are called wave-generated structures (Table 5.2). Note that not all of the lithofacies could be categorized as either wave- or current-dominated.

Table 5.2: Approximate percentage of mudstone in the lithofacies and dominant agent generating the structures in the lithofacies: currents (unidirectional currents) or waves (oscillatory currents).

Lithofacies	1A	1B1	1B2	1C	1D	2A	2A-C	2B	3A
Percentage of mudstone (%)	0	0	0	10	0	50	50	70	100
Current- or wave generated structures	Current	Wave	Wave	Wave	Current	Wave	Current		

Based on the approximate percentage of mudstone in the respective lithofacies (Table 5.2), the dominant depositional process (Table 5.2), and the vertical thicknesses of lithofacies, statistical information was extracted. For every bayfill unit, the total percentage of mudstone and the percentages of current- versus wave-generated structures were calculated. For data extracted from the sedimentary logs, see Appendix I.

The percentage of mud, wave-generated structures, and current-generated structures are plotted in a ternary diagram to classify the facies association either as a sub-bay, bayhead delta, or wave-dominated bayfill (Fig. 5.15) (Kjærefjord et al., 2018). Lithofacies 3B and coal are interpreted as continental and were not considered when doing these calculations. If a bayfill unit contains <60% mud, and >50% of the unit is composed of wave-generated structures, it is characterized as a wave-dominated bayfill (Fig. 5.15). If a bayfill contains <60% mud, and >50% of it consists of current-generated structures, it is considered a bayhead delta (Fig. 5.15). The third category comprises the sub-bay facies association, with a requirement of >60% mud (Fig. 5.15). This classification by Kjærefjord et al. (2018) aims to reflect reservoir properties in a good way, where the acting processes contribute to predicting the facies associations' position. For example, a bayhead delta usually has the best petrophysical properties, containing higher porosity and permeability. In this setting, bayfill units with up to 60% mud can create better reservoirs. 60% mud also turn out to be the value that best separates the facies associations along the margins from those in the middle of a bay. Hence, 60% mud is used to separate the sub-bay from the wave-dominated bayfill and bayhead delta.

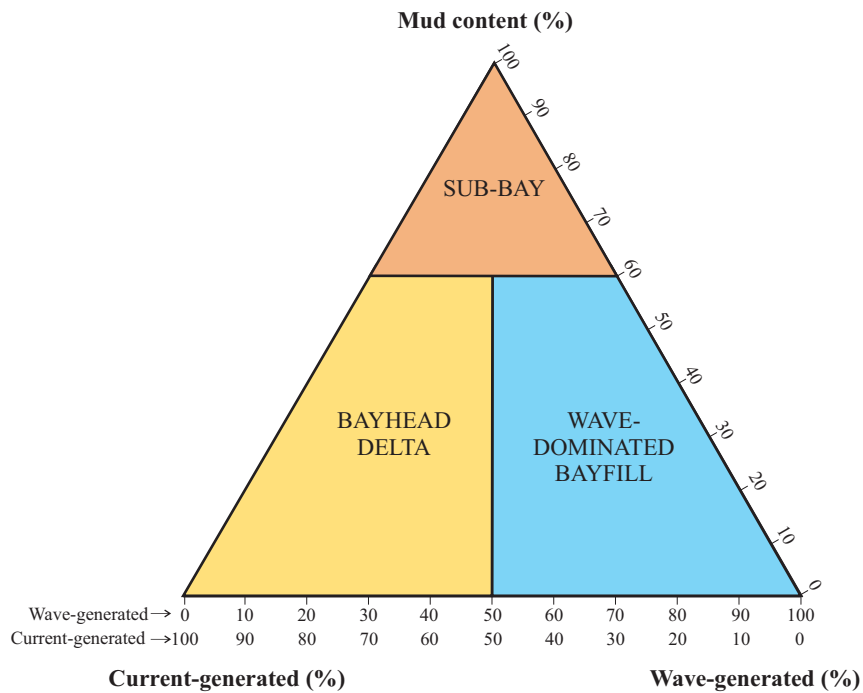


Figure 5.15: Ternary plot showing the classification of a bayfill unit based on the amount of mud (%), the amount of current-generated structures (%), and the amount of wave-generated structures (%).

Further, a specific location of a point in the ternary plot (Fig. 5.15) can represent a position within the interdistributary bay, exemplified in Figure 5.16. In the outer and middle parts of a bay, the wave-dominated bayfill is most common (Kjærefjord, 1999). The wave-dominated bayfill may also occur in inner parts but then often with a higher mud content. Bayhead deltas are commonly closer to distributary channels, therefore dominated by current-generated structures. The amount of current-generated structures in a bayfill unit reflects the proximity to a distributary mouth during deposition. Sub-bays are more protected from waves and currents, and often anoxic, resulting in higher silt- and clay content than the bayhead delta and wave-dominated bayfill.

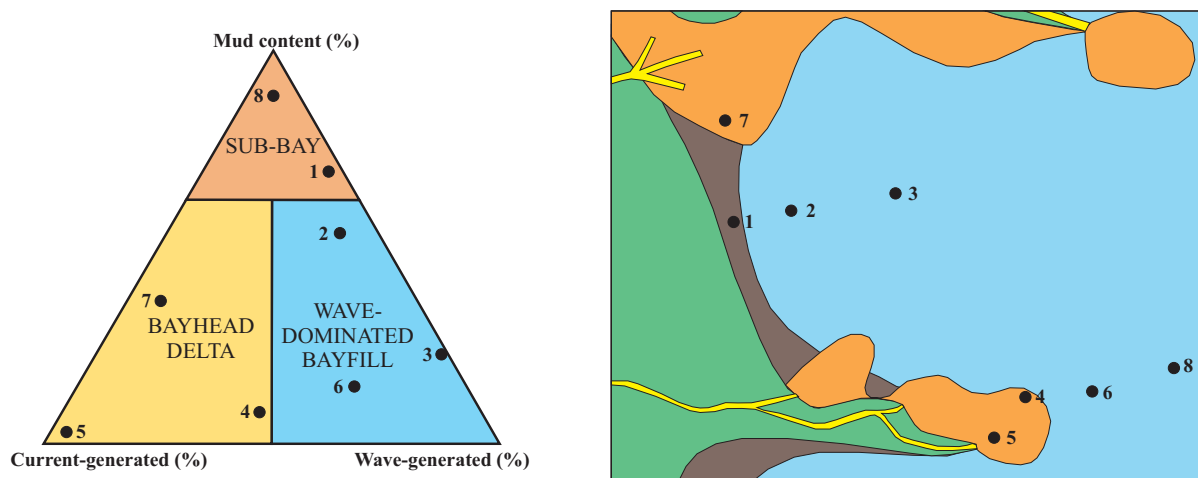


Figure 5.16: Ternary plot showed in Figure 5.15 and a map of an interdistributary bay area. Theoretical numbered points in the ternary plot coincide with the numbered points in the map.

6 Sand- and shale-body geometry

This chapter addresses cross-sections with correlations displaying the spatial distribution of the lithofacies. The cross-sections' vertical intervals are restricted to the area between the channel-fill deposits or organic-rich mudstones in the Lower Neslen Interval at the base and a flooding surface separating the Bayfill #3 and #4 units at the top. The correlation panels are flattened at the flooding surface at the base of the Bayfill #3 unit. Sub-chapters 6.1 and 6.2 describe the vertical and lateral variations of the bayfill units in the study area.

6.1 Vertical variations in geometry

To gain an improved understanding of how the bayfill units vary in facies associations, thickness, and mud content upwards in the succession, this sub-chapter addresses a description of the vertical variations observed between Bayfill units #1, #2, and #3 in the Middle Neslen Interval.

6.1.1 Distribution of facies associations

In total, 56 bayfill units are logged and described, all of them categorized either as a wave-dominated bayfill, bayhead delta, or sub-bay (Fig. 5.6). The bayhead delta facies association is the dominating one, making up 64% of the 56 studied units. The wave-dominated bayfill facies association makes up 25%, whereas the sub-bay facies association makes up 11%. Figure 5.6 shows the distribution of facies associations within each of the bayfill units, demonstrating an upwards increase in the bayhead delta facies association, simultaneously with a decrease in wave-dominated bayfill- and sub-bay facies associations.

6.1.2 Bayfill unit thickness and percentage of mudstone

The thickness of a bayfill unit (Fig. 6.1) indicates available accommodation space during deposition. Periods of limited accommodation cause thinner bayfill units to deposit, whereas periods generating more accommodation contribute to thicker bayfill units. The content of mud (Fig. 6.1) is also an indicator of available accommodation space. Bayfill units with abundant mud reflect more generation of accommodation. This implies that units with less mud are deposited during a period of less available accommodation space.

The average thickness of the bayfill units decreases upwards in the succession (Fig. 6.1). The average percentage of mud within the bayfill units follows the same trend (Fig. 6.1), with a decreasing mud content upwards. The average amount of mud in all the studied bayfill units is

57% in Bayfill #1, 25% in Bayfill #2, and 11% in Bayfill #3 unit, but both the thickness and mud content varies laterally in the study area, as described in Sub-chapter 6.2.

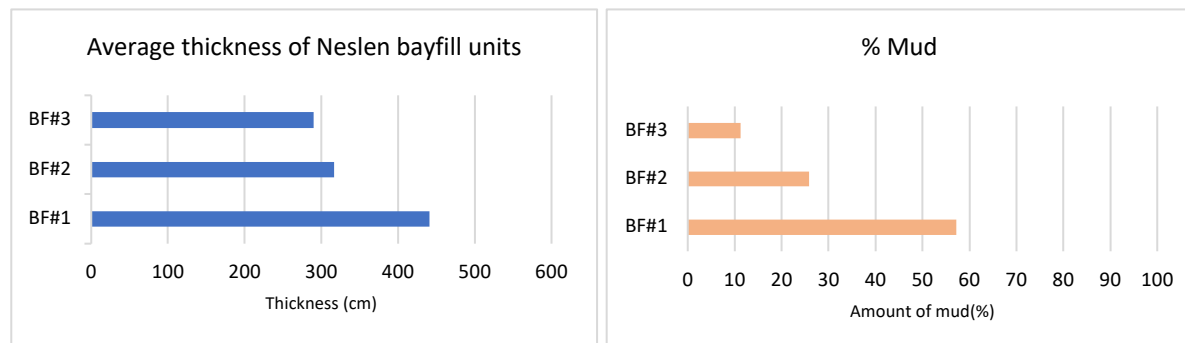


Figure 6.1: Graphs showing the average thickness (cm) and the amount of mud (%) in the Bayfill units #1, #2, and #3. A thick bayfill unit coincides with a high mud content.

6.1.3 Description of bayfill units

The character of the studied bayfill units changes upwards in the vertical succession. As shown in Figures 6.1 and 6.2, the amount of mud in the units decreases upwards in the succession. This sub-chapter addresses a description of the vertical variations of the Bayfill units #1, #2, and #3 in the Middle Neslen Interval.

Most of the Middle Neslen Interval is interpreted as bay- and lagoonal deposits within the study area, with a gradual shift from bay deposition in the west to lagoonal deposition in the east (Kjærefjord et al., 2021, Accepted). This implies that the studied bayfill succession is deposited in a bay sheltered behind barrier island(s) or spit(s). According to Kirschbaum & Hettlinger (2004), equivalent wave-dominated shoreface deposits are present eastwards of the study area, supporting the interpretation of the study area to be located proximal to the coast. Westwards of the study area, there is a gradual shift towards fluvial deposits (Kjærefjord et al., 2021, Accepted). The shift in facies towards east and west supports the suggestion that Neslen Formation generally prograded eastward from the Sevier orogen (Kirschbaum & Hettlinger, 2004). However, Kjærefjord et al. (2021, Accepted) interpret a southwest - northeast orientation of the shoreline in the local study area of this thesis. A description of the overall trends in dominating process and mud content of Bayfill units #1, #2, and #3 follows.

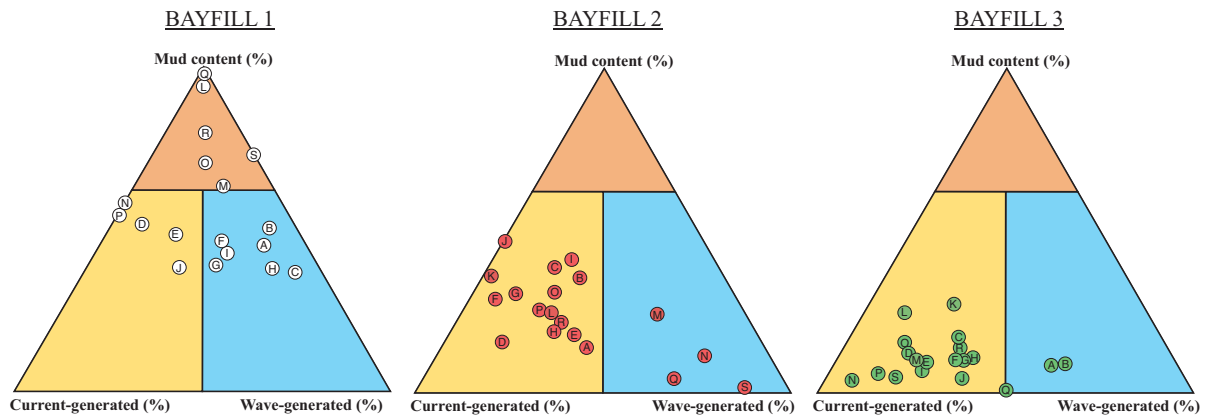


Figure 6.2: Ternary diagrams of Bayfill units #1, #2, and #3, respectively, with plotted values of mud content, current- and wave-generated structures. A decrease in mud content is observed upwards in the succession, and the units become classified more uniformly.

Bayfill #1 unit

Bayfill #1 unit is the only unit where the sub-bay facies association is interpreted (Fig. 6.2). The facies associations are more evenly distributed than in the overlying units (Fig. 6.2). In the northern part of the study area, which includes Neslen Canyon, East Canyon Window, and Keane Creek (logs K - S), the mud content is greater than in the Outer East Canyon and Exit Canyon (logs A - J) (Figs. 1.1 and 1.2). This can indicate that the northern part was located in a calmer area, more sheltered from waves and currents. Locations N and P in East Canyon Window (Fig. 1.2) are interpreted as a bayhead delta, suggesting proximity to a river mouth in an otherwise sub-bay environment area. The southern area was exposed to wave-reworking to a greater degree (Fig. 6.2). Outer East Canyon is wave-dominated, as well as logs F - I in Exit Canyon (Fig. 1.2). Locations D, E, and J in Exit canyon (Fig. 1.2) are interpreted as bayhead delta.

Bayfill #2 unit

The unit is dominated by bayhead delta facies association, with an overall low amount of mud compared to Bayfill #1 unit (Fig. 6.2). This means that during the Bayfill #2 unit deposition, the environment was more actively transporting sand-rich sediments, for example through crevasse channels extending into interdistributary bays. Logs M, N, Q, and S in the northern part of the study area (Fig. 1.2) are characterized as wave-dominated bayfill facies association (Fig. 6.2). This means that the surrounding area (Keane Creek, East Canyon Window, Neslen Canyon) (Fig. 1.1) was located close to the transition between a bayhead delta and a more wave-dominated bayfill, probably in the middle parts of a bay.

Bayfill #3 unit

Facies associations interpreted within Bayfill #3 unit show less spread in the ternary diagram (Fig. 6.2) than Bayfill units #1 and #2, and the mud content and dominating process seem to be more uniform along the unit. The mud content is lower in the Bayfill #3 unit (Fig. 6.2). This could be a consequence of deposition close to a river mouth actively transporting sand-rich sediments. Bayfill #3 unit is interpreted to have been fed from a bayhead delta in the northern part of the study area (logs K - S) and another bayhead delta covering major parts of the southern area (logs A - J) (Fig. 1.2). Logs A and B in Outer East Canyon (Fig. 1.2) are interpreted as wave-dominated bayfills. Deposition close to the channel mouth, in the middle of a bay, where some wave-reworking occurs, is suggested for logs A and B.

6.2 Lateral variations in geometry

This sub-chapter addresses descriptions of the lateral variations of the Bayfill units #1, #2, and #3 in the Middle Neslen Interval and the upper part of the Lower Neslen Interval, intending to improve our understanding of the spatial distribution of lithofacies.

The Lower Neslen Interval is described from the top downwards because it is expected that the uppermost meters are the most important regarding the development of the overlying bayfill units. This is due to a higher degree of early compaction in the upper meters. However, the following Middle Neslen Interval is described from the base upwards.

6.2.1 Outer East Canyon

Outer East Canyon is located in a steep area with good exposures of both channel-fill deposits and bayfill units. The three logs (A, B, C) (Fig. 1.2) are positioned along a ~150 m long, north-south trending transect (Fig. 6.3). Log C is more detailed than logs A and B in the Lower Neslen Interval due to varying original logging scales.

Lower Neslen Interval

The northern- and southernmost logs have thick channel-fill deposits present below the bayfill units, while the middle log has thinner sandstone packages (Fig. 6.3). The northern log (A) has two ~2.6 m thick sandstone packages below the bayfill units, one just below and the other ~6 m below. The two channel-fill deposits are separated by thinner, more laterally extensive deposits of current-rippled sandstones and heteroliths (Lithofacies 1D, 2A-C), as well as a layer of organic-rich mudstone (Lithofacies 3B). In the middle log (B), there is an alternation between 20 - 80 cm thick organic-rich mudstones and 20 - 80 cm thick sandstones with current-ripple

cross-lamination. Several of the sandstones are pinching out laterally. The southernmost log (C) has a ~4 m thick channel-fill deposit below the bayfill units. Below is a 23 cm thick interval of organic-rich mudstone, followed by a ~2.6 m thick channel-fill deposit with marsh deposits below. The observed channel-fill deposits have thin beds (2 - 12 cm) of finer-grained material associated with lateral accretion surfaces (Fig. 6.3). Due to different scales used during logging, such small beds (<20 cm) fall below the scale in logs A and B.

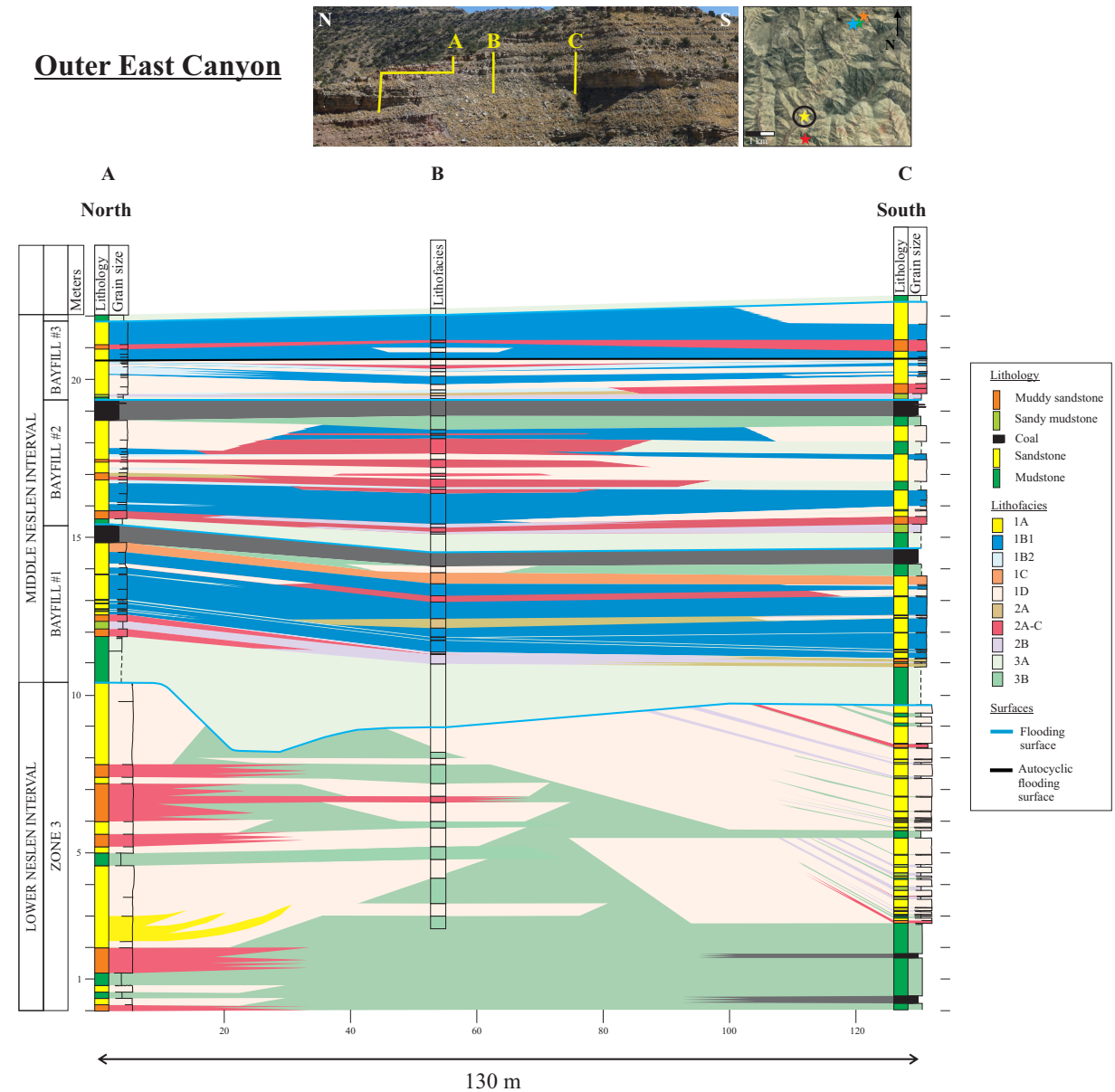


Figure 6.3: Correlation panel of the logged vertical sections A, B, and C in the Outer East Canyon. See Figure 1.2 for position of logs. Note that the ratio between the lateral- and horizontal scale is 1:5. Correlation is based on all observed lithofacies. The upper left photo shows the area of the logged sections, with yellow as logging paths. For full-size photo of the outcrop, see Appendix III. The upper right photo shows where the canyon is located in the study area (© Google Earth 2020).

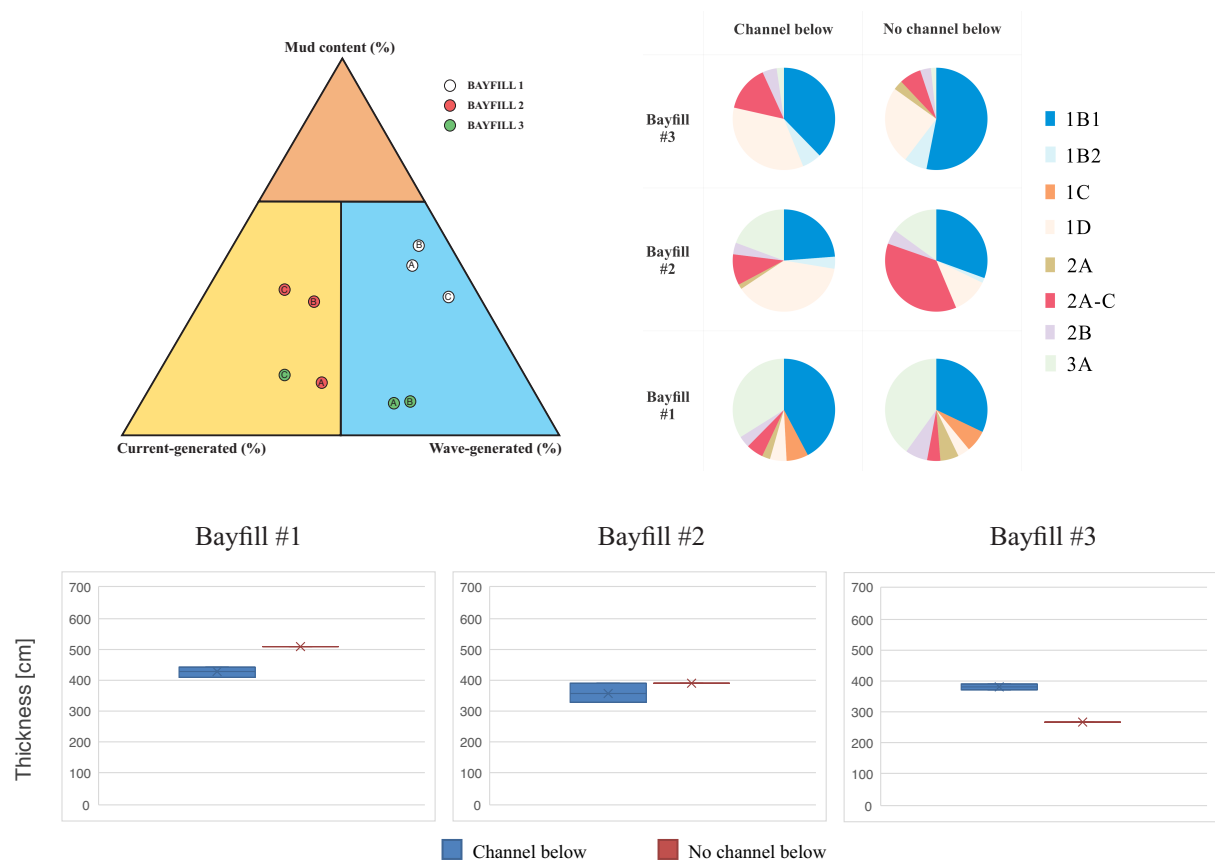


Figure 6.4: Figures summarizing the characteristics of the bayfill succession in logs A, B, and C in Outer East Canyon. See Figure 1.2 for position of logs. Ternary diagram with plotted values of mud content, current- and wave-generated structures within Bayfill units #1, #2, and #3. Pie charts showing the lithofacies distribution within the Bayfill units #1, #2, and #3. Box Whisker plots showing comparisons of the bayfill unit thicknesses above a sandstone-rich channel-fill deposit (blue), and the unit thicknesses above finer-grained materials (red), in Bayfill units #1, #2, and #3, respectively.

Bayfill #1 unit description

The lower part of the unit comprises a mudstone interval, which is thicker in log B (Fig. 6.3). Above this unit, a southward thinning heterolithic interval is observed from A (70 cm) to C (25 cm). This heterolithic interval translates from current-ripple- to wave-ripple cross-laminated from log A to C.

Above, a ~2 m thick hummocky cross-stratified sandstone (Sub-facies 1B1) interval is present, with several thin mudstone-rich layers (Fig. 6.3). One of the mudstone layers in log C is inclined with an apparent dip of $\sim 0.15^\circ$ towards the north. Above, two 20 - 30 cm thick wavy bedded heteroliths are observed in log B. One of them constitutes a northward dipping clinof orm surface with an apparent dip of $\sim 0.15^\circ$. The other one correlates to current-ripple cross-laminated sandstone layers towards the north and south. A bioturbated sandstone bed (~ 30 cm) (Lithofacies 1C) is capping the hummocky cross-stratified sandstone interval (Fig. 6.3). Above, log B comprises a current-ripple cross-laminated sandstone interval, whereas logs A and C have marsh deposits.

The thickness of the unit varies along the transect. Log B has a thicker unit (509 cm) than logs A (445 cm) and C (409 cm). A higher percentage of mudstone is also observed in log B (51%), compared to A (45%) and C (37%). The total amount of wave-generated structures increases from 78% in log A to 88% towards log C (Fig. 6.4). The Bayfill #1 unit is interpreted as a wave-dominated bayfill in all three logs, as shown in the ternary plot (Fig. 6.4)

Bayfill #1 interpretation

The Bayfill #1 unit thickness may be associated with early compaction in Lower Neslen Interval, as the unit thickness is inversely correlated with the thickness of the sandstone-rich channel-fill deposit below. Hence, it can be inferred that more early compaction takes place in the inter-channel mudstones (log B) than in the channel-fill sandstones (logs A and C) in the Lower Neslen Interval, providing deeper water above the inter-channel mudstones (Fig. 6.3). The mudstone interval in the lower part has the greatest thickness variations. This suggests that the finer-grained material in Bayfill #1 unit consumes most of the bathymetrical variations generated by early differential compaction in Lower Neslen Interval. As the mudstone is interpreted as deposited from suspension, hence as mud drapes, the mud was probably extracted from suspension by currents (e.g., bayhead delta currents, crevasse currents, tidal currents). The clinofolds indicate progradation towards the north. The northward thickening trend of the heterolithic interval suggests that the energy level decreases gradually towards the north. Log B is therefore interpreted to be located in a deeper part of the bay compared to log A. Observed current-ripple cross-laminated sandstone could represent the fringe of a bayhead delta. The vertical lithofacies distribution in log A with dominating hummocky cross-stratified sandstone in the middle and upper parts seems to reappear in log C. Just below the capping coal bed in log B, a crevasse channel-fill is interpreted. Consequently, the Bayfill #1 unit thickness and lithofacies distribution seem to be highly affected by the sand content in Lower Neslen Interval, with the thickness variations mainly observed in the finer-grained material.

Bayfill #2 unit description

A mudstone bed thinning from log B (58 cm) towards logs A (19 cm) and C (49 cm) is present at the base of the Bayfill #2 unit (Fig. 6.3). Above, there is a heterolithic interval with a thickening trend and increasing mud content from log A to C. Sandstone with wave-generated structures dominate the next ~1 m, but log C displays a northward prograding unit of current-ripple, cross-laminated sandstone within this interval.

Upwards in the unit, log A comprises thin beds of current-ripple cross-laminated sandstone (Fig. 6.3). In this interval, log B has rapid vertical alternation between heteroliths and sandstones with current-generated structures. Towards log C, those heteroliths translate into mudstones. Logs A and C exhibit prograding sandstone packages with current-generated structures in the uppermost part, whereas log B displays hummocky cross-stratified sandstone.

Bayfill #2 unit is at its thickest in log B (389 cm) and is thinning towards log A (331 cm) (Fig. 6.3). From north to south, there is a gradual increase in structures generated by current-processes, from 55% to 71% (Fig. 6.4), and the amount of silt and clay also increases from 15% to 39%. A bayhead delta is interpreted in Bayfill #2 unit within all the logs in the area, shown in the ternary diagram (Fig. 6.4).

Bayfill #2 unit interpretation

The unit thickness is greater where the Lower Neslen Interval contains less sandstone, but the thickness variations are minor compared to Bayfill #1 unit (Fig. 6.4). The mudstones at the base show more significant thickness variations compared to the deposits above. This implies that the mudstones consume most of the thickness variations created by early differential compaction. Prograding current-ripple cross-laminated sandstones from logs A and C suggest that a bayhead delta builds out into a more wave-influenced bay. The higher amount of heteroliths in log B can be explained by a greater distance from a prograding bayhead delta. Consequently, Bayfill #2 unit thickness is inversely correlated to the channel-fill thickness in Lower Neslen Interval, and the lithofacies distribution shows more heterolithic bedding above inter-channel mudstones.

Bayfill #3 unit description

The base of Bayfill #3 unit comprises mudstones and heteroliths thickening from log A (18 cm) to C (52 cm) (Fig. 6.3). Wave-dominated heteroliths are present in log B and current-dominated heteroliths in log C. Above, there is a ~1 m thick interval with current-ripple cross-laminated heteroliths and sandstones. A ~20 - 30 cm thick wave-dominated sandstone interval indicates coexistence of wave- and current processes. Above, clinoforms are building out from the north with an apparent dip of $\sim 0.53^\circ$. A sharp transition into a ~1 - 2 m thick hummocky cross-stratified sandstone interval follows. This uppermost layer contains a northward thinning heterolithic bed (Fig. 6.3). Log B also has a thin (14 cm) current-ripple cross-laminated sandstone layer within this interval, whereas log C has a 71 cm thick, prograding current-ripple cross-laminated sandstone interval in the uppermost part.

There are slightly more current-generated structures in log C compared to A and B. The mud content is somewhat uniform along the transect, ranging from 9 - 15% from A to C (Fig. 6.4). The thickness of the unit increases from log A (250 cm) towards B (270 cm) and C (311 cm), and the amount of silt and clay is higher in log C than in logs A and B (Figs. 6.3 and 6.4). The ternary plot (Fig. 6.4) shows that the two northernmost logs (A and B) are classified as wave-dominated bayfill and the southernmost log (C) as a bayhead delta.

Bayfill #3 unit interpretation

A positive correlation is found between unit thickness, abundance of current-generated structures, and amount of silt and clay. As the observed clinoforms are dipping towards the south, it is suggested that log B was positioned farther out in the bay compared to log A. The 71 cm thick current-ripple cross-laminated sandstone at the top of log C may indicate progradation of a bayhead delta.

A possible autogenic flooding surface is interpreted at the sudden transition from the current- to the wave-dominated sandstone interval because of the lateral extension of this approximately horizontal surface (Fig. 6.3). It is formed by delta lobe switching or distributary channel avulsion, causing wave processes to dominate and redistribute the sediments. As shown in the Box Whisker plot (Fig. 6.4), the Bayfill #3 unit's potential to obtain thickness variations caused by early differential compaction in Lower Neslen Interval seems to be depleted by Bayfill units #1 and #2. Lithofacies distribution varies laterally, but as log C stands out, the lithofacies distribution of Bayfill #3 unit is less affected by early differential compaction in Lower Neslen Interval.

6.2.2 Exit Canyon

Exit Canyon comprises seven logs in total (Figs. 1.2 and 6.5). Logs D, E, F, G, and H, are placed along a ~300 m west-east trending transect. This transect is perpendicular to a ~60 m north-south trending transect, including logs I and J (Fig. 6.5).

Lower Neslen Interval

In general, the presence of sandstone-rich channel-fill deposits below the bayfill units varies (Fig. 6.5). Logs D, E, and F have thin sandstone beds (20 - 60 cm) underneath and are characterized as not having channel-fill deposits in Lower Neslen Interval. Log I comprises a 2.6 m thick channel-fill deposit 2.8 m below, which is a lateral pinch-out of a channel-fill deposit observed in log J. Due to the relatively thin thickness of this sandstone interval, it is

characterized as not having channel-fill deposits in Lower Neslen Interval. The two logs G and H have thick channel-fill deposits (1.6 - 2.6 m) just below Bayfill #1 unit and 2.4 - 6 m thick channel-fill deposits 3.4 - 5.2 m below. Log J has three thin (20 - 40 cm) sandstone beds in the six first meters below the bayfill units and a 5 m thick channel-fill deposit beneath. Consequently, logs G, H, and J are interpreted as having channel-fill deposits underneath the bayfill succession.

As several of the Exit Canyon logs have channel-fill deposits that are placed up to several (~6) meters below the bayfill units (Fig. 6.5), this cross-section allows studying how early differential compaction of deeper deposits affects the bayfill units as the effect of early compaction decreases upwards in the succession (Sub-chapter 7.2).

Exit Canyon

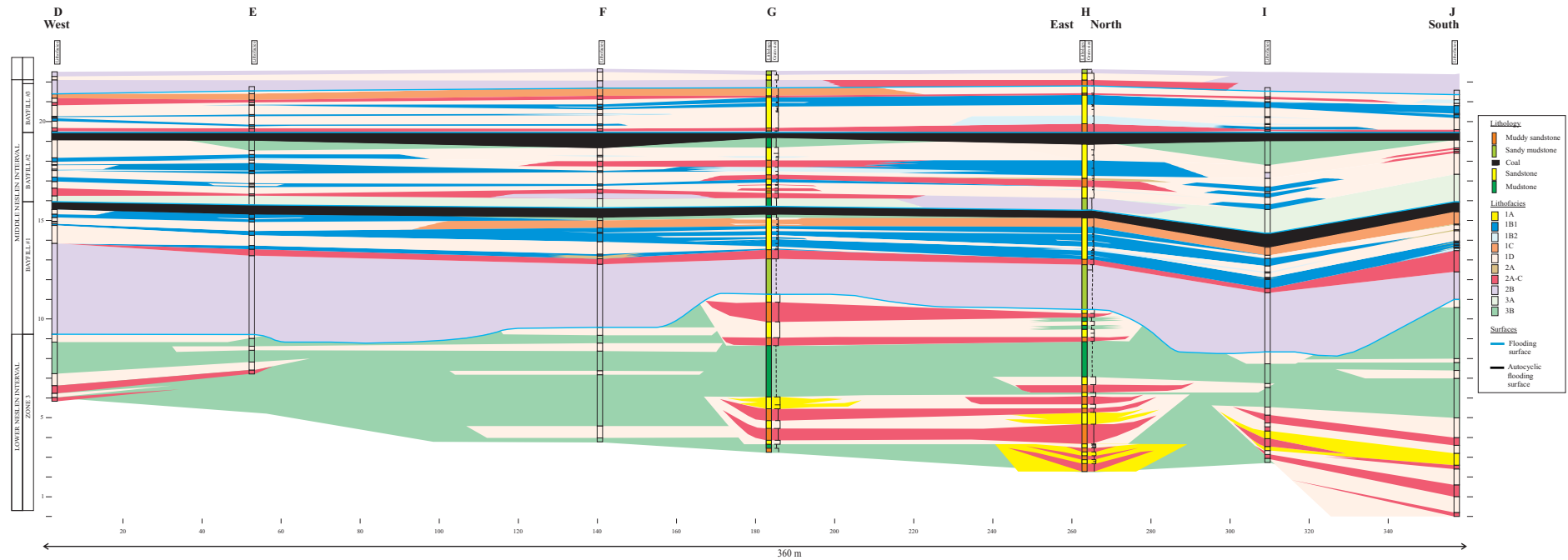
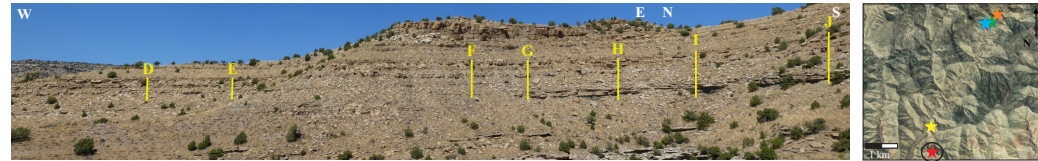


Figure 6.5: Correlation panel of the logged vertical sections D, E, F, G, H, I, and J in the Exit Canyon. See Figure 1.2 for position of logs. Note that the ratio between the lateral- and horizontal scale is 1:5. Correlation is based on all observed lithofacies. The upper left photo shows the area of the logged sections, with yellow as logging paths. For full-size photo of the outcrop, see Appendix III. The upper right photo shows where the canyon is located in the study area (© Google Earth 2020).

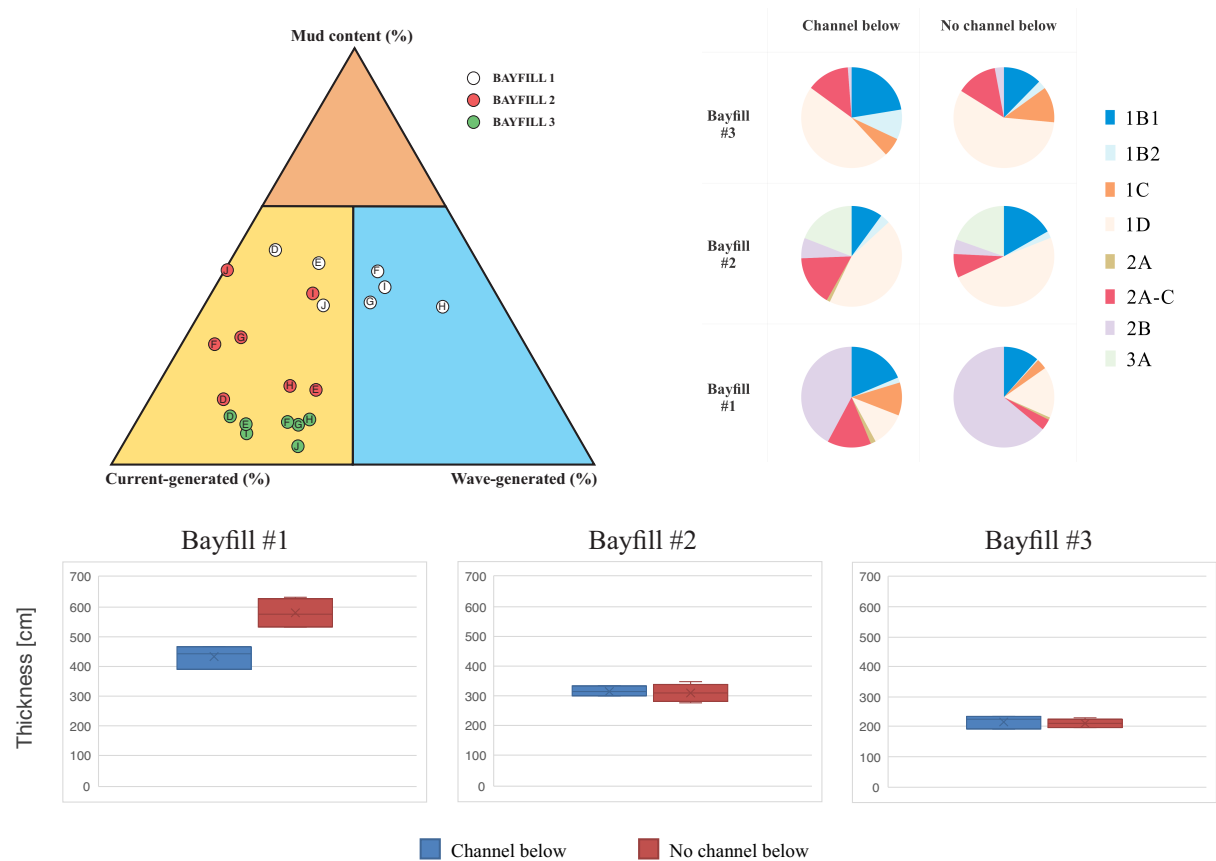


Figure 6.6: Figures summarizing the characteristics of the bayfill succession in logs D, E, F, G, H, I, and J in Exit Canyon. See Figure 1.2 for position of logs. Ternary diagram with plotted values of mud content, current- and wave-generated structures within Bayfill units #1, #2, and #3. Pie charts showing the lithofacies distribution within the Bayfill units #1, #2, and #3. Box Whisker plots showing comparisons of the bayfill unit thicknesses above a sandstone-rich channel-fill deposit (blue), and the unit thicknesses above finer-grained materials (red), in Bayfill unit #1, #2, and #3, respectively.

Bayfill #1 unit description

Bayfill #1 unit is characterized by a lenticular bedded heterolithic interval (Lithofacies 2B) at the base (Fig. 6.5). In logs D, E, F, and I, this interval is thicker (3.2 - 4.6 m) than in logs G, H, and J (2.3 - 2.5 m). The six easternmost logs are followed by a 0.2 - 1.1 m thick wavy bedded heterolith with current-ripple cross-lamination (Lithofacies 2A-C).

The following sandstone interval has a uniform thickness (Fig. 6.5). Thick (<92 cm) current-ripple cross-laminated sandstones (Lithofacies 1D) separated by thinner (6 - 20 cm) hummocky cross-stratified sandstone beds (Sub-facies 1B1) characterize logs D, E, and J (Fig. 6.5). Logs F - I are dominated by hummocky cross-stratified sandstone with thinner beds of current-ripple cross-laminated sandstones. Bioturbated sandstone characterizes the upper part of the bayfill unit in logs F - J, whereas logs D - E contain sandstones with current-ripple cross-lamination and hummocky cross-stratification.

The three logs (G, H, and J) with the thickest sandstones in the Lower Neslen Interval have the thinnest successions (389 - 464 cm) and the lowest mud content (38 - 39%) (Fig. 6.6). Logs D, E, F, and I are 531 - 632 cm thick, containing more mud (43 - 51%). An overall increase in abundance of wave-generated structures is observed from log D - H, followed by a decrease from log H - J. Pie charts (Fig. 6.6) show that Bayfill #1 unit contains less lenticular bedded heteroliths in areas where the channel-fill deposits are present in Lower Neslen Interval (Logs G, H, and J). Shown in the ternary plot (Fig. 6.6), a bayhead delta is interpreted in logs D, E, and J, and a wave-dominated bayfill is interpreted for logs F, G, H, and I.

Bayfill #1 unit interpretation

The prograding sandstone packages in logs D - F and J suggest a bayhead delta building out both from the west towards the east (Log D) and from the south towards the north (Log J). Northward dipping clinofolds support progradation towards the north.

Logs G and H, with the thinnest units, the highest sand fraction, and the abundant wave-generated structures, suggest that shallow parts of the bay were more affected by waves. As the thickness of the sandstone interval is uniform along the transect, it can be inferred that the lenticular bedded heterolith consumes most of the thickness variations created by early differential compaction. This implies that a current generated by a bayhead delta channel, a crevasse channel, or a tidal channel, took the finer-grained material out of suspension to distribute it and fill the topography. The unit thickness coincides with the fraction of sandstone in Lower Neslen Interval. Hence, the Bayfill #1 unit thickness is inversely correlated to the channel-fill thickness, even at the positions where the thick channel-fill deposits are several meters below the bayfill units. Lithofacies distribution somewhat reflects the composition of Lower Neslen Interval, as the Bayfill #1 unit contains less mud with the presence of channel-fill deposits.

Bayfill #2 unit description

A mudstone layer (Lithofacies 3A) is present in the lower part of the Bayfill #2 unit, thickening from log D to J (Fig. 6.5). Log H comprises lenticular bedded heteroliths in this interval. The upper part of the mudstone layer gradually translates into heteroliths in logs D - G.

Sandstones dominate the interval above (Fig. 6.5). From log D to E, there is an increase in the abundance of hummocky cross-stratified sandstone. In logs F and G, current-ripple, cross-laminated wavy bedded heteroliths are abundant, with a gradual decrease against log H. Log I

is dominated by current-ripple cross-lamination with interbeds of hummocky cross-stratification. In contrast, log J more or less comprises current-ripple cross-lamination with no hummocky cross-stratified interbeds.

Above, a layer of organic-rich mudstone (Lithofacies 3B) is present in logs E, G, and I. Logs F and H have a relatively thick coal bed compared to the remaining, explaining their lack of organic-rich mudstone. Log I has a 123 cm thick layer of organic-rich mudstone. There is uncertainty related to the sedimentary description of this interval, as it is partly covered.

The pie charts (Fig. 6.6) show that units positioned above a channel-fill deposit contain more current-ripple, cross-laminated wavy bedded heterolith, and less hummocky cross-stratified sandstone than the logs above inter-channel mudstones. The ternary plot (Fig. 6.6) displays scattered results regarding mud content and dominating depositional process. The four most western logs (D - G) display an eastward increase in abundance of mud, and logs I and J stand out with a higher mud content. Bayfill #2 unit is in Exit Canyon interpreted as a bayhead delta (Fig. 6.6).

Bayfill #2 unit interpretation

Logs D, F, G, and J were possibly positioned closer to a prograding bayhead delta, whereas logs E, H, and I were placed farther out in the bay, where wave processes contribute to the reworking of sediments. As no clinofolds are observed within Bayfill #2 unit, the cross-section may be oriented along the strike of the clinofold surfaces. Plotting of the logged units within the ternary diagram and the Box Whisker plot (Fig. 6.6) is not correlatable with the presence of channel-fill deposits in Lower Neslen Interval. As Bayfill #1 unit thickness was affected by early differential compaction in Lower Neslen Interval, it can be inferred that underlying strata partly deplete the potential of compaction.

Bayfill #3 unit description

The unit has a thin (<8 cm) layer of lenticular bedded heteroliths in the lower part, followed by current-ripple, cross-laminated wavy bedded heteroliths (8 - 44 cm) (Fig. 6.5). The sandstone interval above is characterized by current-ripple cross-lamination in logs D - F, and hummocky cross-stratification in logs G - J (Fig. 6.5). Logs D - G is characterized by heavily bioturbated sandstone in the upper part, whereas logs H - J contain current-ripple cross-laminated sandstone.

In the ternary diagram (Fig. 6.6), the seven logs plot with a narrow spread in mud content (4 - 16%) and dominating depositional process (60 - 79% current processes). The Bayfill #3 unit thickens (196 - 236 cm) from log D to H and thins (236 - 192 cm) from H to J. Generally, the lithofacies distribution exhibits abundant wave-generated structures in the logs where a channel-fill deposit is present in Lower Neslen Interval (Fig. 6.6). Figure 6.6 shows that Bayfill #3 unit is interpreted as a bayhead delta in the seven logs.

Bayfill #3 unit interpretation

The higher amount of current-generated structures in logs D, E, F, and I is associated with more current-processes acting at the bayhead delta. This means that logs G, H, and J, which were more exposed to wave-reworking, were located farther out in the bay. As more hummocky cross-stratification is observed in the logs where a channel-fill deposit is present below, the lithofacies distribution can be related to the presence of channel-fill deposits in Lower Neslen Interval. The Box Whisker plot (Fig. 6.6) shows that the Bayfill #3 unit thickness is independent of the sandstone fraction in Lower Neslen Interval, as there are little thickness relation between the logs situated above channel-fill deposits and the ones above inter-channel mudstones.

6.2.3 Keane Creek

The three logged sections (K, L, M) in Keane Creek are located along a ~100 m transect, trending west-east (Figs. 1.2 and 6.7). Logs K, L, and M are located from west eastwards. The Lower Neslen Interval and Bayfill #1 unit were not logged at location K due to availability.

Lower Neslen Interval

A channel-fill deposit is located just below Bayfill #1 unit in the eastern log (log M) (Fig. 6.7). The channel-fill deposit is ~4.2 m thick in log M. Log L only has a ~1.2 m thick lateral pinch-out/channel margin in Lower Neslen Interval (Fig. 6.7). The westernmost log (K) was not logged at Lower Neslen Interval depth. Therefore, the log K is not incorporated in the comparisons regarding sandstone fraction in Lower Neslen Interval and overlying unit thickness and lithofacies distribution.

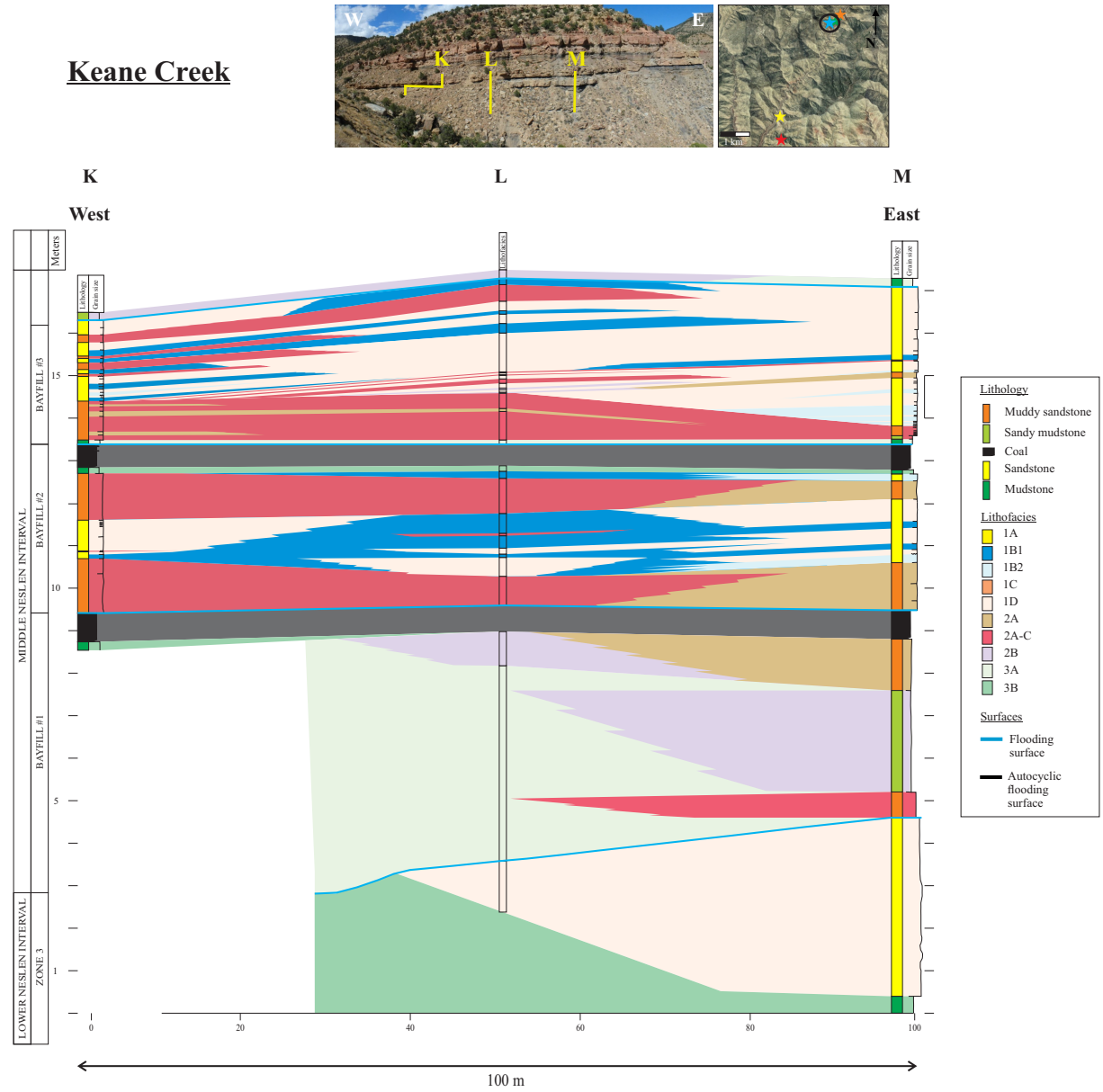


Figure 6.7: Correlation panel of the logged vertical sections K, L, and M in the Keane Creek. See Figure 1.2 for position of logs. Note that the ratio between the lateral- and horizontal scale is 1:5. Correlation is based on all observed lithofacies. The upper left photo shows the area of the logged sections, with yellow as logging paths. Outcrop photo: Jostein Kjærefjord. For full-size photo of the outcrop, see Appendix III. The upper right photo shows where the canyon is located in the study area (© Google Earth 2020).

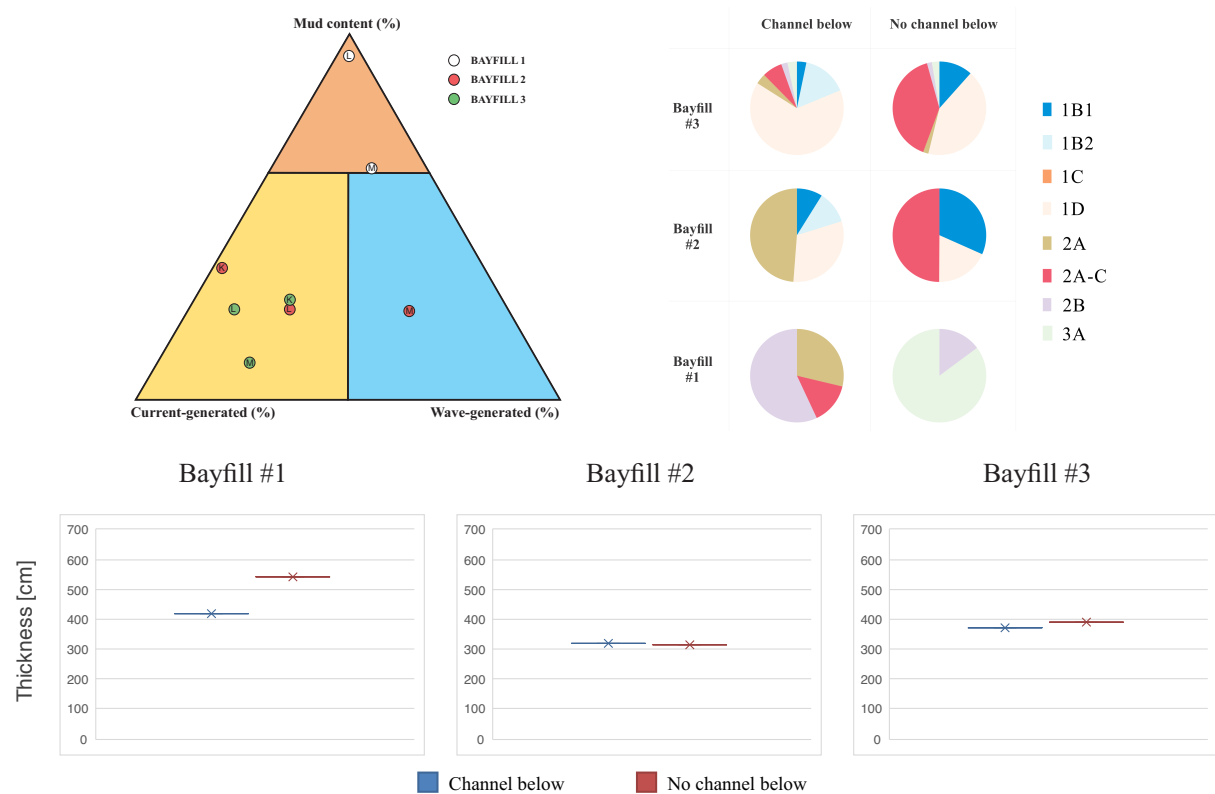


Figure 6.8: Figures summarizing the characteristics of the bayfill succession in logs K, L, and M in Keane Creek. See Figure 1.2 for position of logs. Ternary diagram with plotted values of mud content, current- and wave-generated structures within Bayfill units #1, #2, and #3. Pie charts showing the lithofacies distribution within the Bayfill units #1, #2, and #3. Box Whisker plots showing comparisons of the bayfill unit thicknesses above a sandstone-rich channel-fill deposit (blue), and the unit thicknesses above finer-grained materials (red), in Bayfill unit #1, #2, and #3, respectively.

Bayfill #1 unit description

The Bayfill #1 unit comprises mudstones (Lithofacies 3A) and heteroliths (Lithofacies 2A, 2A-C, 2B) (Fig. 6.7). Log L has a 4.6 m thick mudstone package (Lithofacies 3A) followed by 80 cm of lenticular bedded heteroliths (Lithofacies 2B). Heteroliths predominates in log M, with current-ripple cross-lamination (Lithofacies 2A-C) at the base. Above, lenticular bedded heteroliths (Lithofacies 2B) are present, followed above by wave-ripple, cross-laminated wavy bedded heteroliths (Lithofacies 2A).

The Bayfill #1 unit thins eastward (540 - 421 cm) (Fig. 6.7), and the mud content decreases eastward (96 - 61%) (Fig. 6.8). Log L shows no dominant process, while log M is dominated by wave-processes (Fig. 6.8). Bayfill #1 unit is interpreted as a sub-bay in logs L and M (Fig. 6.8).

Bayfill #1 unit interpretation

A bayhead delta was likely feeding the sub-bay from the east, as log M contains coarser material with more current-generated structures. There is a positive correlation between the unit thickness and the unit's mud content. This could be associated with the presence of a channel-

fill deposit in Lower Neslen Interval, as a deeper area of the bay was generated in log L due to early differential compaction (Fig. 6.7).

Bayfill #2 unit description

A cross-laminated wavy bedded heterolithic layer (70 - 128 cm) predominates in the lower part of the Bayfill #2 unit, with wave-ripples in log M and current-ripples in logs K and L (Fig. 6.7). The next interval is sandstone-dominated, with prograding current-ripple cross-lamination in logs K and M, and hummocky cross-stratification in log L. Logs L and M exhibit similar thickness of the sandstone unit, and log K has a thinner sandstone unit.

The upper part of the bayfill unit is heterolithic, with current-ripple, cross-laminated wavy bedding in logs K and L, prograding above wave-ripple, cross-laminated wavy bedding in log M. This heterolithic unit is thinning towards the east. Above, the two easternmost logs comprise a 16 cm thick layer of wave-generated structures.

An increase in wave-generated structures (3 - 69%) and a decrease in the content of silt and clay (36 - 24%) are observed towards the east (Fig. 6.8). Log L has more hummocky cross-stratified sandstones and current-ripple, cross-laminated wavy bedded heteroliths compared to log M. The thickness variations are minor along the transect (± 11 cm). In Bayfill #2 unit, a bayhead delta is interpreted in the two most western logs (K and L), and a wave-dominated bayfill is interpreted at the easternmost log (M) (Figs. 6.7 and 6.8).

Bayfill #2 unit interpretation

The observed trends show higher mud content in the bayhead delta than in the wave-dominated bayfill. Overall, the amount of current-generated structures increases towards the east. Thus, it can be inferred a gradually increasing distance from a feeding bayhead delta towards the east. As log M also contains smaller, prograding sandstone packages, there might be a bayhead delta building out from the east as well, likely to be smaller or at a greater distance from log M. There may be a relation between the presence of a channel-fill deposit in Lower Neslen Interval and the lithofacies distribution as a thin channel-fill deposit correlates to abundant current-generated structures. Nevertheless, the channel-fill thickness within Lower Neslen Interval does not seem to impact Bayfill #2 unit thickness in Keane Creek significantly.

Bayfill #3 unit description

The lower part of the Bayfill #3 unit consists of a 10 - 12 cm layer of mudstone followed by a heterolithic layer, thinning from logs K (92 cm) and L (112 cm) towards M (32 cm) (Fig. 6.7).

Above, eastward thinning wave-ripple, cross-laminated wavy bedded heterolithic intervals are observed in log M. The next interval is sandstone-dominated, with an increase in thickness towards the east. This interval comprises heterolithic clinoforms building out from the east, also seen on the upper left photo in Figure 6.7. The apparent dip of the clinoforms is $\sim 1^\circ$ towards the west. In the upper part, an increase in current-ripple cross-laminated sandstones and a decrease in hummocky cross-stratified sandstones are observed from log K to M.

Total unit thickness is greater in log L (390 cm) than logs K (292 cm) and M (370 cm). The ternary diagram (Fig. 6.8) indicates a decrease in mud content towards the east. Pie charts (Fig. 6.8) show that log M has a high content of sandstones with current-ripple cross-lamination and low content of heteroliths with current-ripple cross-lamination. The logged units are interpreted as a bayhead delta (Fig. 6.8).

Bayfill #3 unit interpretation

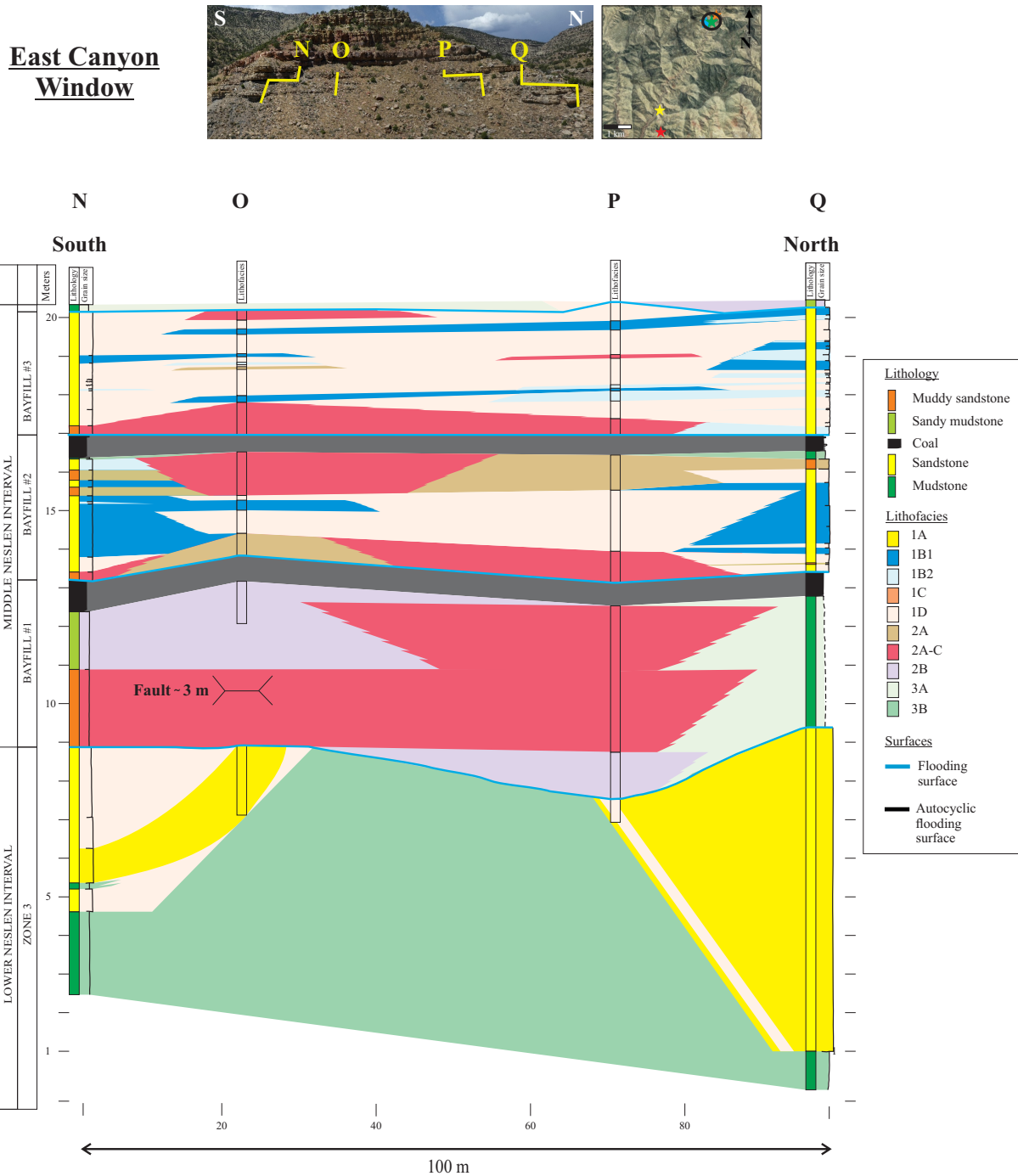
The wave-ripple, cross-laminated sandstone lenses in log M may be associated with fair-weather waves reworking the sediments. Due to the westward dipping clinoforms, a bayhead delta building out from the east is suggested. The increased wave-reworking towards the west supports the interpretation, as more distal parts would be more exposed to wave-processes. The mud content is noticeably lower where the channel-fill deposit is thicker, and the Box Whisker plot (Fig. 6.8) demonstrates that the unit thickness is inversely correlated to the Lower Neslen Interval channel-fill thickness. This implies that in Keane Creek, early differential compaction still can have a small effect on the unit thickness even after 8 - 9 m (Figs. 6.7 and 6.8).

6.2.4 East Canyon Window

The East Canyon Window area is faulted, causing the stratigraphy in the south to be at a higher elevation than in the north. The south-north trending outcrop length is ~ 100 m, with a ~ 20 m area in the middle covered by finer-grained material (Fig. 6.9). Two of the logs (N, O) are positioned left of this poorly exposed area, whereas the other two (P, Q) are to its right. Locations N, O, P, and Q (Fig. 1.2) are defined from south northwards. The cross-section (Fig. 6.9) displays a ~ 3 m thick area that is faulted in Bayfill #1 unit in log O. Because of that, there is a missing section in log O. Hence, thickness comparisons are not conducted in this log, but the log itself is included because of correlation in Bayfill units #2 and #3.

Lower Neslen Interval

Lower Neslen Interval is characterized by a 4 - 5 m thick channel-fill deposit in log N and a ~1.8 m thick channel-fill deposit in log O (Fig. 6.9). Log P comprises a thin sandstone (~60 cm) that gradually thickens towards the north. In log Q, the channel-fill deposit is 8 - 9 m thick. The channel-fill deposits are positioned just below the vertical stacked bayfill units.



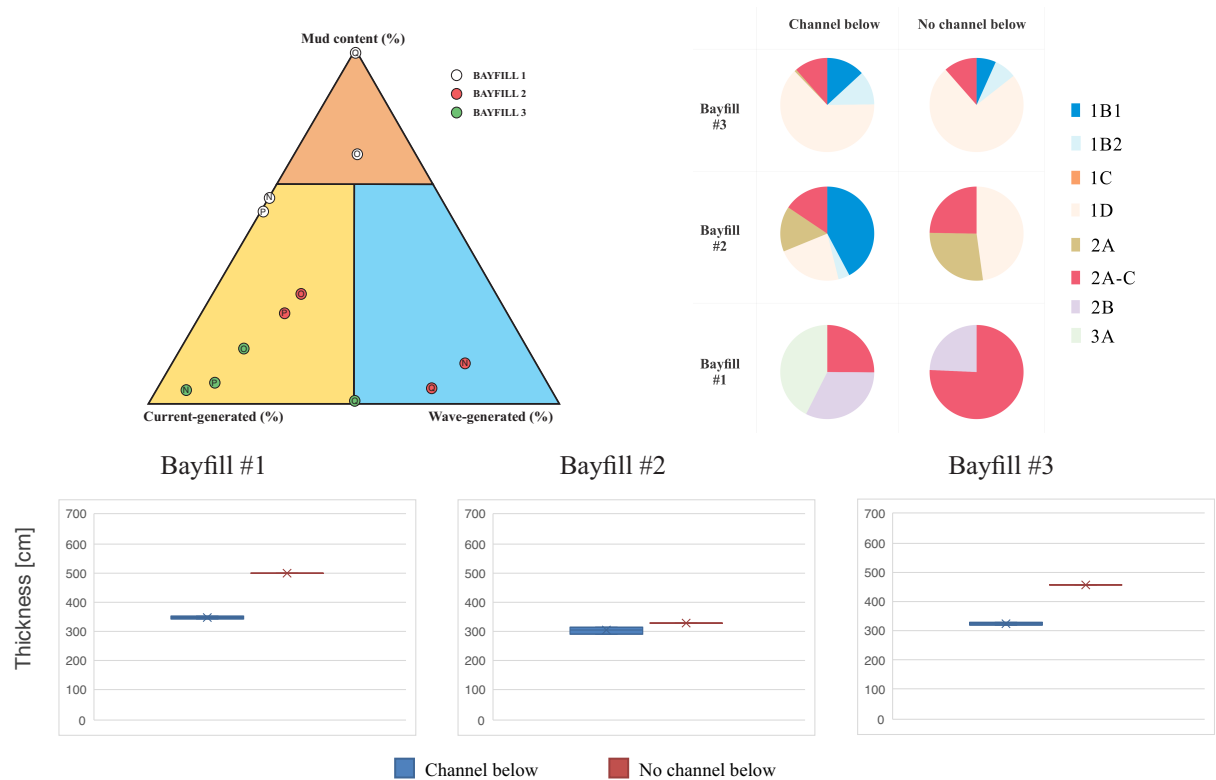


Figure 6.10: Figures summarizing the characteristics of the bayfill succession in logs N, O, P, and Q in East Canyon Window. See Figure 1.2 for position of logs. Ternary diagram with plotted values of mud content, current- and wave-generated structures within Bayfill units #1, #2, and #3. Pie charts showing the lithofacies distribution within the Bayfill units #1, #2, and #3. Box Whisker plots showing comparisons of the bayfill unit thicknesses above a sandstone-rich channel-fill deposit (blue), and the unit thicknesses above finer-grained materials (red), in Bayfill unit #1, #2, and #3, respectively.

Bayfill #1 unit description

Bayfill #1 unit is composed of mudstones (Lithofacies 3A) and heteroliths (Lithofacies 2A-C, 2B) (Fig. 6.9), causing parts of the units to form slopes in the landscape. Heteroliths predominates in logs N, O, and P. In contrast, mudstones constitute log Q. Based on the observations in logs N and P, the faulted area in log O is interpreted similarly to log N. Logs N and O have a layer of current-ripple, cross-laminated wavy bedded heterolith (Lithofacies 2A-C) followed by a lenticular bedded heterolith (Lithofacies 2B). Log P has a thin lenticular bedded heterolith followed by two thicker packages of current-ripple, cross-laminated wavy bedded heteroliths. Log Q differs from the others, only containing mudstones.

Generally, there is an overall high mud content (55 - 100%) in the unit (Fig. 6.10). There are notable differences in the unit thickness along the cross-section. Log P has a significantly thicker unit (501 cm) than the remaining logs (341 - 428 cm) (Fig. 6.9). Bayfill #1 unit in logs N, O, and P are interpreted as bayhead deltas (Fig. 6.10). In log O, the mud content of the logged section is high (70%), plotting it as a sub-bay. However, with the assumptions made in the

cross-section, the mud content is ~60% and is interpreted as a bayhead delta. Log Q is interpreted as a sub-bay due to its high amount of mudstone.

Bayfill #1 unit interpretation

As seen on the cross-section, a bayhead delta is building out from the south towards the sub-bay in the north. Upwards in the succession, the same bayhead delta may have prograded above the underlying deposits, as observed in log P.

What can be observed is that log P, with the thinnest channel-fill deposit in Lower Neslen Interval, has the greatest Bayfill #1 unit thickness, whereas log Q, with the thickest channel-fill deposit, has the thinnest unit. Thus, there may be an inverse correlation between the Bayfill #1 unit thickness and the presence of a channel-fill deposit in the Lower Neslen Interval. The lithofacies distribution implies that thicker channel-fills coincide with a higher amount of mud in Bayfill #1 unit.

Bayfill #2 unit description

The lowermost part of the Bayfill #2 unit comprises heteroliths dominated by current-ripple, cross-lamination in logs N and P, and wave-ripple, cross-lamination in log O. The northernmost log (Q) mainly comprises current-ripple cross-laminated sandstones in this interval, with only a thin layer of current-ripple, cross-laminated wavy bedded heteroliths (Lithofacies 2A).

Above, sandstones with wave-generated structures dominate in logs N and Q, and current-generated structures dominate in logs O and P (Fig. 6.9). There are little vertical variations in these intervals. The upper part comprises various wave-generated structures in log N. Log O contains current-ripple, cross-laminated wavy bedded heteroliths, and log P has wave-ripple, cross-laminated wavy bedded heteroliths in the equivalent stratigraphic interval. Log Q displays a combination of prograding current-ripple cross-laminated sandstones and wave-ripple, cross-laminated wavy bedded heteroliths.

Pie charts (Fig. 6.10) reveal higher amounts of hummocky cross-stratified sandstones and less current-ripple cross-laminated sandstones where the units are situated on top of a channel-fill deposit. The mud content and amount of current-generated structures are also lower in the logs positioned above a channel-fill deposit (Fig. 6.10). Logs N (317 cm) and Q (293 cm), with a channel-fill deposit below, have thinner units compared to log P (331 cm). Logs N and Q are interpreted as deposited as wave-dominated bayfills, whereas logs O and P are part of a bayhead delta (Fig. 6.10).

Bayfill #2 unit interpretation

Logs O and P were positioned closer to a prograding delta, probably building out from the west. This is supported by the high amount of current-ripple cross-laminated sandstone in logs O and P and the prograding heterolith in log O. The ternary diagram (Fig. 6.10) reveals higher mud content in the bayhead delta than in the wave-dominated bayfill. The Box Whisker plot (Fig. 6.10) implies that the Bayfill #2 unit thickness may be moderately affected by the sandstone-rich channel-fill deposits in Lower Neslen Interval. It can be inferred that it is available compactional potential after 4 - 6 m, during Bayfill #2 unit deposition. The low amount of current-generated structures above channel-fill deposits is similar to what is seen in Bayfill #1 unit.

Bayfill #3 unit description

Current-generated structures mostly dominate the Bayfill #3 unit, but the northernmost log (log Q) has an approximately uniform distribution of current- and wave-generated structures (Fig. 6.9). Logs N, O, and P begin with a heterolithic layer with current-ripple cross-lamination, translating into sandstones upwards. This current-ripple cross-laminated sandstone is prograding above the current-ripple, cross-laminated wavy bedded heteroliths towards the north. Overall, current-ripple cross-laminated sandstone predominates the bayfill unit, occurring with beds of both wave- and current-generated structures of varying lateral extent. A 15 - 24 cm thick layer of hummocky cross-stratified sandstone is identified through the three northernmost logs (O, P, Q).

Overall, the total amount of current-generated structures decreases northwards (Fig. 6.10), caused by an increased amount of wave-ripple cross-laminated sandstone. No mudstones are observed in log Q, giving a slightly lower mud content than the remaining logs (N, O, P) (Fig. 6.10). Log P exhibits the thickest unit (459 cm), whereas logs N (319 cm) and Q (331 cm) have significantly thinner units. The Bayfill #3 unit is interpreted as a bayhead delta within all four logs (Fig. 6.10).

Bayfill #3 unit interpretation

Log Q is significantly more affected by waves, suggesting a northward increase in distance from the bayhead delta and more wave reworking in the northern part of East Canyon Window. The Box Whisker plot (Fig. 6.10) shows a relationship between the sandstone fraction in Lower Neslen Interval and the Bayfill #3 unit thickness: Log P, with no channel-fill deposit below, has a considerably thicker unit than logs N and Q. Hence, it can be inferred that effect of early

differential compaction in Lower Neslen Interval is not fully consumed after ~10 m overburden.

6.2.5 Neslen Canyon

Two sections are logged (R, S) along a ~200 m northwest-southeast trending transect within Neslen Canyon (Figs. 1.2 and 6.11). Log R is positioned adjacent to a roadcut and logged along the road, as shown in the upper left photo in Figure 6.11.

Lower Neslen Interval

A ~2 m thick channel-fill deposit is observed 1 m below the vertical stacked bayfill units in the southeastern log (S) (Fig. 6.11). Below, several 40 - 80 cm thick sandstone packages (Lithofacies 1A, 1D) are observed, separated by several meters of organic-rich mudstone (Lithofacies 3B). No channel-fill deposit is observed in the northwestern log (R), but thinner sandstone layers (14 - 40 cm) are found just below Bayfill #1 unit and up to 3 m below. Due to limited availability along the roadcut, log R is not logged deeper. This means that channel-fill deposits could be present deeper than ~3 m below the stacked bayfill units. The Lower Neslen Interval is mostly characterized by organic-rich mudstone in log R (Fig. 6.11).

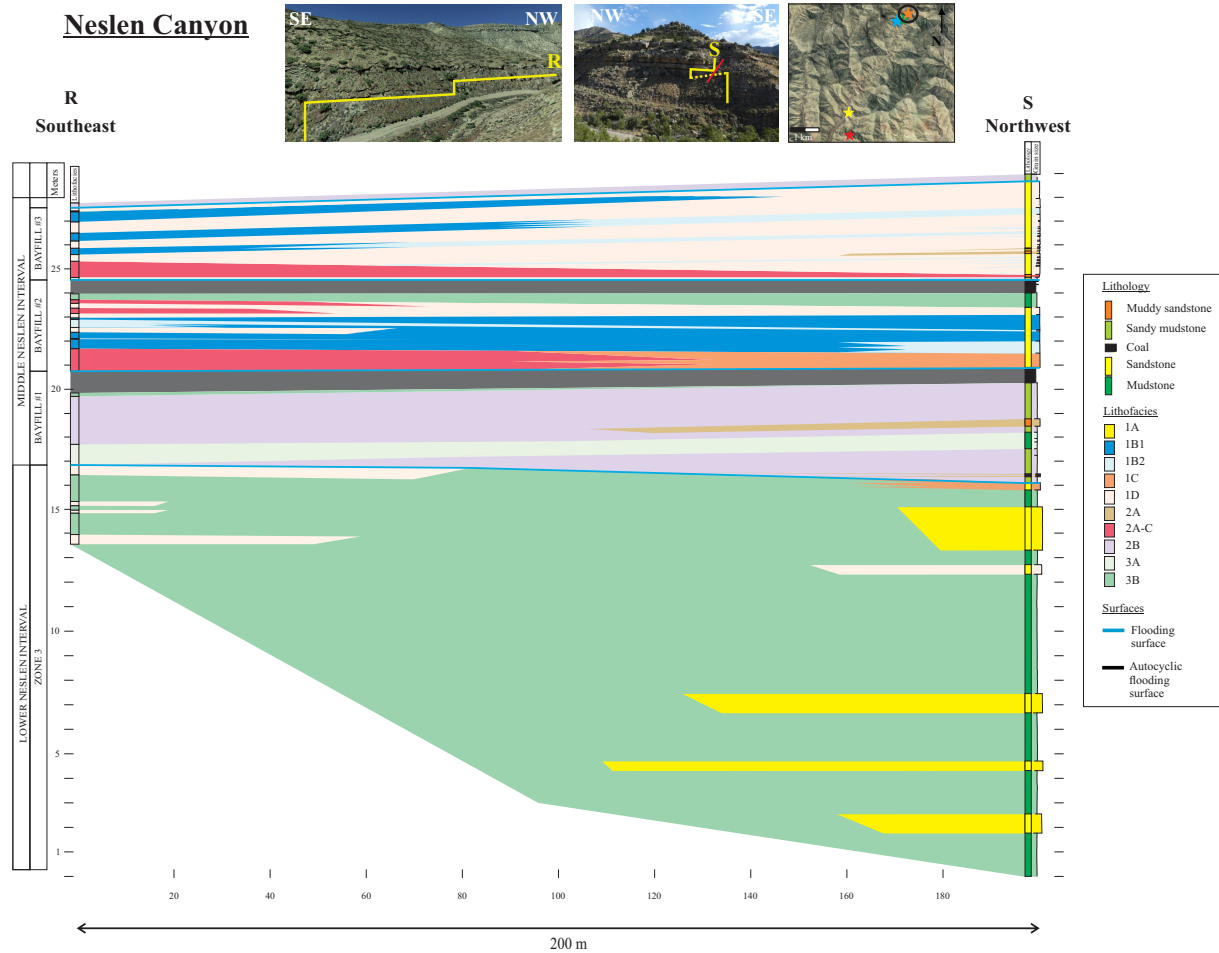


Figure 6.11: Correlation panel of the logged vertical sections in logs R and S in the Neslen Canyon. See Figure 1.2 for position of logs. Note that the ratio between the lateral- and horizontal scale is 1:5. Correlation is based on all observed lithofacies. The two upper left photos show the area of the logged sections, with yellow as the logging path. The red line indicates a normal fault crossing the log path. The photo showing logging path R is retrieved from © Google Earth 2020. The upper right photo shows where the canyon is located in the study area (© Google Earth 2020).

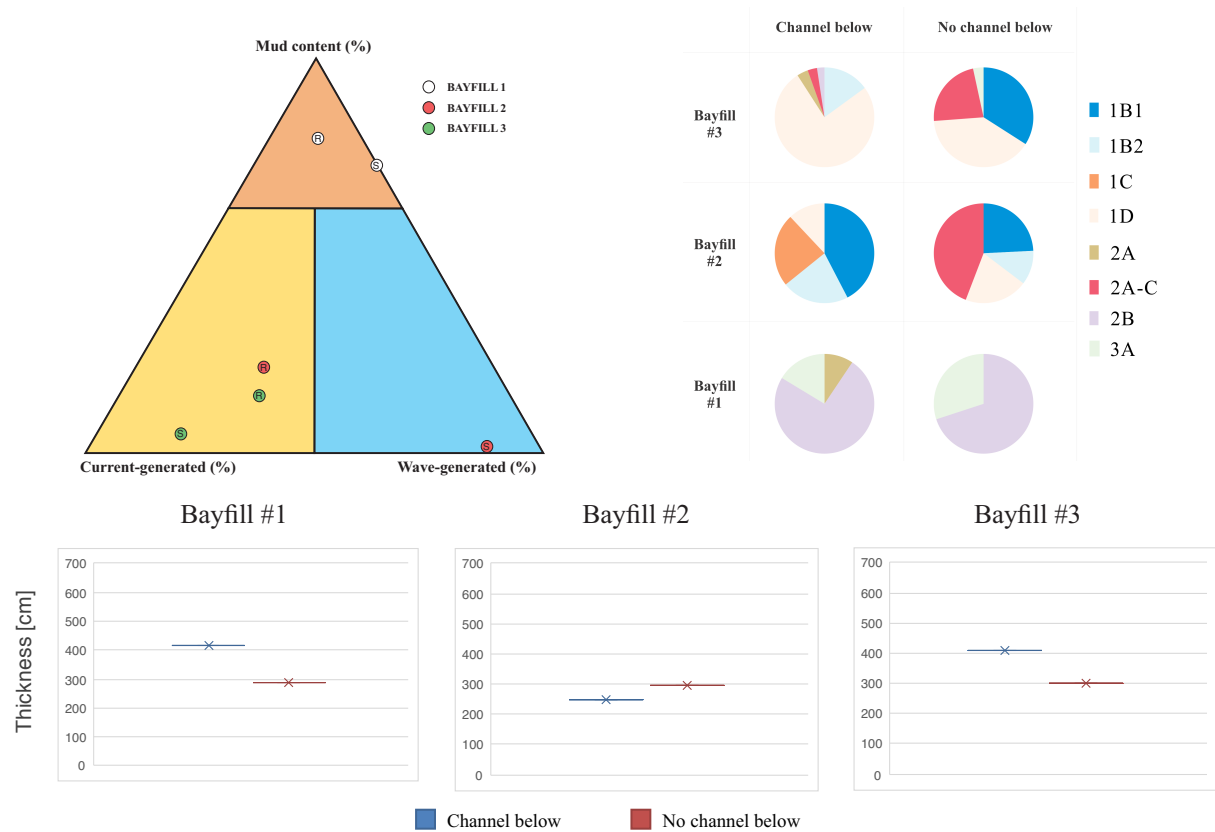


Figure 6.12: Figures summarizing the characteristics of the bayfill succession in logs R and S in Neslen Canyon. See Figure 1.2 for position of logs. Ternary diagram with plotted values of mud content, current- and wave-generated structures within Bayfill units #1, #2, and #3. Pie charts showing the lithofacies distribution within the Bayfill units #1, #2, and #3. Box Whisker plots showing comparisons of the bayfill unit thicknesses above a sandstone-rich channel-fill deposit (blue), and the unit thicknesses above finer-grained materials (red), in Bayfill unit #1, #2, and #3, respectively.

Bayfill #1 unit description

Bayfill #1 unit in log R comprises an 85 cm thick mudstone (Lithofacies 3A), followed by a 2 m thick lenticular bedded heterolith (Lithofacies 2B) (Fig. 6.11). Log S is mainly composed of lenticular bedded heteroliths interbedded with thinner layers (4 - 31 cm) of southeastward dipping, wave-ripple, cross-laminated wavy bedded heteroliths (Lithofacies 2A). A 68 cm thick layer of mudstone is found in the middle of the unit in log S. This mudstone layer correlates to the lowermost part in log R and is dipping towards the southeast.

In log S, only wave-generated structures are present. The dominant process is undefined in log R due to the high amount of mudstone and lenticular bedded heteroliths. A lower mud content (73%) is observed in log S compared to log R (79%) (Fig. 6.12), and the Bayfill #1 unit is thicker in log S (416 cm) than in log R (286 cm). A sub-bay is interpreted in the Bayfill #1 unit (Fig. 6.12).

Bayfill #1 unit interpretation

The ternary diagram (Fig. 6.12) shows that the amount of wave-generated structures increases concurrently with the decreasing mud content in log S. The southeastward dipping layers and the change in lithofacies indicate a sub-bay becoming filled from the northwest. From the Box Whisker plot (Fig. 6.12), it can be inferred that the Bayfill #1 unit is thicker when situated on top of a sandstone-rich channel-fill deposit. Hence, the unit thickness is positively correlated to the channel-fill thickness in Lower Neslen Interval and therefore differs from what was observed in Bayfill #1 unit in the other canyons/creeks. As these observations differ from the other locations, one has to keep in mind that log R could have channel-fill deposits below the logged depth. Another uncertainty is the measuring of this section, as the logging was done over a great horizontal distance.

Bayfill #2 unit description

Noticeable lateral variations occur along the Bayfill #2 unit (Fig. 6.11). In log R, the lower part contains a layer of current-ripple, cross-laminated wavy bedded heteroliths (Lithofacies 2A-C), passing into bioturbated sandstone (Lithofacies 1C) towards log S. Above, a wave-dominated sandstone interval (Lithofacies 1B) is present in both logs. Log R has a 20 cm thick sandstone with current-ripple cross-lamination (Lithofacies 1D) within this interval. The uppermost 1 m is characterized by current-ripple cross-lamination in both logs, with two layers of current-ripple, cross-laminated wavy bedded heteroliths in log R.

Lithofacies distribution (Fig. 6.12) shows that log R is dominated by current-generated structures and contains a great amount of mud (22%). Log S has only 2% mud content and is dominated by wave-generated structures. Log R has a thicker (298 cm) unit compared to log S (250 cm). Bayfill #2 unit is interpreted as a wave-dominated bayfill in the southeast (log S) and as a bayhead delta in the northwest (log R) (Fig. 6.12).

Bayfill #2 unit interpretation

It is suggested that a bayhead delta is building out from log R, becoming more affected and reworked by waves towards log S. As shown in the Box Whisker plot (Fig. 6.12), the unit thickness is inversely correlated to the channel-fill thickness. The lithofacies distribution reveals that units situated on top of channel-fill deposits in Lower Neslen Interval have more wave-generated structures and lower mud content, whereas the units above inter-channel mudstones contain more mud and current-generated structures (Fig. 6.12).

Bayfill #3 unit description

The Bayfill #3 unit comprises a 10 cm thick layer of fine-grained material at the base, passing from mudstones in log R into lenticular bedded heteroliths in log S (Fig. 6.11). A southeastward-thinning layer (68 - 12 cm) of current-ripple, cross-laminated wavy bedded heteroliths follows. Current-ripple cross-laminated sandstone dominates the next interval, but dipping layers of hummocky cross-stratified- and wave-ripple cross-laminated sandstone occur within. They have an apparent dip of $\sim 0.53^\circ$ towards the southeast and indicate clinofolds. Log S is dominated by current-ripple cross-laminated sandstone, whereas log R is more interbedded and wave-reworked. The wave-reworked sandstone layers are characterized by hummocky cross-stratification in log R and pass into wave-ripple cross-lamination in log S.

In log S, the unit essentially consists of current-ripple cross-lamination, whereas log R has a greater variety of lithofacies (Fig. 6.12). The southeastern log (S) has a 409 cm thick unit with 5% mud and 81% current-generated structures. In comparison, the unit in log R is 301 cm thick, with 15% mud and 65% current-generated structures. Logs R and S are dominated by current-generated structures with an overall low content of mud, hence, interpreted as part of a bayhead delta (Fig. 6.12).

Bayfill #3 unit interpretation

The interpreted bayhead delta was likely building out from log S to log R and gets more affected by waves towards log R. Log R is interpreted as positioned at the margin of the bayhead delta where the waves become more prominent. The clinofolds support this interpretation.

The thickness- and lithofacies variations imply that log S, situated above a channel-fill deposit in Lower Neslen Interval, is thicker, has more current-generated structures, and has less mud (Fig. 6.12) than log R, which is positioned above inter-channel mudstone. It can be inferred that Bayfill #3 unit thickness is independent of the Lower Neslen Interval channel-fill thickness, probably due to the vertical distance.

7 Analysis of the geometry

A description of how the individual bayfill unit thicknesses in the five studied areas (Fig. 1.1) were affected by the presence of a channel-fill deposit was presented in Chapter 6. This chapter addresses a more quantitative analysis of the channel-fill deposits' effect on the lateral variations in unit thicknesses and the lithofacies distribution.

Four different outcomes are found by quantifying the effect from early differential compaction in Lower Neslen Interval on the Middle Neslen Interval bayfill unit's lateral thickness- and lithofacies variations. The outcomes are based on the presence of channel-fill deposits in Lower Neslen Interval and how the overlying bayfill thickness and lithofacies distribution are affected by its presence. The outcomes A, B1, B2, and B3 are shown in Table 7.1.

Table 7.1: Overview of four possible outcomes related to the presence of a channel-fill deposit and early differential compaction in Lower Neslen Formation.

Influence or no influence by channel-fill deposit	No influence (A)	Influence (B)		
Outcome	A	B1	B2	B3
Explanation	Neither thinning of the bayfill units nor differences in lithofacies distribution	Thinning of the bayfill units, but no differences in lithofacies distribution	Thinning of the bayfill units and differences in lithofacies distribution	No thinning of the bayfill units, but differences in lithofacies distribution

In the five studied areas, one of the four outcomes A, B1, B2, and B3 is assigned to each Bayfill unit #1, #2, and #3, as shown in Table 7.2.

Table 7.2: Overview of the interpreted outcomes in Bayfill units #1, #2, and #3, respectively, within the five studied areas.

Interpretation of outcomes			
	Bayfill #1	Bayfill #2	Bayfill #3
Outer East Canyon	B2	B2	B3
Exit	B2	B3	B3
Keane Creek	B2	B3	B2
East Canyon Window	B2	B2	B1
Neslen Canyon	A	B2	B3

Based on the division into four outcomes (Tables 7.1 and 7.2), almost all of the bayfill units seem to be affected, to some extent, by the sand content in Lower Neslen Interval. However, the degree of influence varies, and especially the unit thickness seems to be less affected by channel-fill deposits upwards in the succession. The following Sub-chapters, 7.1 and 7.2, address these variations in more detail.

7.1 Lateral variations in lithofacies

Almost every bayfill unit's lithofacies distribution is interpreted to be affected by the presence of a channel-fill deposit in Lower Neslen Interval (Table 7.2). This sub-chapter discusses the more specific effect from channel-fill deposits on the abundance of wave- versus current-generated structures, and on the abundance of sandstone versus mudstone.

7.1.1 Wave- versus current-generated structures

Most of the studied bayfill units demonstrate an increase in abundance of wave-generated structures when the amount of sand increases in the Lower Neslen Interval (Fig. 7.1). In the northern part of the study area, comprising Keane Creek, East Canyon Window, and Neslen Canyon (Fig. 1.1), the Bayfill #2 unit is interpreted as a wave-dominated bayfill above the channel-fill deposits (Logs M, N, Q, S) and as a bayhead delta above the inter-channel mudstones (Logs L, P, R). As shown in the heat map (Table 7.3), the amount of wave-generated structures is inversely correlated to the bayfill unit thickness in most logs.

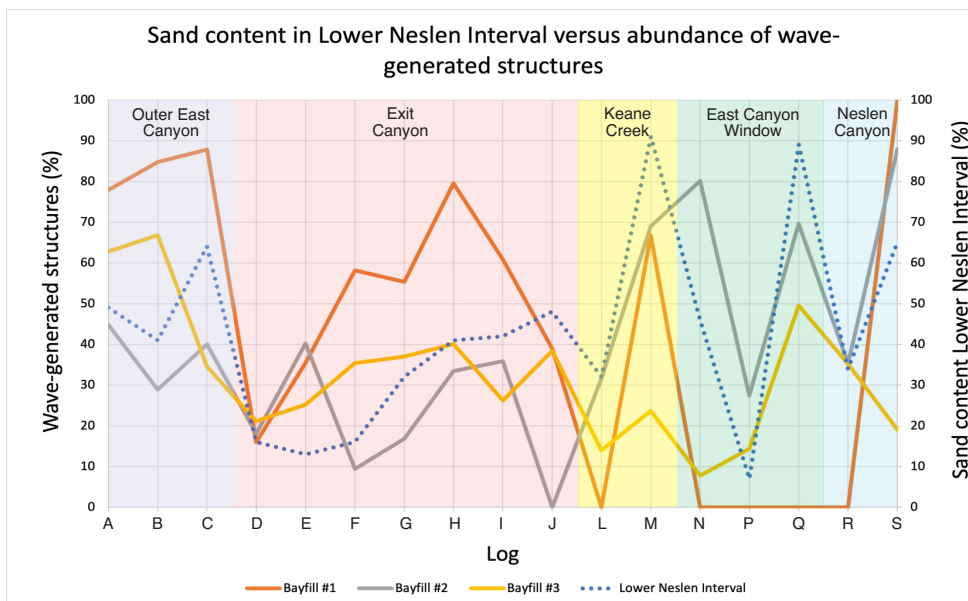


Figure 7.1: Relationship between the sand content (%) in Lower Neslen Interval versus the abundance of wave-generated structures (%) in the Middle Neslen Interval bayfill units. See Figure 1.2 for locations of logs A - S. The overall trend shows an increase in wave-generated structures in the Bayfill units where the sand content in Lower Neslen Interval is higher. This trend is observed in Exit Canyon, Keane Creek, and Neslen Canyon in Bayfill #1 unit and all canyons except Exit Canyon in Bayfill #2 unit. For Bayfill #3 unit, this trend is demonstrated in Exit Canyon, Keane Creek, and East Canyon Window.

Table 7.3: Heat map showing correlations between the bayfill unit thicknesses (cm) and the abundance of wave-generated structures (%) in the studied canyons. Correlation coefficient is from -1 (red) (100% inverse correlation) to +1 (green) (100% positive correlation). Most of the correlation coefficients are inverse, which means that thicker bayfill units correlate to a lower amount of wave-generated structures.

	Outer East Canyon	Exit Canyon	Keane Creek	East Canyon Window	Neslen Canyon
Bayfill #3	-0.91	0.52	-1.00	-0.30	-1.00
Bayfill #2	-0.72	0.10	1.00	-0.64	-1.00
Bayfill #1	-0.14	-0.58	-1.00		1.00

7.1.2 Content of sandstone versus mudstone

In addition to looking at variations in wave- versus current-generated structures, the abundance of sandstone versus mudstone in the bayfill units is considered. Three different scenarios regarding the sand content in the bayfill units above a channel-fill deposit are made, shown in Figure 7.2. As shown in Figure 7.3, the sand content in the bayfill units increases or remains the same when the sand content in Lower Neslen Interval increases. A decreased sand content (scenario II) (Fig. 7.2) does not appear in any of the bayfill units. Four out of five areas show an increase in sand content in the Bayfill #1 unit above channel-fill deposits (Fig. 7.3). Three of the Bayfill #2 and #3 units exhibit this trend.

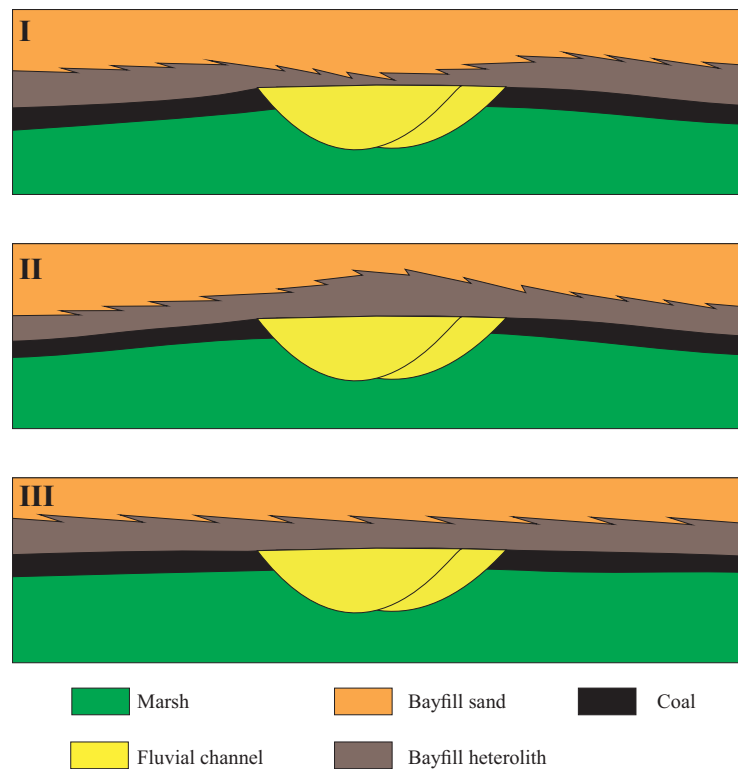


Figure 7.2: Three different scenarios showing how the sand content is affected by the presence of a channel-fill deposit. I: Increased sand content above channel-fill deposits. II: Decreased sand content above channel-fill deposits. III: No trend in the sand content above channel-fill deposits.

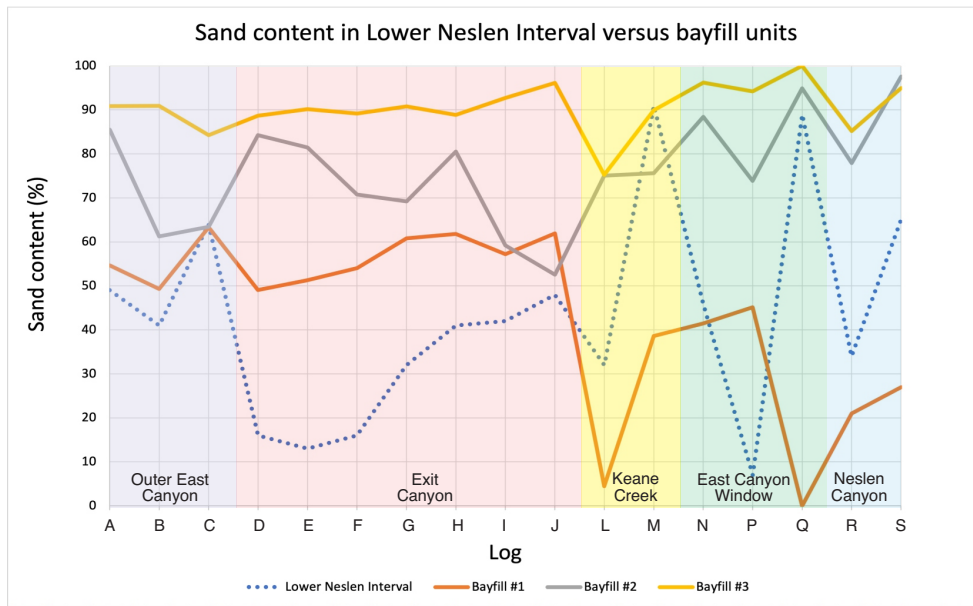


Figure 7.3: Relationship between the sand content (%) in Lower Neslen Interval versus the sand content (%) in the Middle Neslen Interval bayfill units. See Figure 1.2 for locations of logs A - S. The overall trend shows an increase in sand content in the Bayfill units where the sand content in Lower Neslen Interval is higher. Among Bayfill #1 units, this observed trend is found in all canyons except East Canyon Window. In Bayfill #2 unit, the trend is observed in Outer East Canyon, East Canyon Window, and Neslen Canyon. For the Bayfill #3 unit, the trend is observed in Keane Creek, East Canyon Window, and Neslen Canyon. Notice that the expected trend is found in all bayfill units in the Neslen Canyon.

The sand content of the bayfill units is correlatable to the thickness of the unit. Most of the areas and bayfill units demonstrate that thicker bayfill units have a lower content of sand (Table 7.4).

Table 7.4: Heat map showing correlations between the bayfill unit thicknesses (cm) and the amount of sand (%) in the studied canyons. Correlation coefficient is from -1 (red) (100% inverse correlation) to +1 (green) (100% positive correlation). Most of the correlation coefficients are inverse, which means that thicker bayfill units correlate to a lower sand content.

	Outer East Canyon	Exit Canyon	Keane Creek	East Canyon Window	Neslen Canyon
Bayfill #3	-0.95	-0.57	-1.00	-0.71	1.00
Bayfill #2	-1.00	-0.32	1.00	-0.93	-1.00
Bayfill #1	-0.96	-0.94	-1.00	0.61	1.00

7.2 Lateral thickness variations

The thickness of individual bayfill units tends to correlate with the sand content in the underlying deposits, as shown in Figure 7.4 and the Box Whisker Plots in Chapter 6 (Figs. 6.4, 6.6, 6.8, 6.10, 6.12). How far up in the succession there is this dependency varies from one area to another. Four out of five areas show an inverse correlation between sand content in Lower Neslen Interval and the thickness of Bayfill #1 unit (Table 7.5). Upwards in Bayfill units #2 and #3, the inverse correlation is weaker. Most of the Bayfill #3 unit thicknesses do not show

a thinning trend above the channel-fill deposits (Fig. 7.4), which means that the effect usually does not exceed 8 m of overburden. In Exit Canyon, some of the channel-fill deposits are located up to ~6 m below the Bayfill #1 unit’s base, which could explain why only the Bayfill #1 unit displays a thinning above the channel-fill deposits in this canyon (Fig. 7.4). Typical for the Bayfill #1 unit is that finer-grained deposits (heteroliths) exhibit thickness variations that reflect the presence of a channel-fill deposit below (Figs. 6.3 and 6.5). In East Canyon Window, all the three bayfill units are thinning above channel-fill deposits, suggesting an influence as far as 10 m of overburden.

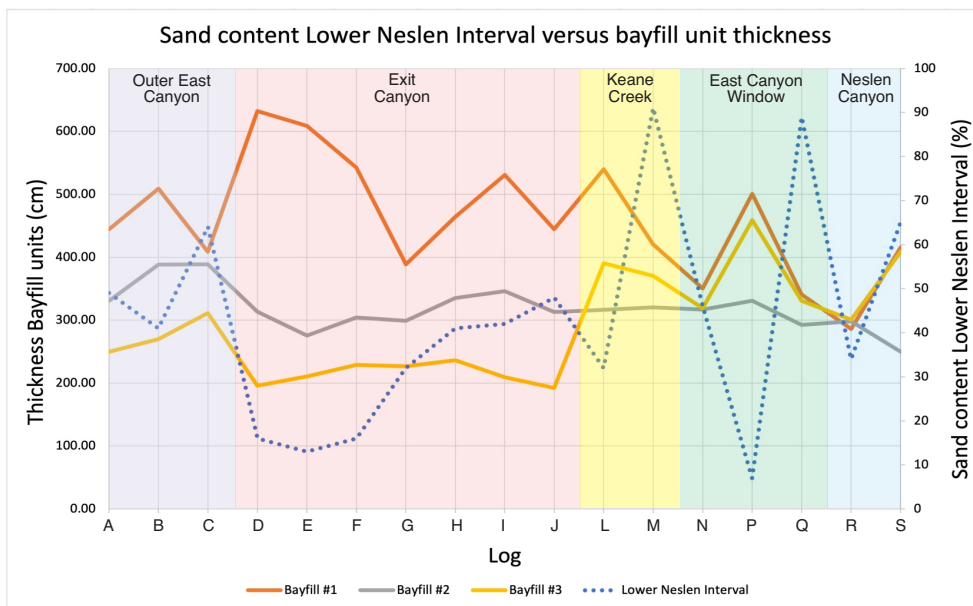


Figure 7.4: Relationship between the sand content (%) in Lower Neslen Interval versus the thickness (cm) of the Middle Neslen Interval bayfill units. See Figure 1.2 for locations of logs A - S. The overall trend shows a decrease in thickness of the Bayfill units where the sand content in Lower Neslen Interval is higher. For the Bayfill #1 units, this trend is observed in all canyons except for Neslen Canyon. Bayfill #2 unit shows this trend in Outer East Canyon, East Canyon Window, and Neslen Canyon, whereas Bayfill #3 unit demonstrates the same trend in Keane Creek, East Canyon Window, and Neslen Canyon.

Table 7.5: Heat map showing correlations between the sand content in Lower Neslen Interval (%) and the bayfill unit thicknesses (cm) in the studied canyons. Correlation coefficient is from -1 (red) (100% inverse correlation) to +1 (green) (100% positive correlation). Most of the correlation coefficients are inverse, especially in the Bayfill #1 unit, which means that a lower sand content in Lower Neslen Interval correlates to thicker bayfill units.

	Outer East Canyon	Exit Canyon	Keane Creek	East Canyon Window	Neslen Canyon
Bayfill #3	0.78	-0.05	-1.00	-0.81	1.00
Bayfill #2	0.18	0.67	1.00	-0.99	-1.00
Bayfill #1	-0.94	-0.71	-1.00	-0.88	1.00

7.3 Other factors controlling lateral thickness variations

In addition to looking at how the sand content in Lower Neslen Interval controls the thickness, other possible factors must be considered. Even if Lower Neslen Interval differential compaction is interpreted as the main cause in most cases, such an interpretation lacks in some areas. Other expected controlling factors are listed below:

- Autocompaction: The amount of mud within the bayfill unit will determine the compaction-generated thickness decrease. This causes bayfill units with abundant mud to be thinner than bayfill units with abundant sand. As shown in Table 7.4, most bayfill units are thinner when the sand content is higher, but this is not the case in every studied bayfill unit.
- Differential compaction of the bayfill unit below: If the underlying bayfill unit has a high amount of mud, it is believed to coincide with thicker, overlying bayfill units. Bayfill units with more sandstone generate thinner, overlying bayfill units.
- Differential compaction of underlying coal beds: A thicker mire below a bayfill unit, now presented as a coal bed, will probably generate more space for a bayfill unit above compared to what a thin coal bed does.
- Differential compaction of coal and organic-rich mudstone (Lithofacies 3B) in Middle Neslen Interval: If these layers are thick, a thicker overlying bayfill unit is suggested. Thinner layers of coal and organic-rich mudstone lead to thinner overlying bayfill units.

Table 7.6 shows which of the aforementioned factors control the bayfill units in the five studied areas. Lower Neslen Interval is the dominant factor, followed by autocompaction and compaction of coal and organic-rich mudstone (Lithofacies 3B). Differential compaction of an underlying bayfill unit does not significantly control the thickness variations in any of the areas. Some of the units are partly controlled by several factors, while others are controlled by only one factor (Table 7.6). What can be observed is that several other factors do not control many of the units controlled by differential compaction of Lower Neslen Interval.

Table 7.6: Overview of the factors interpreted as controls on the thickness variations in the bayfill units. Interpreted controls are marked with an «X». The five controlling factors are (1) Differential compaction of Lower Neslen Interval, (2) Autocompaction within the bayfill unit, (3) Differential compaction of underlying bayfill units in Middle Neslen Interval, (4) Differential compaction of underlying coal beds in Middle Neslen Interval, and (5) Differential compaction of underlying coal beds and organic-rich mudstones (Lithofacies 3B) in Middle Neslen Interval.

	Bayfill #	(1) Lower Neslen Interval	(2) Auto-compaction	(3) Bayfill units below	(4) Coal beds below	(5) Coal and organic-rich mudstone below
Outer East Canyon	1	X				
	2	X				X
	3			X		X
Exit Canyon	1	X				
	2				X	X
	3				X	X
Keane Creek	1	X				
	2		X		X	X
	3	X				
East Canyon Window	1	X	X			
	2	X	X (weak)			
	3	X	X (weak)	X (weak)	X	
Neslen Canyon	1		X			
	2	X		X	X	X
	3		X			X

7.4 Summary

Several trends have been observed in connection with the presence of channel-fill deposits in Lower Neslen Interval:

- The bayfill units demonstrate a thinning above channel-fill sandstones, normally up to 8 m of overburden above the sandstone (Fig. 7.4 and Table 7.5).
- The bayfill units contain a higher amount of sand and an increase in wave-generated structures when positioned above a channel-fill deposit (Figs. 7.1 and 7.3).

The increase in sand content and wave-generated structures above a channel-fill deposit co-occurs with the thinning of the bayfill units above channel-fill deposits in most areas (Tables 7.3 and 7.4). This implies that thinner bayfill units correlate to more sandstone-rich units, and thicker bayfill units coincide with mudstone-rich bayfill units.

8 Controls of thickness within bayfill successions

The studied bayfill units show lateral variations in the sand- and shale-body geometry, reflected in lithofacies distribution and unit thickness. The overall stratigraphic controls on architecture are changes in accommodation space, sediment supply, and sediment distribution. These controls are subdivided into tectonic subsidence and uplift, compaction, isostasy, eustatic sea-level fluctuations, sediment supply and distribution, and basin physiography. As the bayfill units are relatively thin, limited accommodation space was available during deposition. Therefore, they are interpreted to be highly sensitive to changes in relative sea-level and sediment supply (Simms et al., 2018). The following chapter will focus on factors controlling the vertical and lateral distribution of sediments and bayfill unit thicknesses. For the lateral part, the main focus will be on early differential compaction of the substrata and its effect on the development of bayfill successions.

8.1 Vertical thickness controls

8.1.1 Autogenically versus allogenicly controlled flooding

For stacked bayfill sequences, the reestablishment of bays occurs by repeated flooding episodes and an associated increase in water depth. Interdistributary bays are reestablished in the studied succession after deposition of Bayfill units #1 and #2. A flooding event has also occurred between deposition of Lower Neslen Interval and Bayfill #1 unit. Flooding events reflect a change in the rate of accommodation versus the rate of sediment supply.

Changes in accommodation are primarily driven by a movement of the sea surface (eustatic sea-level) and the sea floor (tectonics). The reestablishment of a bay environment caused by a flooding event can be related to both allogenic (external) and autogenic (internal) controls, as the stratigraphic architecture of marginal-marine successions results from the interaction between them (Shiers et al., 2014). Allogenic controls are caused by the action or influence of external environmental factors such as eustatic sea-level, climate, tectonic subsidence, and regional changes in sediment supply. The autogenic controls are self-generated within the depositional system and include river avulsion and delta lobe shifting. Previous studies of the Mesaverde Group interpret the bayfill successions as a response to allogenic controls (Kjærefjord et al., 2021, Accepted), but Shiers et al. (2014) also suggest that autogenic controls affected the succession.

The flooding surface's lateral extension must be considered to determine whether the flooding events between the studied bayfill units are allogenicly or autogenicly controlled. If a flooding event is regionally extensive, it may be considered an allogenicly controlled flooding event, but if its lateral extent is restricted, it could be determined as autogenicly controlled. According to Olariu (2014), autogenicly controlled flooding surfaces in Holocene deltas can extend over tens of kilometers. Therefore, one should be careful in determining the stratigraphic responses as either autogenicly or allogenicly controlled.

Large delta complexes, such as the Yellow River delta, China, comprise two types of channel avulsions, with accompanying delta lobes at two scales: delta superlobes and delta lobes (Fig. 8.1) (Xue, 1993). A delta superlobe results from avulsion in the lower river channel and consists of several smaller delta lobes, resulting from avulsion in the distributary channels (Fig. 8.1). Superlobes persist for longer times (up to hundreds of years) than delta lobes (<20 years). Roberts (1997) also developed a hierarchical structure of deltaic components for the fluvially-dominated Holocene Mississippi River, consisting of deposits of different temporal and spatial scales (1st to 5th order), called «deltas within deltas». This means that autogenicly controlled floodings take place at different scales. The delta superlobes (2nd order) within the Holocene Mississippi River delta plain (1st order) covered up to 15 000 km². As the shoreline in the study area was characterized by barrier islands with a predominance of wave processes (Kirschbaum & Hettinger, 2004; Kjærefjord et al., 2018), a comparison with a fluvially-dominated delta complex may be inaccurate. Holocene sub-deltas (4th order) at the Mississippi deltaic plain, which often fill shallow bays, can cover ~300 km² at periods of maximum development (Welder, 1959; Coleman & Gagliano, 1964).

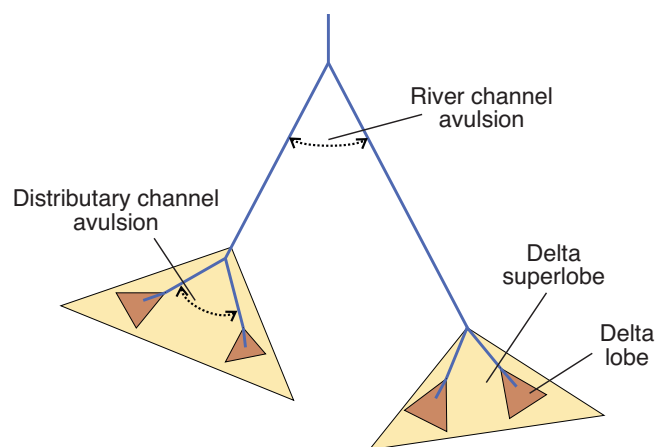


Figure 8.1: Illustration of two scales of channel avulsions and associated delta lobe switching in large delta complexes. Delta superlobes result from river channel avulsion and delta lobes result from avulsion of distributary channels. Modified from Hori & Saito (2007).

The flooding surface below Bayfill #2 unit is interpreted as the maximum flooding surface and is contiguous to the mudstone tongue between the more distal members (Corcoran and Cozzette) of the Iles Formation (Fig. 2.5) (Shiers et al., 2017). Given that the studied succession was deposited at the margin of the fluctuating (transgressive and regressive) shoreline of the Western Interior Seaway, it is likely that allogenic controls affected the study area that was located immediately behind the coastline of the Seaway (Ryer et al., 1984; Johnson, 2003; Miall et al., 2008; Shiers et al., 2014).

The flooding surfaces between the vertical stacked bayfill units in this thesis' study area are traceable from Coal Gulch, Colorado in the east to Sejo Canyon, Utah in the west, representing a distance of ~90 km. Each bayfill unit constitutes the marginal-marine part of a distal, marine parasequence eastward of the study area (Kjærefjord et al., 2021, Accepted). The flooding surfaces separating the bayfill units are also found in the more distal shoreface deposits. The correlation of flooding surfaces between Bayfill #1, #2, and #3 units to marine parasequences indicate allogenic controlled flooding surfaces (Kjærefjord et al., 2018).

8.1.2 Relative sea-level changes

Interdistributary bays sheltered behind barrier island systems are more sensitive to sea-level changes than areas exposed to the open sea. The sensitivity is mainly due to the shallowness of sheltered bays and the delicate balance between the generation of accommodation and sediment supply in these low gradient settings (Simms et al., 2018). Minor relative sea-level changes in a low gradient and low relief setting result in widespread submerge during transgressions and emergence during regressions (Shiers et al., 2017). The thickness of a bayfill unit reflects the water depth of the bay, and factors such as regional subsidence and compaction of underlying sediments control the paleo water depth.

According to Kjærefjord et al. (2018), the thickness and sand content of a bayfill unit is partly related to the available accommodation during deposition. Primarily, the sand content is a function of how sediments are distributed in the area, but it is also affected by the available accommodation space. Low accommodation periods generate thin, sandstone-rich bayfill units, whereas high accommodation periods give thicker bayfill units with abundant mudstone. This study finds that the bayfill units become thinner and more sandstone-rich upwards in the succession (Fig. 6.1) and that the thickness is inversely correlated to the abundance of sandstone (Table 7.4). This implies that the floodings and subsequent deposition of Bayfill units #1 - #3 were initiated by smaller, high-frequency relative sea-level rises (Kjærefjord et al., 2021,

Accepted) during an overall lower-frequency decreasing rate of generation of accommodation. The Buck Sequence Boundary (Kirschbaum & Hettinger, 2004), positioned on top of Bayfill #3 unit in the study area (Fig. 2.7), also indicates an overall, gradual decrease in generation of accommodation.

8.1.3 Tectonic subsidence

In a retroarc foreland basin (this study), the flexuring of crust, dynamic subsidence, and sediment loading are the main subsidence mechanisms. The subsidence rates are higher in the proximal part and decrease distally (Catuneanu, 2006). Proarc foreland basins have tectonic subsidence rates of 0.2 - 0.5 mm/year, while the retroarc foreland basins rate rarely exceeds 0.05 mm/year (Allen & Allen, 2013). Tectonic subsidence causes regional changes in relative sea-level. As the study area covers a few square kilometers and is located far out in the foreland basin (~250 km from the source area), tectonic subsidence is believed to affect the study area uniformly. Tectonic subsidence variations are generally of a lower frequency and amplitude compared to the high-frequency eustatic changes. In the Mesaverde Group, tectonic subsidence is assigned to the 3rd order cyclicity (3 million year), compared to the 4th and 5th order cyclicity of eustatic changes (10 000 – 100 000 year) (Howell & Flint, 2003).

8.1.4 Compaction-induced subsidence

Introduction

During burial and overburden of sedimentary deposits, pore sizes reduce, water is squeezed out, and the rock volume is reduced (Chopra & Marfurt, 2012). Earlier studies (e.g., Meckel et al., 2007; Törnqvist et al., 2008) point at sediment compaction as an essential contributor to subsidence patterns in sedimentary basins, and that lateral variations in lithology cause differential subsidence in overlying sediments (Blackwelder, 1920; Davies, 2005). Sediment compaction is an important contributor to relative sea-level rise at a local scale (Brain, 2016). These rates are between 0.7 and 2.2 mm/year on deltas (Syvitski, 2008; Church et al., 2013).

According to Leeder (1988), finer-grained sediments such as mudstones and siltstones have a higher compaction potential than sandstones. Clay has a higher initial porosity than sand, up to 80% (Perrier & Quiblier, 1974), and is readily compressed (Athy, 1930). The initial porosity of sand varies and is dependent on grain-size, typically ranging from 30 - 50%.

Compaction rates

Different lithologies result in varying compaction rates, with a decreasing compaction rate over time and burial depth (Perrier & Quiblier, 1974; Becker & Sultan, 2009; van Asselen, 2011). Keogh (2019) reports that most (~80%) of the compaction in coastal wetlands occurs within the first 100 years after deposition and in the uppermost 1 m of the subsurface. Holocene subsidence rates for worldwide deltas are 0.5 - 4.5 mm/year on average (Becker & Sultan, 2009).

In the Mississippi Delta system, the compaction rate during the first 10's - 100's years after deposition ranges from 5 - 10 mm/year (Becker & Sultan, 2009). According to Meckel et al. (2007), 80% of the Holocene compaction rates at the Mississippi Delta system are between 0.69 and 2.2 mm/year, and Törnqvist et al. (2008) demonstrate an average Holocene compaction rate of <3 mm/year for the same system.

Both studies from the Mississippi- and Nile Delta systems conclude that compaction rate is greatest shortly after deposition, slowing with age and depth of burial (Morton et al., 2005; Meckel et al., 2007; Törnqvist et al., 2008; Becker & Sultan, 2009; van Asselen, 2011). In the Mississippi Delta system, the high subsidence rates for the younger deposits demonstrate that early compaction is the main driver for deltaic subsidence, particularly subsequent to deposition. Some modern deltas also have particularly high subsidence rates due to, i.e., groundwater extraction and infrastructural loading (Minderhoud et al., 2017).

8.2 Lateral thickness controls

8.2.1 Differential compaction

Different lithologies have different porosities, mineral compositions, and pore shapes, and therefore respond differently to burial. Lateral lithological variations contribute to lateral differences in compaction (Chopra & Marfurt, 2012). Differential compaction of the shallow stratigraphic units on a delta is suggested as a reason for lateral variations in subsidence rates (Higgins et al., 2014). This study focuses on the compaction of muds and sands, which compact at varying degrees, resulting in differential compaction. This sub-chapter addresses three types of differential compaction affecting the study area:

1. Differential compaction of Lower Neslen Formation
2. Differential compaction due to autocompaction within a bayfill unit
3. Differential compaction of coals and organic-rich mudstones

1. *Lower Neslen Interval differential compaction*

The described correlation between the presence or absence of a channel-fill deposit in the Lower Neslen Interval and the thickness of the bayfill units can partly be explained by early differential compaction in the Lower Neslen Interval (Table 7.5 and Fig. 7.4).

Box Whisker plots (Figs. 6.4, 6.6, 6.8, 6.10, 6.12) show the relation between the thickness of the bayfill units positioned above sandstone-rich channel-fill deposits and those situated on top of finer-grained material, such as floodplain fines. According to Bjørlykke & Høeg (1997), the compaction versus burial profile is different from sandstones to shales. Shales have the highest porosity gradient during shallow burial (<2 - 3 km), whereas sandstones compact the most at greater depths (>2 - 3 km), where chemical compaction dominates. This supports the idea that early differential compaction of shales versus sandstones in Lower Neslen Interval influences the overlying bayfill units.

As demonstrated, the inter-channel mudstones undergo more post-depositional compaction than adjacent channel-fill sandstones. Studies of submarine fans in the North Sea demonstrate that submarine channel-fill deposits in an otherwise mudstone-dominated environment will often not undergo as much compaction as the finer-grained surroundings (Heritier et al., 1979). At the Po Plain, floodplain muds are more susceptible to compaction than the channel sands (Amorosi & Marchi, 1999; Teatini et al., 2011). The above studies support the trends observed in this thesis, demonstrating that bayfill units become thicker where they overlie inter-channel mudstones in Lower Neslen Interval (Table 7.5 and Fig. 7.4).

On average, Bayfill #1 unit and some of the Bayfill units #2 and #3 are thinner when positioned above a channel-fill deposit (Fig. 7.4). In most areas, the potential for thickness variations generated by early differential compaction in Lower Neslen Interval is consumed after 7 - 8 m overburden, but it may locally be recorded up to 10 m overburden (East Canyon Window) (Fig. 6.9).

In addition to lateral thickness variations, lateral lithofacies variations are interpreted as a result of the presence or absence of underlying channel-fill deposits (Figs. 7.1 and 7.3). Observed variations in sandstone content and wave-generated structures coincide with the thinning of units above channel-fill deposits (Tables 7.3 and 7.4). Thin bayfill units reflect shallow water. Thus, a high amount of wave-generated structures would be expected in the thin units, as well

as coarser sediments. Shallow parts of the bay are more wave-reworked due to their position above wave-base.

Bayhead delta facies association is more common above the inter-channel mudstones (Fig. 7.3) and is therefore often thicker than the wave-dominated bayfill and sub-bay facies associations (Fig. 5.6). This could be explained by distributary channel mouths targeting deeper parts of the bays. Only the deposits above wave-base become reworked by waves; thus, the lower part of the bayhead delta is better preserved.

2. Differential compaction due to autocompaction within a bayfill unit

Autocompaction occurs due to the sediment's self-weight (Allen, 1999). Any grain-size or grain-size-mix has a certain compaction potential. Autocompaction results in thinner units than the initial water depth and is a controlling factor regarding the bayfill unit thickness. When a bay is being filled with sediments, the effective stress initiates compaction. Depending on the compactional potential, the bayfill units may obtain varying thickness reductions. Thinner units are expected when the bayfill unit contains a high amount of mud relative to sand, whereas less mud and more sand are believed to cause thicker units. Differential compaction due to autocompaction of bayfill units is interpreted as a possible reason for thickness variations in some of the bayfill units in the Neslen Formation (Table 7.6).

3. Differential compaction of coals and organic-rich mudstones

It is demonstrated that peat compaction in modern delta plains plays a significant role in the generation of bathymetrical variations during early burial (Törnqvist et al., 2008; van Asselen et al., 2010; van Asselen, 2011). Factors such as peat type, amount of organic matter, and effective stress control the amount- and rate of compaction.

The studied succession has thick layers (39 - 115 cm) of coal and organic-rich mudstones between the bayfill units. A wide range of peat:coal compactional ratios are described in the literature, but a 10:1 peat:coal compactional ratio is often used (e.g., McCabe, 1985). However, Nadon (1998) argued that remarkably lower ratios (1.2:1 to 2.2:1) are more realistic.

The thickness differences in the bayfill units of the Middle Neslen Formation are partly due to the differential compaction of marsh deposits, presently occurring as both coal and highly compacted organic-rich mudstone (Table 7.6). Consequently, the logs with the thickest marsh deposits below would be expected to possess the thickest bayfill units above. This is observed in eight of the bayfill units (Table 7.6).

9 Conclusions

This study aims to investigate the vertical and lateral controls on thickness and lithofacies distribution of the Bayfill units #1 - #3 in the Upper Cretaceous Middle Neslen Interval of the Book Cliffs, focusing on early differential compaction in the Lower Neslen Interval. The aim was reached by establishing schemes of lithofacies and facies associations based on logged sections. From the lithofacies, facies associations, log correlations, and thickness controls presented in this thesis, the following conclusions are drawn:

- Eleven descriptive lithofacies and sub-facies are established. These have been assigned to 3 facies associations: FA1 (fluvial channel-fill deposits), FA2 (marsh/levee deposits), and FA3 (bay deposits). The bay deposits are divided into sub-facies associations FA3a (wave-dominated bayfill), FA3b (bayhead delta), and FA3c (sub-bay) based on their mud content and relative abundance of wave- versus current-generated structures.
- The relatively thin (1.7 - 6.3 m) bayfill units show an upward-coarsening trend, suggesting upward-shallowing water depth and progradation of a bay shoreline.
- In the study area, the Middle Neslen Interval represents a lower delta plain depositional environment with marine influence, sheltered behind barrier islands. Three vertical stacked bayfill units (#1, #2, and #3) are identified, bounded by allogenic flooding surfaces. An autogenically controlled flooding surface is found within Bayfill #3 unit in Outer East Canyon. An upwards decrease in unit thickness and increase in abundance of sand from Bayfill #1 - #3 suggests a decreasing rate of generation of accommodation.
- Lateral variations in lithofacies distribution and unit thickness occur locally, with early differential compaction as the main control. An increase in sand content and abundance of wave-generated structures characterizes the units positioned above an underlying channel-fill deposit in the Lower Neslen Interval. Concurrently, 80% of the Bayfill #1 units, 40% of the Bayfill #2 units, and 60% of the Bayfill #3 units demonstrate a thinning above channel-fill deposits. Typical for the Bayfill #1 unit is that there are more thickness variations in the finer-grained deposits (heteroliths) than in the sandstones. This means that early differential compaction of Lower Neslen Interval usually impacts bayfill thickness up to 8 m of burial, but the impact is related to the vertical distance to underlying channel-fill deposits.
- In addition to Lower Neslen Interval differential compaction, autocompaction of the bayfill units and compaction of marsh deposits is believed to have affected the thickness of the bayfill units.

List of references

- Allen, J. R. L. (1965). A review of the origin and characteristics of recent alluvial sediments. *Sedimentology* 5(2), 89-191.
- Allen, J. R. L. (1999). Geological impacts on coastal wetland landscapes: some general effects of sediment autocompaction in the Holocene of northwest Europe. *The Holocene* 9(1), 1-12.
- Allen, P. A., & Allen, J. R. L. (2013). *Basin Analysis: Principles and Application to Petroleum Play Assessment*: John Wiley & Sons.
- Amorosi, A., & Marchi, N. (1999). High-resolution sequence stratigraphy from piezocone tests: an example from the Late Quaternary deposits of the southeastern Po Plain. *Sedimentary Geology* 128(1-2), 67-81.
- Arndorfer, D. J. (1973). Discharge patterns in two crevasses of the Mississippi River delta. *Marine Geology* 15(4), 269-287.
- Aschoff, J. L. (2010). Preliminary Regional Sequence Stratigraphic Framework and Characterization of Potential Fluvial Reservoirs of the Upper Mesaverde Group, Uinta Basin, Utah. *Utah Geologic Survey* 569.
- Aschoff, J. L., Olariu, C., & Steel, R. J. (2018). Recognition and significance of bayhead delta deposits in the rock record: A comparison of modern and ancient systems. *Sedimentology* 65(1), 62-95.
- Aschoff, J. L., & Steel, R. J. (2011). Anatomy and development of a low-accommodation clastic wedge, upper Cretaceous, Cordilleran Foreland Basin, USA. *Sedimentary Geology* 236(1-2), 1-24.
- Ashley, G. M. (1990). Classification of large-scale subaqueous bedforms: a new look at an old problem. *Journal of Sedimentary Reserach* 60, 160-172.
- Athy, L. F. (1930). Density, porosity, and compaction of sedimentary rocks. *AAPG Bulletin* 14(1), 1-24.
- Becker, R. H., & Sultan, M. (2009). Land subsidence in the Nile Delta: inferences from radar interferometry. *The Holocene* 19(6), 949-954.
- Benyoucef, M., Mebarki, K., Ferré, B., Adaci, M., Bulot, L. G., Desmares, D., Villier, L., Bensalah, M., Frau, C., & Ifrim, C. (2017). Litho-and biostratigraphy, facies patterns and depositional sequences of the Cenomanian-Turonian deposits in the Ksour Mountains (Saharan Atlas, Algeria). *Cretaceous Research* 78, 34-55.
- Bhatt, N. Y., & Patel, S. J. (2017). Ichnology and Sequence Stratigraphy of Wave-Dominated Prograding Delta, Bhuj Formation (Cretaceous), Khatrod Hill Range, Mainland Kachchh, Western India. *Journal of Geosciences* 2(2), 121-137.
- Bhattacharya, J., & Walker, R. G. (1991). River-and wave-dominated depositional systems of the Upper Cretaceous Dunvegan Formation, northwestern Alberta. *Bulletin of Canadian Petroleum Geology* 39(2), 165-191.
- Bhattacharya, J. P. (2010). Deltas. In N. P. James & R. W. Dalrymple (Eds.), *Facies models : 4* (Vol. 6). St. John's, Newfoundland: Geological Association of Canada.
- Bjørlykke, K., & Høeg, K. (1997). Effects of burial diagenesis on stresses, compaction and fluid flow in sedimentary basins. *Marine and Petroleum Geology* 14(3), 267-276.
- Blackwelder, E. (1920). The origin of the central Kansas oil domes. *AAPG Bulletin* 4(1), 89-94.
- Blakey, R. C. (Cartographer). (2017). Deep Time Maps: maps of ancient Earth. Retrieved from <https://deeptimemaps.com/western-interior-seaway-thumbnails/>
- Blakey, R. C., Peterson, F., & Kocurek, G. (1988). Synthesis of late Paleozoic and Mesozoic eolian deposits of the Western Interior of the United States. *Sedimentary Geology* 56(1-4), 3-125.

- Blakey, R. C., & Ranney, W. D. (2018). *Ancient Landscapes of Western North America: A Geologic History with Paleogeographic Maps*. Cham, Switzerland: Springer Nature.
- Brain, M. J. (2016). Past, present and future perspectives of sediment compaction as a driver of relative sea level and coastal change. *Current Climate Change Reports* 2(3), 75-85.
- Burst, J. F. (1965). Subaqueously formed shrinkage cracks in clay. *Journal of Sedimentary Research* 35(2), 348-353.
- Catuneanu, O. (2006). *Principles of Sequence Stratigraphy*: Elsevier.
- Chopra, S., & Marfurt, K. J. (2012). Seismic attribute expression of differential compaction. *The Leading Edge* 31(12), 1418-1422.
- Church, J. A., Clark, P. U., Cazenave, A., Gregory, J. M., Jevrejeva, S., Levermann, A., Merrifield, M. A., Milne, G. A., Nerem, R. S., & Nunn, P. D. (2013). Sea Level Change. In T. F. Stocker, D. Qin, G.-K. Plattner, M. Tignor, S. K. Allen, J. Boschung, A. Nauels, Y. Xia, V. Bex, & P. M. Midgley (Eds.), *IPCC, 2013: Climate Change 2013: The Physical Science Basis. Contribution of Working Group I to the Fifth Assessment Report of the Intergovernmental Panel on Climate Change*. United Kingdom and New York, NY, USA: Cambridge University Press.
- Coleman, J. M. (1969). Brahmaputra River: channel processes and sedimentation. *Sedimentary Geology* 3(2-3), 129-239.
- Coleman, J. M., & Gagliano, S. M. (1964). Cyclic sedimentation in the Mississippi River deltaic plain. *Gulf Coast Association of Geological Societies Transactions* 14, 67-80.
- Coleman, J. M., & Prior, D. B. (1982). Deltaic Environments of Deposition In P. A. Scholle & D. Spearing (Eds.), *Sandstone Depositional Environments* (Vol. 31, pp. 139 - 178). Memoir: American Association of Petroleum Geologists.
- Coleman, J. M., & Wright, L. D. (1975). Modern river deltas: variability of processes and sand bodies. In M. L. Broussars (Ed.), *Deltas* (pp. 99-149). Models for Exploration: Houston Geological Society.
- Collinson, J. D., Thompson, D., & Mountney, N. (2006). *Sedimentary Structures* (3rd ed.). Harpenden: Terra Publishing.
- Crimes, T. P., & Anderson, M. M. (1985). Trace Fossils from Late Precambrian-Early Cambrian Strata of Southeastern Newfoundland (Canada): Temporal and Environmental Implications. *Journal of Paleontology*, 310-343.
- Dalrymple, R. W., & Choi, K. (2007). Morphologic and facies trends through the fluvial-marine transition in tide-dominated depositional systems: a schematic framework for environmental and sequence-stratigraphic interpretation. *Earth-Science Reviews* 81(3-4), 135-174.
- Davies, R. J. (2005). Differential compaction and subsidence in sedimentary basins due to silica diagenesis: A case study. *Geological Society of America Bulletin* 117(9-10), 1146-1155.
- DeCelles, P. G., & Giles, K. A. (1996). Foreland basin systems. *Basin Research* 8(2), 105-123.
- Dreyer, T. (1990). Sand Body Dimensions and Infill Sequences of Stable, Humid-Climate Delta Plain Channels. In T. A. Buller, Berg, E., Hjelmeland, O., Kleppe, J., Torsæter, and O., Aasen, J.O. (Ed.), *North Sea Oil and Gas Reservoirs II* (pp. 337-351). Dordrecht: Springer.
- Dumas, S., & Arnott, R. W. C. (2006). Origin of hummocky and swaley cross-stratification - The controlling influence of unidirectional current strength and aggradation rate. *Geology* 34, 1073-1076.
- Dumas, S., Arnott, R. W. C., & Southard, J. B. (2005). Experiments on oscillatory-flow and combined-flow bed forms: implications for interpreting parts of the shallow-marine sedimentary record. *Journal of Sedimentary Research* 75, 501-513.
- Elliott, T. (1974). Interdistributary bay sequences and their genesis. *Sedimentology* 21, 611-622.

- Elliott, T. (1986). Deltas. In H. G. Reading (Ed.), *Sedimentary Environments and Facies (2d ed)* (pp. 113-154).
- Erslev, E. A. (1993). Thrusts, back-thrusts and detachment of Rocky Mountain foreland arches. In C. J. Schmidt, R. B. Chase, & E. A. Erslev (Eds.), *Laramide Basement Deformation in the Rocky Mountain Foreland of the Western United States* (Vol. 280, pp. 339-358): Geological Society of America Special Paper.
- Fenn, C. A. (2012). *Outcrop to Subsurface Reservoir Characterization of the Lower Mesaverde Group, Red Wash Field, Uinta Basin and Douglas Creek Arch, Utah and Colorado*. (Doctoral dissertation), University of Colorado, Boulder.
- Fisher, D. J. (1936). *The Book Cliffs Coal Field in Emery and Grand Counties, Utah*: US Government Printing Office.
- Fisher, D. J., Erdmann, C. E., & Reeside, J. B. (1960). *Cretaceous and Tertiary formations of the Book Cliffs, Carbon, Emery, and Grand counties, Utah, and Garfield and Mesa counties, Colorado*: US Government Printing Office.
- Franczyk, K. J., Pitman, J. K., & Nichols, D. J. (1990). Sedimentology, mineralogy, palynology, and depositional history of some uppermost Cretaceous and lowermost Tertiary rocks along the Utah Book and Roan Cliffs east of the Green River. *U.S. Geological Survey Bulletin 1787-N*, 27.
- Frisch, W., Meschede, M., & Blakey, R. C. (2011). *Plate Tectonics : Continental Drift and Mountain Building* (1st ed. 2011. ed.). Heidelberg, Dordrecht, London, New York: Springer.
- Harper, E. S. (2011). *Fluvial architecture of the lower Williams Fork Formation (middle Mesaverde Group), Douglas Creek Arch, Colorado*. (Master of Science), University of Colorado,
- Heritier, F. E., Lossel, P., & Wathne, E. (1979). Frigg field—large submarine-fan trap in lower Eocene rocks of North Sea Viking graben. *AAPG Bulletin 63*(11), 1999-2020.
- Hettinger, R. D., & Kirschbaum, M. A. (2002). Stratigraphy of the Upper Cretaceous Mancos Shale (upper part) and Mesaverde Group in the southern part of the Uinta and Piceance basins, Utah and Colorado. *U.S. Geological Survey, Geologic Investigation Series I-2764*.
- Higgins, S. A., Overeem, I., Steckler, M. S., Syvitski, J. P., Seeber, L., & Akhter, S. H. (2014). InSAR measurements of compaction and subsidence in the Ganges-Brahmaputra Delta, Bangladesh. *Journal of Geophysical Research: Earth Surface 119*(8), 1768-1781.
- Hintze, L. F. (1988). Geologic History of Utah. In (Vol. 7, pp. 202). Provo, Utah, United States: Brigham Young University Geology Studies Special Publication.
- Hori, K., & Saito, Y. (2007). Classification, architecture, and evolution of large-river deltas. *Large rivers: Geomorphology and management*, 75-96.
- Howell, J. A., & Flint, S. S. (2003). Siliciclastics Case Study: The Book Cliffs. In A. L. Coe (Ed.), *The Sedimentary Record of Sea-Level Change* (pp. 135-208). Cambridge: Cambridge University Press.
- Johnson, R. C. (1985). Early Cenozoic history of the Uinta and Piceance Creek basins, Utah and Colorado, with special reference to the development of Eocene Lake Uinta. In R. M. Flores & S. S. Kaplan (Eds.), *Cenozoic paleogeography of the west-central United States, Rocky Mountain Paleogeography Symposium 3* (pp. 247-276). Society of Economic Paleontologists and Mineralogists: Rocky Mountain Section (SEPM).
- Johnson, R. C. (2003). Depositional framework of the Upper Cretaceous Mancos Shale and the lower part of the Upper Cretaceous Mesaverde Group, western Colorado and eastern Utah. *Petroleum Systems and Geologic Assessment of Oil and Gas in the Uinta–Piceance Province, Utah and Colorado: United States Geological Survey, Digital Data Series DDS-69-B*.

- Kauffman, E. (1984). Paleobiogeography and evolutionary response dynamic in the Cretaceous Western Interior Seaway of North America. *Jurassic-Cretaceous biochronology and biogeography of North America, Geological Association of Canada Special Paper 27*, 273-306.
- Kauffman, E., & Caldwell, W. (1993). The Western Interior Basin in space and time. *Geological Association of Canada Special Paper 39*.
- Keith, S. B. (1978). Paleosubduction geometries inferred from Cretaceous and Tertiary magmatic patterns in southwestern North America. *Geology* 6(9), 516-521.
- Keogh, M. E. H. (2019). *Accretion, Compaction, and Restoration: Sediment Dynamics and Relative Sea-level Rise in Coastal Wetlands*. (Doctoral dissertation), Tulane University School of Science and Engineering,
- Kirschbaum, M. A., & Hettinger, R. D. (2004). Facies analysis and sequence stratigraphic framework of Upper Campanian strata (Neslen and mount Garfield Formations, Bluecastle Tongue of the Castlegate Sandstone, and Mancos Shale), eastern Book cliffs, Colorado and Utah. *U.S. Geological Survey Digital Data Series DDS-69-G*.
- Kjærefjord, J. M. (1999). Bayfill Successions in the Lower Jurassic Åre Formation, Offshore Norway: Sedimentology and Heterogeneity Based on Subsurface Data from the Heidrun Field and Analog Data from the Upper Cretaceous Neslen Formation, Eastern Book Cliffs, Utah. In T. F. Hentz (Ed.), *Advanced Reservoir Characterization for the 21st century* (Vol. 19, pp. 149-157). Houston: SEPM Gulf Coast Section 19th Annual Research Conference Proceedings, Society of Economic Paleontologists and Mineralogists.
- Kjærefjord, J. M., Thrana, C., & Bullimore, S. (2021, Accepted). *Stratigraphic architecture within delta plain deposits in the Upper Cretaceous Neslen and Farrer formations, Book Cliffs, Utah*.
- Kjærefjord, J. M., Thrana, C., Bullimore, S., & Stenbakk, T. C. (2018). *Stratigraphic Architecture and Bayfill Classification in the Upper Cretaceous Neslen Formation, Eastern Book Cliffs, Utah*. Paper presented at the AAPG Annual Convention and Exhibition
- Krystinik, L. F., & DeJarnett, B. B. (1995). Lateral Variability of Sequence Stratigraphic Framework in the Campanian and Lower Maastrichtian of the Western Interior Seaway. In J. C. Van Wagoner & G. T. Bertram (Eds.), *Sequence Stratigraphy of Foreland Basin Deposits: Outcrop and Subsurface Examples from the Cretaceous of North America*. Tulsa, Oklahoma, U.S.A.: American Association of Petroleum Geologists.
- Lawton, T. F. (1986). Fluvial systems of the Upper Cretaceous Mesaverde Group and Paleocene North Horn Formation, Central Utah - A record of transition from thin-skinned to thick-skinned deformation in the foreland region. In J. A. Peterson (Ed.), *Paleotectonics and Sedimentation in the Rocky Mountain region, United States* (Vol. 41, pp. 423-442): American Association of Petroleum Geologists Memoir.
- Lawton, T. F. (2008). Laramide sedimentary basins. *Sedimentary basins of the world* 5, 429-450.
- Leeder, M. R. (1988). Recent developments in Carboniferous geology: a critical review with implications for the British Isles and NW Europe. *Proceedings of the Geologists' Association* 99(2), 73-100.
- Li, Y., & Bhattacharya, J. (2014). Facies architecture of asymmetrical branching distributary channels: Cretaceous Ferron Sandstone, Utah, USA. *Sedimentology* 61(5), 1452-1483.
- MacEachern, J. A., Bann, K. L., Bhattacharya, J. P., & Howell Jr, C. D. (2005). Ichnology of deltas: organism responses to the dynamic interplay of rivers, waves, storms, and tides. *Society of Sedimentary Geology* 83, 49-85.

- MacEachern, J. A., Pemberton, S. G., Gingras, M. K., Bann, K. L., James, N. P., & Dalrymple, R. W. (2010). Ichnology and facies models. *Facies models* 4, 19-58.
- Mack, G. H., James, W. C., & Monger, H. C. (1993). Classification of paleosols. *Geological Society of America Bulletin* 105(2), 129-136.
- McCabe, P. J. (1985). Depositional environments of coal and coal-bearing strata. *Sedimentology of coal and coal-bearing sequences*, 11-42.
- Meckel, T. A., Ten Brink, U. S., & Williams, S. J. (2007). Sediment compaction rates and subsidence in deltaic plains: numerical constraints and stratigraphic influences. *Basin Research* 19(1), 19-31.
- Miall, A. D., Catuneanu, O., Vakarelov, B. K., & Post, R. (2008). The Western interior basin. *Sedimentary basins of the world* 5, 329-362.
- Minderhoud, P. S. J., Erkens, G., Pham, V. H., Bui, V. T., Erban, L., Kooi, H., & Stouthamer, E. (2017). Impacts of 25 years of groundwater extraction on subsidence in the Mekong delta, Vietnam. *Environmental research letters* 12(6).
- Morton, R. A., Bernier, J. C., Barras, J. A., & Ferina, N. F. (2005). Historical subsidence and wetland loss in the Mississippi delta plain. *Gulf Coast Association of Geological Societies Transactions* 5, 555-571.
- Mozley, P. S., & Wersin, P. (1992). Isotopic composition of siderite as an indicator of depositional environment. *Geology* 20(9), 817.
- Nadon, G. C. (1998). Magnitude and timing of peat-to-coal compaction. *Geology* 26(8), 727-730.
- Olariu, C. (2014). Autogenic process change in modern deltas: lessons for the ancient. *From depositional systems to sedimentary successions on the Norwegian continental margin*, 149-166.
- Payenberg, T. H. D., Sidi, F. H., & Lang, S. C. (2003). Paleocurrents and reservoir orientation of Middle Miocene channel deposits in Mutiara field, Kutei Basin, east Kalimantan. In F. H. Sidi, D. Nummedal, P. Imbert, H. Darman, & H. W. Posamentier (Eds.), *Tropical Deltas of Southeast Asia; Sedimentology, Stratigraphy, and Petroleum Geology* (Vol. 76, pp. 255-266). Society for Sedimentary Geology Special Publication.
- Perrier, R., & Quiblier, J. (1974). Thickness changes in sedimentary layers during compaction history; methods for quantitative evaluation. *AAPG Bulletin* 58(3), 507-520.
- Plummer, P. S., & Gostin, V. A. (1981). Shrinkage cracks; desiccation or syneresis? *Journal of Sedimentary Research* 51(4), 1147-1156.
- Pratt, B. R. (1998). Syneresis cracks: subaqueous shrinkage in argillaceous sediments caused by earthquake-induced dewatering. *Sedimentary Geology* 117(1), 1-10.
- Roberts, H. H. (1997). Dynamic changes of the Holocene Mississippi River delta plain: the delta cycle. *Journal of Coastal Research*, 605-627.
- Roberts, L. N. R., & Kirschbaum, M. A. (1995). Paleogeography and the Late Cretaceous of the Western Interior of middle North America; coal distribution and sediment accumulation. *U. S. Geological Survey Professional Paper* 1561, 115.
- Ryder, R. T., Fouch, T. D., & Elison, J. H. (1976). Early Tertiary sedimentation in the western Uinta basin, Utah. *GSA Bulletin* 87(4), 496-512.
- Ryer, T. A., Rahmani, R., & Flores, R. (1984). Transgressive-regressive cycles and the occurrence of coal in some Upper Cretaceous strata of Utah, USA. In *Sedimentology of coal and coal-bearing sequences* (Vol. 7, pp. 217-227): Blackwell Scientific Publications Oxford.
- Raaf, J. F. M., Boersma, J. R., & Gelder, A. (1977). Wave-generated structures and sequences from a shallow marine succession, Lower Carboniferous, County Cork, Ireland. *Sedimentology* 24(4), 451-483.

- Shiers, M. N., Hodgson, D. M., & Mountney, N. P. (2017). Response of a coal-bearing coastal-plain succession to marine transgression: Campanian Neslen Formation, Utah, USA. *Journal of Sedimentary Research* 87(2), 168-187.
- Shiers, M. N., Mountney, N. P., Hodgson, D. M., & Cobain, S. L. (2014). Depositional controls on tidally influenced fluvial successions, Neslen Formation, Utah, USA. *Sedimentary Geology* 311, 1-16.
- Simms, A. R., Rodriguez, A. B., & Anderson, J. B. (2018). Bayhead deltas and shorelines: Insights from modern and ancient examples. *Sedimentary Geology* 374, 17-35.
- Smith, N. D., Cross, T. A., Dufficy, J. P., & Clough, S. R. (1989). Anatomy of an avulsion. *Sedimentology* 36(1), 1-23.
- Sonntag, R., Evans, J. P., La Pointe, P., Deraps, M., Sisley, H., & Richey, D. (2014). Sedimentological controls on the fracture distribution and network development in Mesaverde Group sandstone lithofacies, Uinta Basin, Utah, USA. *Geological Society, London, Special Publications* 374(1), 23-50.
- Southard, J. B., Lambie, J. M., Federico, D. C., Pile, H. T., & Weidman, C. R. (1990). Experiments on bed configurations under bidirectional purely oscillatory flow, and the origin of hummocky cross-stratification. *Journal of Sedimentary Petrology* 60, 1-17.
- Spieker, E. M. (1946). *Late Mesozoic and Early Cenozoic History of Central Utah*: U.S. Geological Survey Professional Paper.
- Syvitski, J. P. M. (2008). Deltas at risk. *Sustainability science* 3(1), 23-32.
- Taylor, K. G., Gawthorpe, R. L., Curtis, C. D., Marshall, J. D., & Awwiller, D. N. (2000). Carbonate Cementation in a Sequence-Stratigraphic Framework: Upper Cretaceous Sandstones, Book Cliffs, Utah-Colorado. *Journal of Sedimentary Research* 70(2), 360-372.
- Taylor, K. G., & Machent, P. G. (2010). Systematic sequence-scale controls on carbonate cementation in a siliciclastic sedimentary basin: Examples from Upper Cretaceous shallow marine deposits of Utah and Colorado, USA. *Marine and Petroleum Geology* 27(7), 1297-1310.
- Teatini, P., Tosi, L., & Strozzi, T. (2011). Quantitative evidence that compaction of Holocene sediments drives the present land subsidence of the Po Delta, Italy. *Journal of Geophysical Research: Solid Earth* 116(B8).
- Tonkin, N. S. (2012). Deltas. In D. Knaust & R. G. Bromley (Eds.), *Trace Fossils as Indicators of Sedimentary Environments* (Vol. 64, pp. 507-528). Amsterdam: Elsevier, *Developments in Sedimentology*.
- Törnqvist, T. E., Wallace, D. J., Storms, J. E. A., Wallinga, J., Van Dam, R. L., Blaauw, M., Derksen, M. S., Klerks, C. J. W., Meijneken, C., & Snijders, E. M. A. (2008). Mississippi Delta subsidence primarily caused by compaction of Holocene strata. *Nature Geoscience* 1(3), 173-176.
- van Asselen, S. (2011). The contribution of peat compaction to total basin subsidence: implications for the provision of accommodation space in organic-rich deltas. *Basin Research* 23(2), 239-255.
- van Asselen, S., Stouthamer, E., & Smith, N. D. (2010). Factors controlling peat compaction in alluvial floodplains: a case study in the cold-temperate Cumberland Marshes, Canada. *Journal of Sedimentary Research* 80(2), 155-166.
- Van Wagoner, J. C. (1992). High-frequency sequence stratigraphy and facies architecture of the Sego Sandstone in the Book Cliffs of western Colorado and eastern Utah. In J. C. Van Wagoner, D. Nummedal, C. R. Jones, D. R. Taylor, D. C. Jennette, & G. W. Riley (Eds.), *sequence stratigraphy applications to shelf sandstone and sandstone reservoirs; outcrop to subsurface examples* (pp. 1-10): AAPG Field Conference.

- Van Wagoner, J. C. (1995). Sequence stratigraphy and marine to nonmarine facies architecture of foreland basin strata, Book Cliffs, Utah, USA. In J. C. Van Wagoner & G. T. Bertram (Eds.), *Sequence Stratigraphy of Foreland Basin Deposits: Outcrop and Subsurface Examples from the Cretaceous of North America*. Tulsa, Oklahoma, U.S.A.: AAPG.
- Van Wagoner, J. C., Mitchum, R. M., Campion, K. M., & Rahmanian, V. D. (1990). Siliciclastic sequence stratigraphy in well logs, cores, and outcrops: concepts for high-resolution correlation of time and facies. *AAPG Methods in Exploration Series 7*, 55.
- Welder, F. A. (1959). Processes of deltaic sedimentation in the lower Mississippi River. *Coastal Studies Institute Technical Report 12*, 90.
- Willis, A. (2000). Tectonic control of nested sequence architecture in the Sego Sandstone, Neslen Formation and upper Castlegate Sandstone (Upper Cretaceous), Sevier foreland basin, Utah, USA. *Sedimentary Geology 136*(3-4), 277-317.
- Willis, B. J., & Gabel, S. (2001). Sharp-based, tide-dominated deltas of the Sego Sandstone, Book Cliffs, Utah, USA. *Sedimentology 48*(3), 479-506.
- Wright, L. D. (1977). Sediment transport and deposition at river mouths: a synthesis. *Geological Society of America Bulletin 88*(6), 857-868.
- Xue, C. (1993). Historical changes in the Yellow River delta, China. *Marine Geology 113*(3-4), 321-330.
- Yang, B., Dalrymple, R. W., & Chun, S. (2006). The significance of hummocky cross-stratification (HCS) wavelengths: evidence from an open-coast tidal flat, South Korea. *Journal of Sedimentary Research 76*, 2-8.
- Yonkee, W. A., & Weil, A. B. (2015). Tectonic evolution of the Sevier and Laramide belts within the North American Cordillera orogenic system. *Earth-Science Reviews 150*, 531-593.
- Young, R. G. (1955). Sedimentary facies and intertonguing in the Upper Cretaceous of the Book Cliffs, Utah-Colorado. *Geological Society of America Bulletin 66*(2), 177-202.

APPENDIX

APPENDIX I:
Data from sedimentary logs

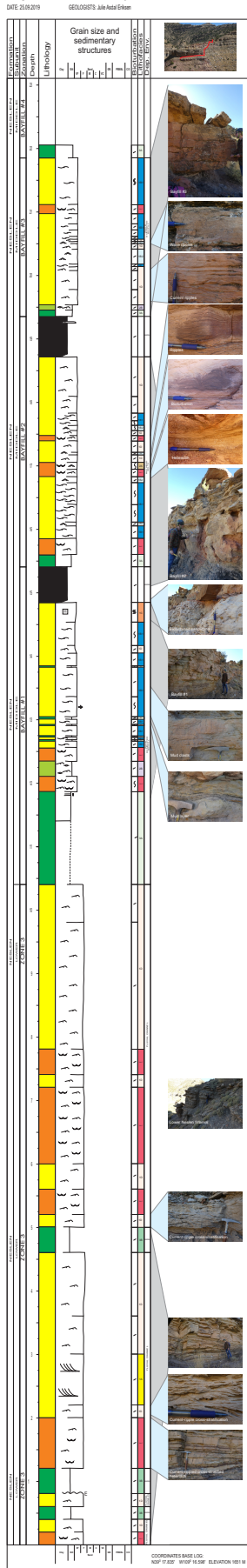
Appendix I: Data extracted from the sedimentary logs. For log positions, see Figures 1.1 and 1.2.

Log	Bayfill #	Thickness (cm)	Thickness marsh (cm)	%Silt and clay	%Sand	%Current	%Wave	%Sand Lower Neslen Interval
A	1	444.59	56.07	45.34	54.66	22.05	77.95	49
	2	330.752	63.80	14.5	85.50	55.2	44.8	
	3	249.91		9.11	90.89	37.224	62.776	
B	1	509.124	44.78	50.69	49.31	15.22	84.78	41
	2	388.15	94.35	38.73	61.27	71.09	28.91	
	3	269.626		9.06	90.94	33.198	66.802	
C	1	408.82	88.02	36.69	63.31	12.18	87.82	64
	2	388.84	81.67	36.58	63.42	59.98	40.02	
	3	311.018		15.72	84.28	65.435	34.565	
D	1	632.3	39.75	50.97	49.03	84.03	15.97	16
	2	313.462	37.60	15.7	84.30	81.91	18.09	
	3	195.992		11.28	88.72	78.852	21.148	
E	1	608.84	48.91	48.67	51.33	64.53	35.47	13
	2	275.368	91.38	18.53	81.47	59.77	40.23	
	3	210.768		9.79	90.21	74.772	25.228	
F	1	542.28	64.28	45.95	54.05	41.83	58.17	16
	2	304.296	77.43	29.23	70.77	90.56	9.44	
	3	228.984		10.82	89.18	64.587	35.413	
G	1	388.59	57.36	39.19	60.81	44.61	55.39	32
	2	299.164	75.60	30.76	69.24	83.11	16.89	
	3	226.54		9.19	90.81	63.007	36.993	
H	1	463.91	39.13	38.21	61.79	20.46	79.54	41
	2	335.126	59.37	19.47	80.53	66.52	33.48	
	3	236.472		11.13	88.87	59.92	40.08	
I	1	530.54	71.45	42.8	57.20	39.15	60.85	42
	2	346.11	164.58	40.82	59.18	64.15	35.85	
	3	209.34		7.26	92.74	73.77	26.23	
J	1	444.268	50.93	38.07	61.93	61.04	38.96	48
	2	313.016	38.57	47.47	52.53	100	0	
	3	192.14		3.87	96.13	61.586	38.414	
K	1		87.48					
	2	328.808	68.41	36.58	63.42	97.06	2.94	
	3	292.284		26.78	73.22	69.027	30.973	
L	1	540	60.73	95.54	4.46	0	0	32
	2	316.562	63.51	24.95	75.05	68.33	31.67	
	3	390.434		24.73	75.27	85.99	14.01	
M	1	420.57		61.39	38.61	33.24	66.76	91
	2	320.41	70.03	24.4	75.60	31.01	68.99	
	3	370.41		10.06	89.94	76.33	23.67	
N	1	350.6	78.61	58.53	41.47	100	0	46
	2	316.952	62.18	11.53	88.47	19.85	80.15	
	3	319.23		3.77	96.23	92.217	7.783	
O	1		66.58					20
	2	268.67	43.65	31.79	68.21	68.74	31.26	
	3	297.938		15.42	84.58	82.118	17.882	
P	1	500.572	59.78	54.86	45.14	100	0	7
	2	330.972	51.80	26.09	73.91	72.54	27.46	
	3	458.644		5.74	94.26	85.59	14.41	
Q	1	340.77	62.02	100	0.00	0	0	89
	2	292.278	62.21	5.09	94.91	30.38	69.62	
	3	330.702		0	100.00	50.433	49.567	
R	1	285.92	104.51	79.01	20.99	0	0	34
	2	298.048	81.96	22.08	77.92	64.71	35.29	
	3	300.604		14.8	85.20	64.766	35.234	
S	1	415.87	64.06	73.02	26.98	0	100	65
	2	249.994	115.34	2.38	97.62	12.02	87.98	
	3	408.92		5.04	94.96	80.909	19.091	

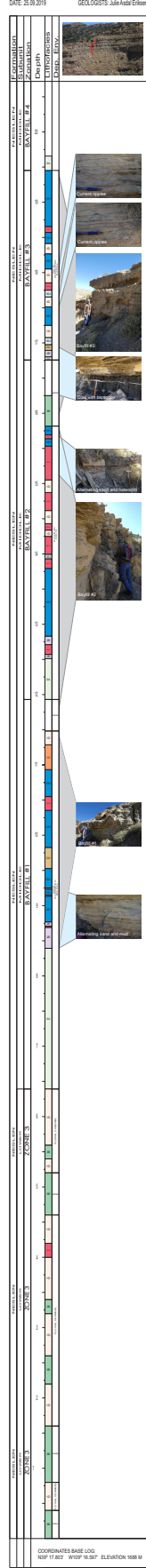
APPENDIX II:
Sedimentary logs

Appendix II: Sedimentary logs from locations A to S. The logs include lithology, grain-size, sedimentary structures, degree of bioturbation, lithofacies, facies association, and photos. The upper right photo shows the outcrop, with the red line as the logging path. At the bottom of each log, the coordinates of the base of the log are written. The location of the logs is also shown in Figures 1.1 and 1.2. Logs should be read digitally with the possibility of zooming. Figure 4.1 shows the legend for symbols and lithology used in the log.

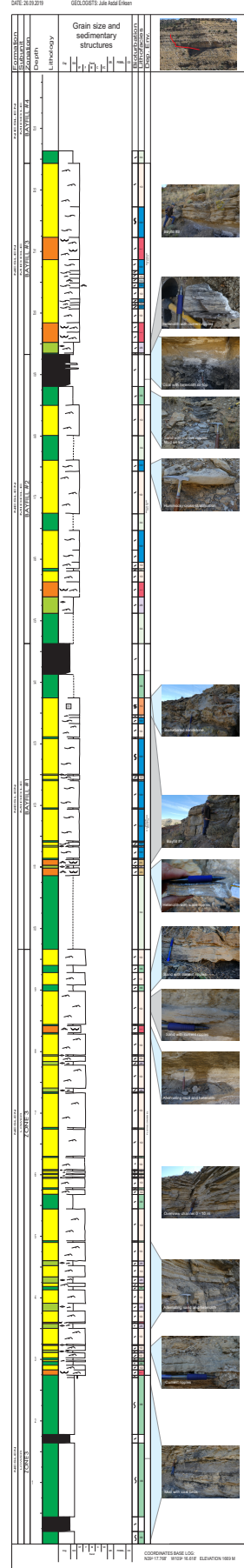
Log A - Outer East Canyon



Log B - Outer East Canyon

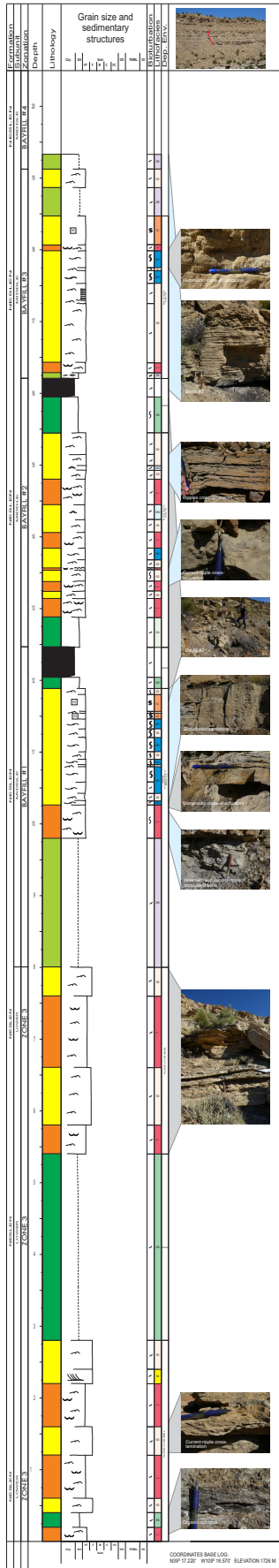


Log C - Outer East Canyon



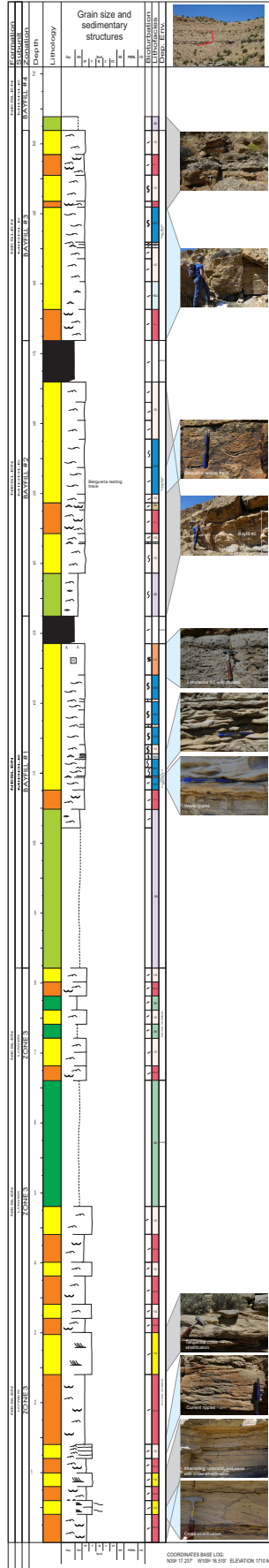
Log G - Exit Canyon

DATE: 14.09.2019 GEOLOGISTS: Julia Ahdal Eriksen



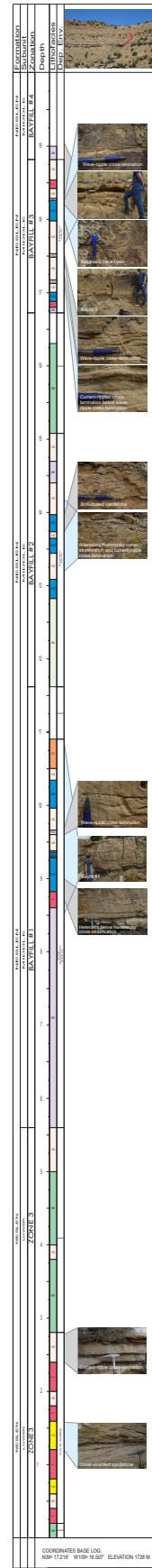
Log H - Exit Canyon

DATE: 13.09.2019 GEOLOGISTS: Julia Ahdal Eriksen

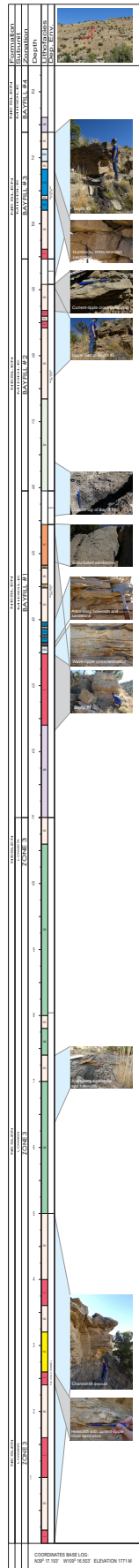


Log I - Exit Canyon

DATE: 14.09.2019 GEOLOGISTS: Julia Ahdal Eriksen

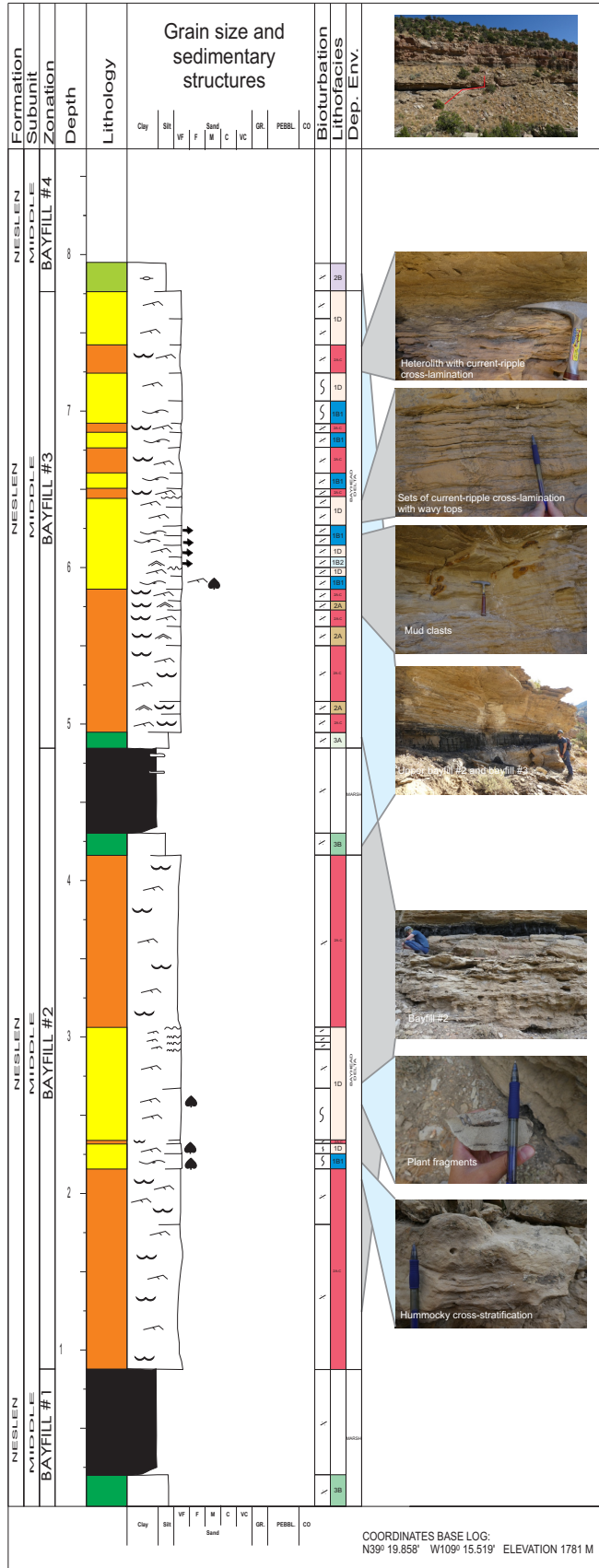


Log J - Exit Canyon
DATE: 10.09.2019 GEOLOGISTS: Julie Asdal Eriksen

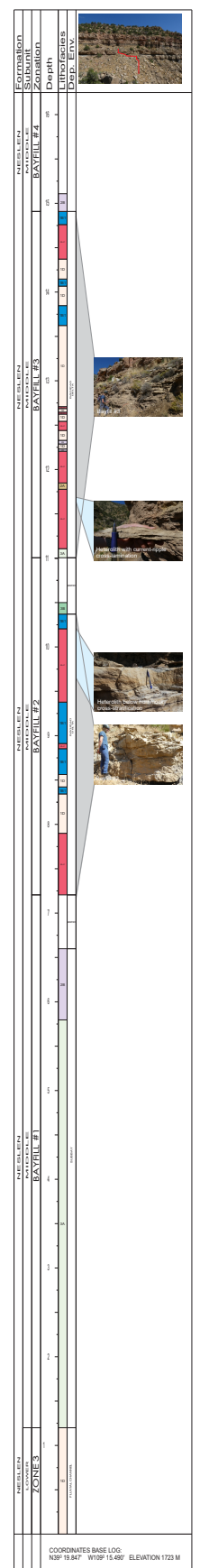


Log K - Keane Creek

DATE: 10.09.2019 GEOLOGISTS: Julie Asdal Eriksen

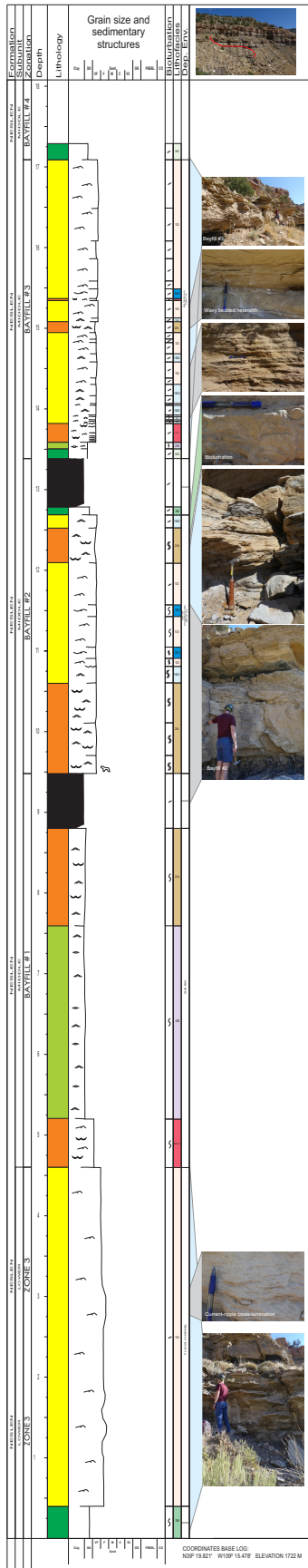


Log L - Keane Creek
DATE: 12.09.2019 GEOLOGISTS: Julie Asdal Eriksen



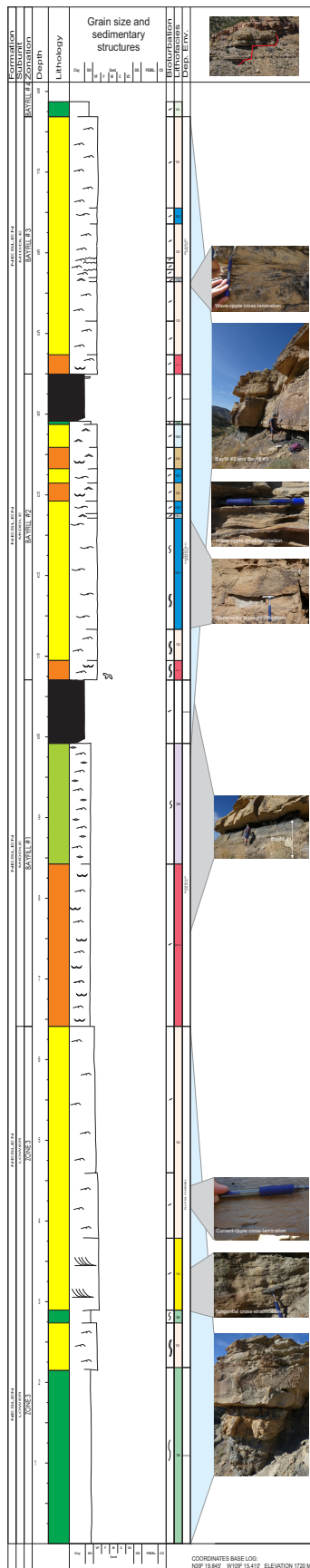
Log M - Keane Creek

DATE: 09.09.2019 GEOLOGISTS: Julie Asdal Eriksen



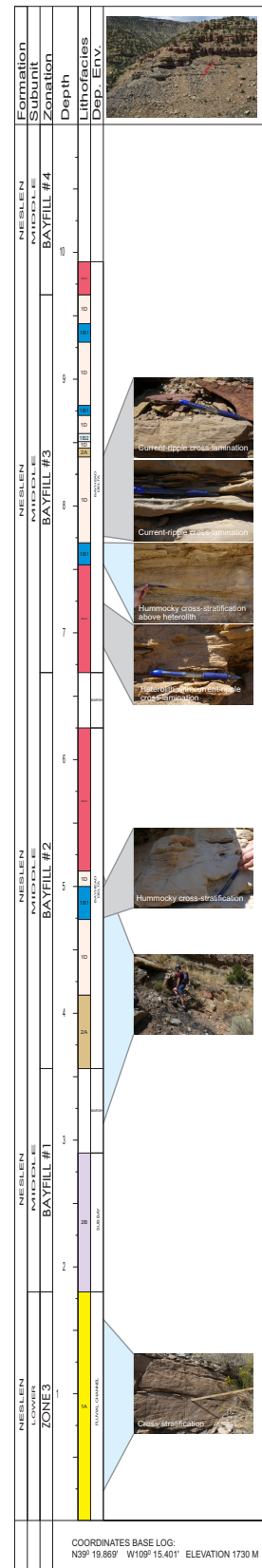
Log N - East Canyon Window

DATE: 07.09.2019 GEOLOGISTS: JULIE ASDAL ERIKSEN



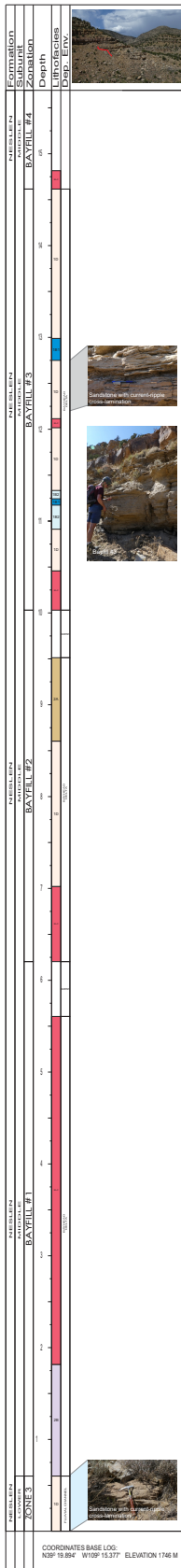
Log O - East Canyon Window

DATE: 09.09.2019 GEOLOGISTS: Julie Asdal Eriksen



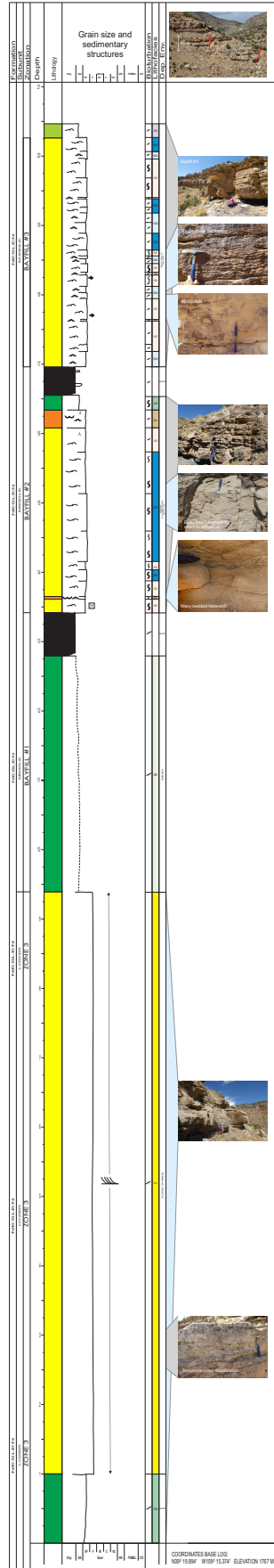
Log P - East Canyon Window

DATE: 09.09.2019 GEOLOGISTS: Julia Astal Erksen



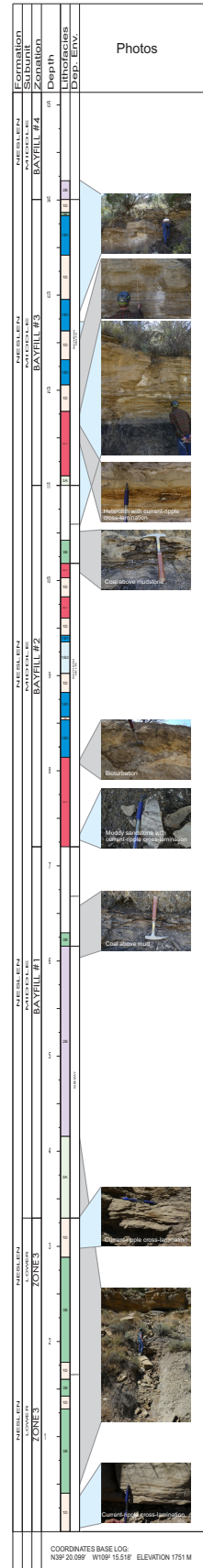
Log Q - East Canyon Window

DATE: 30.08.2019 GEOLOGIST: JULIE ASDAL ERKSEN



Log R - Neslen Canyon

DATE: 12.09.2019 GEOLOGISTS: Julia Astal Erksen



APPENDIX III:
Panoramic photos

Appendix III: Full-size panoramic photos of the studied outcrops in Outer East Canyon, Exit Canyon, Keane Creek, and East Canyon Window. See Figures 1.1 and 1.2 for the location of outcrops.

Outer East Canyon:



Exit Canyon:



Keane Creek: Photo: Jostein Kjærefjord



East Canyon Window:

